Extracellular adenosine deamination primes tip organizer development in *Dictyostelium*

Pavani Hathi and Ramamurthy Baskar*

Bhupat and Jyoti Mehta School of Biosciences, Department of Biotechnology, Indian Institute of Technology-Madras, Chennai 600036, India.

*Correspondence: rbaskar@iitm.ac.in

Abstract

Ammonia is a morphogen in *Dictyostelium* and is known to arise from the catabolism of proteins and RNA. However, we show that extracellular adenosine deamination catalyzed by 'adenosine deaminase related growth factor' (ADGF), is a major source of ammonia, and demonstrate a direct role of ammonia in tip organizer development. The tip formed during early development in *Dictyostelium* functions analogously to the embryonic organizer of higher vertebrates. *Dictyostelium* cell lines carrying mutations in the gene *adgf* fail to establish an organizer, and this could be reversed by exposing the mutants to volatile ammonia. Interestingly, *Klebsiella pneumoniae* physically separated from the *Dictyostelium adgf* mutants in a partitioned dish, also rescues the mound arrest phenotype suggesting a cross-kingdom interaction that drives development. Both the substrate, adenosine and the product, ammonia regulate *adgf* expression, and ADGF acts downstream of the histidine kinase DhkD in regulating tip formation. Thus, the consecutive transformation of extracellular cAMP to adenosine, and adenosine to ammonia are integral steps during *Dictyostelium* development. Remarkably, in higher vertebrates, *adgf* expression is elevated during gastrulation and thus adenosine deamination may be a conserved process driving organizer development in different organisms.

Key words

adenosine deaminase, organizer development, tip formation, volatile ammonia, *Dictyostelium*

Introduction

During early embryonic development, organizers play an important role in patterning and directing the differentiation of surrounding cells into specific tissues and organs. The embryonic organizer establishes the developmental polarity in vertebrates; and similarly, in *Dictyostelium,* the mound/slug tip acts as an organizer (Rubin and Robertson, 1975) playing a pivotal role in guiding collective cell migration and patterning. Despite numerous investigations on *Dictyostelium* tip formation, the processes by which the tip establishes and maintains the primary developmental axis remains elusive. Gaining insights into the mechanisms regulating tip organizer function will offer valuable insights on orchestrated cell movements and processes underlying development.

Dictyostelium transitions from a unicellular amoeba to a multicellular organism in response to starvation. The cells aggregate into a mound, which gives rise to a migrating slug and ultimately a fruiting body composed of spores and a dead stalk (Raper, 1940; Kessin, 2001). This process is regulated by diffusible signals including cAMP, adenosine, ammonia, and a chlorinated hexaphenone, 'differentiation-inducing factor' (DIF) (Bloom and Kay, 1988; Williams, 1988; Gross, 1994; Mahadeo and Parent, 2006; Shu et al., 2006). Importantly, the cell cycle phase soon after starvation is known to strongly influence the cell fate either as prestalk (pst) or prespore (psp) cells (Weeks and Weijer, 1994; Jang and Gomer, 2011).

Tip development in *Dictyostelium* depends on cAMP signaling in turn regulating protein kinase A (PKA) activity, adenosine signaling, and morphogenetic cell movements (Schaap and Wang,

45 1986; Mann and Firtel, 1993; Siegert and Weijer, 1995). Adenosine, a by-product of cAMP
46 hydrolysis, acts as an inhibitory morphogen suppressing additional tip formation (Schaap and
47 Wang, 1986).

48 Adenosine deaminases (ADA) catalyse the breakdown of adenosine to generate inosine and
49 ammonia, and are conserved among bacteria, invertebrates, vertebrates including mammals
50 (Cristalli et al., 2001). In humans, two isoforms of ADA are known including ADA1 and ADA2,
51 and the *Dictyostelium* homolog of ADA2 is adenosine deaminase-related growth factor (ADGF).
52 Unlike ADA that is intracellular, ADGF is extracellular and also has a growth factor activity (Li
53 and Aksoy, 2000; Iijima et al., 2008). Loss-of-function mutations in *ada2* are linked to
54 lymphopenia, severe combined immunodeficiency (SCID) (Gaspar, 2010), and vascular
55 inflammation due to accumulation of toxic metabolites like dATP (Zhou et al., 2014;
56 Notarangelo, 2016). In mice, *ada2* disruption leads to perinatal mortality (Wakamiya et al.,
57 1995), and overexpression of *ada2* results in aberrant heart and kidney development (Riazi et al.,
58 2005). In frogs, mutations in *ada2* manifest in reduced body size and altered polarity (Iijima et
59 al., 2008). In *Drosophila*, certain isoforms of ADGF are known to play a pivotal role in cell
60 proliferation by depleting extracellular adenosine (Zurovec et al., 2002), and loss of function of
61 *adgfA* promotes melanotic tumour formation and larval death (Dolezal et al., 2005). Adenosine
62 deaminases are known to interact with dipeptidyl peptidase IV (DPP), cluster of differentiation
63 (CD26) expressed on T-cells and the adenosine receptor, A2AR (expressed on dendritic cells) to
64 facilitate cell-cell signaling (Moreno et al., 2018). Thus, *adgf* plays a pivotal role in the
65 regulation of cell proliferation and development in several organisms.

66 Four isoforms of ADA are annotated in the *Dictyostelium discoideum* genome (Eichinger et al.,
67 2005) including adenosine deaminase (*ada*; DDB_G0287371), adenosine deaminase acting on

68 tRNA-1 (DDB_G0278943), adenosine deaminase tRNA-specific (DDB_G0288099) and
69 adenosine deaminase-related growth factor (*adgf*; DDB_G0275179), and their role in growth and
70 development is not known. In this study, we demonstrate that ammonia generated by ADGF
71 plays a direct role in establishing the tip organizer, highlighting a novel link between nucleoside
72 metabolism and developmental polarity in *Dictyostelium*.

73 **Results**

74 **Differential regulation of *adgf* expression during growth and development**

75 *Dictyostelium* cell lines carrying mutations in the gene *adgf* were obtained from the genome wide
76 *Dictyostelium* insertion (GWDI) bank, and were subjected to further analysis to know the role of
77 *adgf* during *Dictyostelium* development. To verify the insertion of blasticidin *(bsr)* resistance
78 cassette in *adgf* mutant, a diagnostic PCR was carried out and the integration was validated
79 (Figures 1A and 1B), and qRT-PCR analysis confirmed the absence of *adgf* expression (Figure
80 1C). In vertebrates, adenosine deaminases are expressed in a tissue specific manner to control
81 growth and development. To determine whether *adgf* expression is differentially regulated
82 during *Dictyostelium* development, qRT-PCR was performed using RNA isolated at 0 h, 8 h, 12
83 h, 16 h, 20 h and 24 h post starvation. *adgf* expression peaks at 16 h (Figure 1D) implying an
84 important role for *adgf* later in development. At this time point, the expression of the other three
85 isoforms of ADA were not significantly different from wild-type (WT), suggesting that the loss
86 of *adgf* (data not shown) function is not compensated by the other isoforms.

87 **The predicted structures of *Dictyostelium* ADGF and human ADA2 share a strong**
88 **structural similarity.**

89 The *D. discoideum adgf* gene is predicted to encode a protein of 543 amino acids, and belongs to
90 the metallo-transferases superfamily (Figure S1A), having an ADA and an N- terminal domain
91 similar to human ADA2 (Figure S1B). The ADGF sequence from the protein family database
92 (https://www.ebi.ac.uk/interpro/) was analysed using the online tool SMART (Simple Modular
93 Architecture Research Tool: http://smart.embl-heidelberg.de), to know the presence of
94 structurally similar domains. The different domains of *Dictyostelium* ADGF (DdADGF) show a
95 high degree of similarity with human ADA2. DdADGF shares 37.5% identity with human
96 ADA2 and shares a sequence similarity of 59.5% with *D. fasciculatum*, 61.2% with *D. pupureum,*
97 53.6% with *D. lacteum* and 62.1% with *Polysphondylium pallidum* (www.uniprot.org). Multiple
98 sequence alignment reveals the presence of an N-terminal signal sequence characteristic of
99 extracellular proteins (Figure S1C).and conserved histidine and glutamine residues in the active
100 site of both *D. discoideum* ADGF and human ADA2 (Figure S1D).

101 The phylogenetic relation of ADGF to the classic ADA subfamily has been reported previously
102 (Maier et al., 2005). To determine the evolutionary relationship of DdADGF with that of other
103 organisms, a phylogenetic analysis was carried out, and the amino acid alignment was created
104 using MEGAX software (Kumar et al., 2018). The evolutionary history of ADGF was inferred
105 using a Maximum Likelihood approach with Bootstrap analysis (100 iterations) as described by
106 Felsenstein (1985). The resulting phylogenetic tree indicated that DdADGF is closely related to
107 the ADGF proteins of other Dictyostelids, including *D. purpureum*, *Heterostelium pallidum,* and
108 *Cavenderia fasciculata*. DdADGF forms a distinct clade, likely representing a distant relative of
109 its vertebrate homolog (Figure S1E). Using the crystal structure of human ADA2, Cat eye
110 syndrome critical region protein 1 (CECR1) as a template (PDB-3LGD), the structure of
111 DdADGF was predicted by homology modeling (https://alphafold.ebi.ac.uk/) (Figures S1 F-H).

112 Alignment of DdADGF with human ADA2 yielded a root mean square deviation (RMSD) value
113 of 1 Å, indicating strong structural similarity (Eidhammer et al., 2000; Koehl, 2001).

114 ***adgf* controls aggregate size in *Dictyostelium***

115 To understand the role of *adgf* during *D. discoideum* development, *adgf* mutants were plated at a
116 density of $5x10^5$ cells/cm^2 on non-nutrient phosphate buffered agar plates and monitored
117 thereafter. In comparison to WT, the aggregates of *adgf* $^-$ were larger, and thus the number of
118 aggregates were fewer (Figure 2A) than the WT. To determine the pathways impairing the tissue
119 size in the mutant, RNA expression of countin (*ctn*) and small aggregates (*smlA*) were examined,
120 and their levels were reduced significantly compared to controls (Figure 2B). Countin factor (CF)
121 regulates group size by reducing the expression of cell-cell adhesion proteins cadherin (*cadA*)
122 and contact site A (*csaA*) (Siu et al., 1985; Coates and Harwood, 2001). Compared to WT, both
123 cell-to-cell adhesion and *cadA, csaA* expression were higher in the *adgf* mutant (Figures 2C and
124 2D) suggesting that *adgf* regulates the overall size of the aggregates.

125 cAMP chemotaxis significantly influences cell-cell adhesion (Konijn et al., 1967), and to
126 determine if chemotaxis is impaired in the *adgf* $^-$ lines, an under-agarose chemotaxis assay was
127 carried out. The chemotactic activity was not significantly different between the two cell types
128 (Figure 2E), suggesting that the increased mound size in the mutant is not due to altered
129 chemotaxis.

130 ***adgf* mutants form large, tipless mounds**

131 Subsequent to plating on KK2 agar, WT cells formed mounds by 8-9 h, and culminate to form
132 fruiting bodies by the end of 24 h. In contrast, the *adgf* $^-$ lines were blocked as rotating mounds
133 with no tips till 30 h (Figure 2F; Supplementary videos S1 and S2). Such a mound arrest

134 phenotype could be mimicked by adding the ADA specific inhibitor deoxycoformycin (DCF) to
135 WT cells (Figure 2G). After 36 h, a fraction of *adgf* $^{-}$ mounds (34.77 ± 4%) formed fruiting
136 bodies with bulkier spore sac (79.6 ± 6.3 mm^2) and stalk (Figures 2H and 2I). This late recovery
137 from the mound arrest may be due to the expression of other ADA isoforms after 36 h.

138 **Reduced ADA activity leads to high adenosine levels in the *adgf* mutant**

139 If *adgf* function is compromised, ADA enzyme activity is expected to be low. To verify this,
140 total ADA activity in WT and *adgf* $^{-}$ mounds was measured using a commercial assay kit. This
141 assay relies on the conversion of inosine (derived from ADA activity) to uric acid, and was
142 measured spectrophotometrically. Although ADA activity dropped significantly in the mutant
143 (Figure 3A), it was not completely abolished, and possibly, other isoforms may have a basal
144 activity both at 12 h and 16 h.

145 ADGF quenches extracellular adenosine, and if blocked, as expected in *adgf* $^{-}$*,* the mutants will
146 have increased extracellular adenosine. Using a commercial kit, the total adenosine levels were
147 measured, and both at 12 h and 16 h, the levels were elevated (Figure 3B), and this difference
148 was highly significant at 16 h. *adgf* expression at this time point was also high in WT cells. The
149 elevated adenosine levels at 16 h may result from reduced ADA activity and increased
150 expression of genes such as 5' nucleotidase (*5'nt*) and phosphodiesterases (*pdsA* and *regA*)*,* all
151 involved in adenosine formation (Headrick and Willis, 1989; Godecke, 2008). Hence, their
152 expression levels were examined. Although the expression of both *5'nt* and *regA* were enhanced
153 at 8 h, *pdsA* levels remained unaltered. Interestingly, the expression of all three genes trended
154 lower at 12 h but were significantly upregulated at 16 h (Figure 3C), suggesting an important
155 role of these genes at a specific time in development.

156 **Addition of ADA or overexpression of *adgf* cDNA restored tip development in *adgf*$^{-}$**

157 *adgf* mutants carry significantly high levels of adenosine. By administering ADA enzyme on top
158 of the *adgf*$^{-}$ mounds (Figure 4A), excess adenosine can be quenched resulting in ammonia
159 formation, possibly rescuing the phenotype. Indeed, addition of 10 U ADA onto mutant mounds
160 restored tip development. Besides, overexpression of WT *adgf* cDNA (driven by actin15
161 promoter) complemented the developmental defects of *adgf* mutants (Figures 4B and 4C),
162 confirming that the developmental block is the result of *adgf* gene disruption alone. However,
163 *adgf* cDNA overexpression in WT cells does not result in any observable defects (Figure 4D).
164 Taken together, these findings support an important function of *adgf* in tip development.

165 **WT or its conditioned media (CM) restored tip formation in *adgf*$^{-}$ mounds**

166 To determine whether *adgf* is necessary for tip formation in a cell-autonomous manner, WT and
167 the mutant cells were mixed in different proportions and plated for development. In a mix of
168 50% WT: 50% mutant, the mound defects of *adgf*$^{-}$ were rescued, but with 20% WT and 80%
169 *adgf*$^{-}$, the rescue was partial (31 ± 4 %) (Figure 4E) suggesting that the mound arrest phenotype
170 of the mutant is due to the absence of some secreted factor(s).

171 Further, when developed in the presence of WT CM, *adgf*$^{-}$ cells formed tipped mounds and
172 eventually fruiting bodies (Figure 4F). Conversely, in the presence of *adgf*$^{-}$ CM, WT cells
173 developed as large mounds with no tips (Figure 4G) and the size was comparable to the mounds
174 formed by *adgf*$^{-}$. These findings imply that the developmental phenotype of *adgf*$^{-}$ is not due to a
175 cell autonomous defect but due to faulty secreted factor signaling. While this finding is
176 consistent with the involvement of a secreted factor, it is also possible that a membrane-bound
177 extracellular factor may have a role in complementing the mutant phenotype.

178 **Volatile ammonia rescued the mound arrest phenotype of *adgf*$^-$**

179 If ADGF enzyme activity is compromised, ammonia levels are expected to be low. Hence, the
180 concentration of ammonia from WT and *adgf*$^-$ mounds was measured using a commercial kit.
181 Ammonia levels were significantly reduced in *adgf*$^-$ lines (Figure 5A). By mixing sodium
182 hydroxide and ammonium chloride (Thadani et al., 1977), ammonia could be generated, and in
183 such conditions, tip formation was restored in *adgf*$^-$ mounds (Figure 5B). All the rescue
184 experiments involving ammonia were carried for a 3.5 h time period.

185 **Physically separated WT restored tip development in the mutant**

186 WT mounds are expected to release different set of volatiles including ammonia, possibly
187 rescuing the mound arrest phenotype of the mutants nearby. To verify if this is correct, *adgf*$^-$
188 cells were developed in one half of a compartmentalized Petri dish, and WT cells on the other
189 side. Interestingly, the mound arrest of *adgf*$^-$ was fully rescued (Figure 5C) in the presence of
190 WT, although they were physically separated from each other. This suggests that volatiles, likely
191 to be ammonia released from WT is sufficient enough to rescue the mutant phenotype.

192 The *adgf*$^-$ CM is expected to have high adenosine levels, possibly generating low or no
193 ammonia. Addition of ADA to *adgf*$^-$ CM in one compartment of the partitioned dish led to
194 partial rescue (57 % ± 2) of *adgf*$^-$ kept on the other side of the dish (data not shown) implying
195 that the ammonia generated in such conditions may not be enough for a full rescue.

196 **Adenosine deamination alone drives the rescue of *adgf*$^-$**

197 To know if adenosine deamination is exclusively responsible for the rescue of the mutant, 10 ml
198 cold KK2 buffer mixed with different concentrations of adenosine (10 μM, 0.1 mM, 1 mM) was
199 added in one half of the compartmentalized dish, and the other side of the dish had the mutant on

200 phosphate buffered agar arrested at the mound stage. Addition of ADA enzyme (10 U) to the
201 buffered solution containing adenosine led to a full rescue after 3.5 h (Figure 5D), strongly
202 indicating that volatile ammonia generated from adenosine deamination alone is rescuing the
203 defect. Protein/RNA catabolism also generates ammonia in *Dictyostelium* (White and Sussman,
204 1961; Hames and Ashworth, 1974; Schindler and Sussman, 1977; Walsh and Wright, 1978), but
205 their levels were not significantly different between WT and *adgf* mutants (Figure S2A-B)
206 suggesting that ammonia released from adenosine deamination plays a direct role in tip
207 formation.

208 **Caffeine, not ammonia rescued the mound size of *adgf*$^{-}$**

209 Given that adenosine levels were elevated in the mutants, we attempted to rescue the large
210 mound size observed in the *adgf* mutants by treating them with the adenosine receptor antagonist,
211 caffeine (Costenla et al., 2010; Ribeiro and Sebastiao, 2010). Caffeine rescued this early
212 developmental defect in a dose-dependent manner (Figure 5E), suggesting that *adgf* may be one
213 of the regulators of group size in *Dictyostelium*. Since ammonia levels were reduced in the
214 mutant, we tested whether exposure to ammonia could rescue the large mound size of the *adgf*
215 mutant. Exposing the mutants to 0.01 M ammonia soon after plating or six hours after plating,
216 had no effect on the mound size of the mutants (Figure 5F), suggesting that while some early
217 effects may be mediated through adenosine receptors, the later effects appear to be independent
218 and are likely to be influenced by ammonia.

219 **Faulty expression of cAMP relay genes in *adgf*$^{-}$**

220 cAMP signaling is crucial for tip development and determining cell fate in *Dictyostelium*
221 (Schaap and Wang, 1986; Saxe et al., 1993; Firtel, 1996; Singer et al., 2019). Hence, the
222 expression of genes involved in cAMP relay were measured in WT and *adgf*$^{-}$ cells by qRT-PCR.

223 Total cAMP levels and *acaA* gene expression were both low in the *adgf*$^-$ lines (Figures 6A and
224 6B). Treating the cells with the pkA activator 8-Br-cAMP or the activator of adenyl cyclase,
225 cyclic-di-GMP (Wang and Schaap, 1985; Chen and Schaap, 2012), reversed the *adgf*$^-$ mound
226 arrest phenotype (Figures 6C and D), and increasing the cyclic-di-GMP dose from 0.5 mM to 1
227 mM resulted in multi tipped phenotype (Figure 6E). These observations reinforce that the mound
228 arrest phenotype of the *adgf*$^-$ lines is due to faulty cAMP signaling. A transient increase in
229 cAMP levels can be achieved by blocking the phosphodiesterase (*pde4*) activity. When treated
230 with a known PDE4 inhibitor, 3-Isobutyl-1-methylxanthine (IBMX) (Bader et al., 2007; Siegert
231 and Weijer, 1989), there was no effect on tip formation in *adgf*$^-$ mounds (Figure 6F), although
232 caffeine restored tip formation (Figure 6G).

233 **Circular instead of spiral cAMP waves in *adgf*$^-$ mounds**

234 Low *acaA* expression, reduced cAMP levels and enhanced cell-cell contacts in *adgf*$^-$ is likely to
235 impair cAMP wave propagation, and to ascertain if this is true, the cAMP signal propagation in
236 WT and *adgf*$^-$ mounds were compared using dark field optics. The cAMP wave propagation was
237 spiral in WT, and in contrast, the waves were circular in the *adgf* mutant, suggesting that the
238 cAMP relay is impaired (Figure 6H; Supplementary videos S3 and S4). While this strongly
239 suggests a defect in the mutant's ability to sustain spiral wave formation, the possibility of short-
240 lived or transient spiral waves in the mutant cannot be excluded.

241 **Ammonia restores tip formation by regulating *acaA/pde4* expression**

242 To find if *adgf* expression is regulated by the substrate or the product, WT cells were treated with
243 different concentrations of adenosine (100 nM, 1 µM, 0.5 mM), plated on KK2 agar plates and
244 harvested at 16 h for RNA isolation. Independently, WT mounds on KK2 agar plates were
245 exposed to different concentrations of volatile ammonia (0.1 mM, 1 mM, 10 mM) for 3 h and

246 thereafter, the mRNA expression levels of *adgf*, *acaA* and *pde4* were examined. With 100 nM
247 adenosine, the expression of both *adgf* and *acaA* decreased, but at higher adenosine
248 concentrations (1 μM, 0.5 mM), the expression levels of these two genes were comparable to
249 controls (Figure 7A). Interestingly, *pde4* expression decreased gradually with increasing
250 adenosine concentrations (100 nM to 0.5 mM), but increased steadily with increasing ammonia
251 levels.

252 Exposure of WT mounds to 0.1 mM ammonia, led to decreased *adgf* expression but exposure to
253 1 mM and 10 mM ammonia, respectively caused a 3 and 2.3-fold upregulation of *acaA*
254 expression. These observations suggest that ammonia may be rescuing the mound arrest
255 phenotype by enhancing *acaA* expression and thus cAMP levels. In similar conditions, a
256 considerable increase in *pde4* expression was observed (Figure 7B), which may be necessary for
257 controlling cAMP levels in response to ammonia treatment. In conclusion, the expression of *adgf*
258 is influenced both by the substrate adenosine, as well as the product ammonia in a dose
259 dependent manner. To ascertain if ammonia exposure indeed increases the cAMP levels in the
260 mutant thereby restoring the phenotype, cAMP levels were measured in the *adgf* mutant mounds
261 following the rescue with ammonia. Indeed, the cAMP levels were higher in the rescued mounds
262 compared to untreated *adgf* controls (Figure 7C), supporting the idea that ammonia promotes tip
263 development by restoring the cAMP signaling.

264 ***adgf*$^{-}$ cells sort to prestalk in a chimera with WT**

265 To determine if *adgf* favours the differentiation of one cell type over the other, the expression of
266 pst and psp markers were examined in the mutant by realtime PCR. While the expression of pst
267 markers, *ecmA* and *ecmB* were significantly upregulated, the psp-specific *pspA* gene expression
268 was reduced in the mutant (Figure 7D), suggesting that WT *adgf* favours psp expression.

269 To know the cell type preference of the *adgf* mutants in a chimera with WT, a fraction (20%) of
270 any one cell type was labelled with a cell tracker stain 1,1'-Dioctadecyl-3,3,3',3'-
271 Tetramethylindocarbocyanine Perchlorate (DIL), and the development was tracked thereafter. In
272 the slugs that formed after mixing labelled WT or *adgf* ^{OE} cells with 80% unlabelled *adgf* $^{-}$ cells,
273 the fluorescence was largely confined to the psp region (Figures 8B-C). Conversely, when *adgf* $^{-}$
274 cells stained with DIL were mixed with unlabelled WT or *adgf* ^{OE}, the fluorescence was
275 restricted to the pst part of the slug (Figure 8A). In the chimeric slugs, consistently, labelled WT
276 or *adgf* ^{OE} cells occupy the psp, whereas the *adgf* $^{-}$ cells end up in the pst region. Thus, the
277 distribution of cell types in the mound/slug is significantly influenced by *adgf,* as the mutant
278 cells sort out in a mixture with WT cells and differentiate to pst cells.

279 Further, when *adgf* $^{-}$ slugs were stained with the pst marker, neutral red (Yamamoto and
280 Takeuchi, 1983), the staining was intense in the pst region and anterior-like cells (ALCs), and
281 such an intense coloration was not apparent in WT especially in the ALCs (Figure S3A). To
282 further investigate if reduced ADA activity affects cell type specific marker expression or their
283 pattern in slugs, pst (*ecmA*-GFP, *ecmO*-GFP) or psp (*pspA*-RFP) lines were treated with the
284 ADA inhibitor DCF. While there was no change in pst/psp patterns in the fraction of mounds and
285 slugs that developed after a long delay, the *ecmA*-GFP fluorescence was intense when compared
286 to WT (Figures S3B). Similar to NR staining pattern in *adgf* mutant slugs, a prominent
287 expression of *ecmA*-GFP was observed in the ALC region also. Visually, there was no change in
288 *ecmO* or *pspA* marker expression in DCF treated slugs (Figures S3C and S3D) suggesting that
289 impaired ADGF activity affects tip specific expression.

290 To know if *adgf* expression is differentially regulated between the two major cell types, psp-GFP
291 tagged WT slugs were disaggregated, and using the fluorescence activated cell sorter (FACS),

292 GFP-negative prestalk (pst-GFP^{-}) and GFP-positive prespore (psp-GFP^{+}) populations were
293 obtained (Figures 9A-E), and RNA was isolated from both cell populations. Real time PCR
294 analysis reveals that *adgf* expression is 4.95-fold higher in the psp-GFP^{+} than pst-GFP^{-} cells
295 (Figure 9F). The preferential sorting of WT cells to psp region and the *adgf* mutants (with
296 reduced psp expression) to the pst part of the slug also reinforces the differential expression of
297 *adgf*. Thus, cells with higher *adgf* expression preferentially sorted to the psp region and the
298 absence of *adgf* in mutant cells may hinder their ability to adopt a prespore fate, leading to their
299 preferential sorting in the pst region within the chimera.

300 ***adgf* acts downstream of the histidine kinase, *dhkD***

301 In an effort to identify the pathway by which *adgf* acts during tip development, we selected a
302 number of mutant lines with similar mound arrest phenotype such as cAMP receptor B (*carB* $^{-}$),
303 LIM domain containing protein (*limB* $^{-}$), mound mutant (*mndA* $^{-}$) and histidine kinase (*dhkD* $^{-}$)
304 (Saxe et al., 1993; Carrin et al., 1996; Chien et al. 2000; Singleton and Xiong, 2013), and treated
305 the mounds with ADA enzyme. Treatment with 10 U ADA or exposure to ammonia restored tip
306 formation in *dhkD* $^{-}$ mounds and not others tested (Figures S4A and S4C). An increase in ADA
307 concentration (20 U), resulted in the development of multiple tips in *dhkD*$^{-}$ (Figures 10A-C).
308 Further, in the *dhkD* mutant mounds that were rescued by ammonia, cAMP levels were
309 significantly elevated compared to untreated *dhkD* $^{-}$ controls (Figure S4D). These findings imply
310 that ammonia induced tip formation increased cAMP levels, thereby restoring the phenotype, and
311 *adgf* acts downstream of *dhkD* in controlling tip development. Similarly, we tested few mutants
312 with multi-tipped phenotype, such as tipped mutant (*tipA* $^{-}$), culinB (*culB* $^{-}$), autophagy mutants
313 (*atg7* $^{-}$, *atg8*$^{-}$, and *atg9*$^{-}$) (Stege et al., 1999; Wang and Kuspa, 2002; Otto et al., 2003; Otto et al.,
314 2004, Tung et al., 2010) by adding the ADA inhibitor, DCF (1 mM) to the cell suspension /agar

315 plates and if rescued, those mutants are likely to be in the same pathway as that of *adgf* in
316 controlling tip development. However, DCF treatment had no impact on the phenotype of the
317 mutants with multiple tips (Figure S4B).

318 **Impaired expression of other deaminases also results in aberrant tip formation**

319 Several pathways control ammonia levels during development, and knockouts in other
320 deaminases (2-aminomuconate deaminase: DDB_G0275081, adenosine monophosphate
321 deaminase: DDB_G0292266, dCTP deaminase: DDB_G0293580, threonine deaminase:
322 DDB_G0277245, N-acetyl glucosamine deaminase: DDB_G0286195, glucosamine-6-phosphate
323 deaminase: DDB_G0278873) show a partial mound arrest phenotype (Figures S5A-F) although
324 the expression of some of these candidates is stronger during development, suggesting a
325 prominent and unique role of adenosine deamination in tip development.

326 **High adenosine levels and other related purines do not block tip development**

327 ADA catalyses the conversion of adenosine/deoxy adenosine respectively to inosine/ deoxy
328 inosine. As *adgf* mutants have high adenosine levels, we investigated if the mound arrest could
329 be mimicked in WT by treating with adenosine. However, addition of adenosine does not lead to
330 mound arrest in WT (Figure S6A). It is possible that ADA/ADGF converted adenosine
331 analogues to inosine analogues, which in some manner affected development. Hence, WT cells
332 were treated with adenosine analogue (2'-deoxyadenosine) or guanosine (10 μM each), and they
333 do not cause a mound arrest phenotype either. Similarly, treating *adgf*$^{-}$ mounds with inosine
334 does not restore tip formation (Figures S6B and S6C) suggesting that the blocked tip
335 development is due to faulty adenosine deamination alone.

336 **Cross kingdom rescue of the *adgf*$^{-}$ mound arrest phenotype**

337 Just like WT *Dictyostelum* rescuing the mound arrest phenotype of the *adgf* mutant, we
338 examined if bacteria physically separated from the mutants would rescue the phenotype. To
339 check this, *Klebsiella pneumoniae* and *adgf* mutants were incubated adjacent to each other within
340 a compartmentalized KK2 agar plate. After 12 h incubation period, tip formation was restored in
341 the mutants while in the same time frame, the mounds in controls failed to form tips. Possibly,
342 *Klebsiella* on KK2 plates with no nutrients would die releasing ammonia thereby restoring tip
343 development in *Dictyostelium* (Figure S7).

344 **Discussion**

345 ***Dictyostelium* ADGF is likely to be a secreted growth factor**

346 Multiple sequence alignments, experiments with conditioned media and cell mixing with WT
347 suggests that ADGF is secreted. ADGF is also known to interact with 5′-adenosine
348 monophosphate (AMP) and deoxyadenosine. AMP deaminase, previously characterized in the
349 mollusk *Helix pomatia*, has been identified as a member of ADGF family (Tzertzinis et al.,
350 2023). Studies on the characterization and expression of ADGF in Pacific abalone has shown
351 that it is a secreted protein critical for embryonic and larval development (Hanif et al., 2022).
352 The crystal structure of human ADA2 reveals the presence of a catalytic- and two unique ADA2-
353 specific domains with novel folds, responsible for protein dimerization and interaction with cell
354 surface receptors. Furthermore, the presence of a number of N-glycosylation sites, conserved
355 disulfide bond, and a signal peptide indicate that ADA2 is specifically adapted to function in the
356 extracellular environment (Zavialov et al., 2010).

357 **Possible reasons for increased mound size in the *adgf* mutant**

358 Enhanced cell adhesion influences cohesion and can impact the mound size (Roisin-Bouffay et
359 al., 2000). The expression of *cadA* and *csaA* genes were upregulated in the *adgf* mutant, possibly
360 leading to increased adhesion and larger mound formation. While over-secretion of *ctn* leads to
361 stream breaking and small aggregate formation (Brock and Gomer, 1999), disruption of the *ctn*
362 gene prevents this process, inducing large aggregate formation. *ctn* in turn regulates *smlA* (Brock
363 et al., 2003), impacting the overall aggregate size. Thus, *adgf* mutants that have reduced *ctn* and
364 *smlA* expression manifest in large mound formation. Indeed, cells treated with adenosine are
365 known to form large aggregates (Schaap and Wang, 1986; Jaiswal et al., 2012), and the first
366 genetic evidence supporting the previous work is from *adgf* mutants, which carry excess
367 extracellular adenosine and form large aggregation streams.

368 **Pathways generating ammonia in *Dictyostelium***

369 Proteolysis during starvation is believed to be the main source of volatile ammonia in
370 *Dictyostelium* (Hames and Ashworth, 1974; Schindler and Sussman, 1977; White and Sussman,
371 1961), while RNA degradation is also attributed to yield ammonia during starvation (Walsh and
372 Wright, 1978). During development, amino acids, total protein and RNA levels are reported to
373 reduce with a significant increase in ammonia levels, thus equivocating the source of volatile
374 ammonia (Hames and Ashworth, 1974). The highly acidic, autophagic vesicles in pst cells
375 (Gross, 2009) are believed to catalyze the breakdown of proteins and RNA, also generating
376 ammonia.

377 Furthermore, several deaminases or enzymatic reactions in *Dictyostelium* may also generate
378 ammonia (Supplementary Table S1). The annotated *D. discoideum* genome contains five
379 evolutionarily conserved family of ammonium transporter/methylammonium permease/rhesus
380 protein (Amt/Mep/Rh) encoding genes (Eichinger et al., 2005), *amtA, amtB, amtC, rhgA,* and

381 *rhgB,* which help in regulating ammonia levels during growth and development. *amtA* and *amtC*
382 antagonistically control developmental processes and are involved in ammonium sensing or
383 transport (Follstaedt et al., 2003; Kirsten et al., 2005; Singleton et al., 2006).

384 **Role of ammonia during *Dictyostelium* development**

385 Ammonia is known to inhibit aggregation (Schindler and Sussman, 1979; Williams et al., 1984),
386 affect aggregate territory size (Thadani et al., 1977), aggregate density (Feit, 1988), cell fate
387 (Gross et al., 1988), culmination (Davies et al., 1993) and fruiting body size in *Dictyostelium*
388 (Lonski, 1976). Ammonia promotes psp over pst differentiation (Newell et al., 1969; Sternfeld
389 and David, 1979; Gross et al. 1983; Oyama and Blumberg, 1986), and favors prolonged slug
390 migration called 'slugging' over culmination by suppressing DIF biosynthesis (Neave et al.,
391 1983). Ammonia plays a crucial role in orienting cell masses, accelerating the movement of
392 aggregating cells (Bonner et al., 1986), and prevents the developmental transition of slugs to
393 fruiting bodies (Bradbury and Gross, 1989; Wang and Schaap, 1989). Enzymatic removal of
394 ammonia causes the quick transition from slug to fruiting thus controlling the morphogenetic
395 pathways (Schindler and Sussman, 1977).

396 In slugger mutants, ammonia is known to inhibit tip formation (Gee et al., 1994), but not in WT
397 NC4. Yoshino et al., (2007) have also reported ammonia inhibiting both aggregation and tip
398 formation in WT cells. However, ammonium chloride was used as a source of ammonia, and the
399 potential interference from chloride ions cannot be ruled out. A mutant impaired in
400 mitochondrial function, *midA*$^{-}$, is reported to accumulate high levels of ammonia that inhibited
401 development (Torija et al., 2006). Notably, these cells were developed with overhead light, a
402 condition that may influence ammonia sensitivity and the developmental phenotype. However,
403 ammonia exerts no effect on tip formation in AX4 (data not shown). After the tips are

404 established, the slugs/ fruiting bodies move away from ammonia, reflecting a process by which
405 fruiting bodies position themselves from other structures to increase the possibility of spore
406 dispersal (Kosugi and Inouye, 1989).

407 Cells carrying high ATP, its derivatives cAMP (Bagorda et al., 2009; Singer et al., 2019) and
408 adenosine (Schaap and Wang, 1986), end up in the tip (Hiraoka et al., 2022). Further, 5'-
409 nucleotidase promoter activity is high in pstAB cells (Ubeidat et al., 2002) that significantly
410 covers the tip region suggesting high adenosine levels in the tip. However, extracellular 5'-AMP
411 can be derived from multiple sources such as hydrolysis of cAMP, ATP and RNA (Carpousis et
412 al., 1999).

413 As a gas, ammonia can diffuse generating a gradient. Our results (Figure 6A) also show that the
414 amount of ammonia released from adenosine is in the same order of magnitude as that from other
415 sources (Yoshino et al., 2007). It is interesting that a mutation in *adgf* manifests in arrested tip
416 development, although *adgf* expression was found to be higher in psp than pst cells. If a
417 threshold concentration of ammonia is not present, collective cell movement influencing tip
418 formation may be blocked at the mound stage. Increased *adgf* expression in psp than pst cell
419 types suggest that low extracellular adenosine (Weijer and Durston, 1985; Schaap and Wang,
420 1986) and high levels of ammonia influence psp cell fate. The slime sheath at the back of the
421 slug is believed to prevent the diffusion of ammonia (Gross, 2009), and ammonia escaping
422 through the front of the slug neutralizes the acidic vesicles (Bonner, 1952), causing collective
423 cell movement thereby restoring tip development. The decision between the formation of the tip
424 (pst cells) and the ALC is controlled by the tip's production of ammonia, which prevents the
425 migration of ALCs towards the tip (Sternfeld and David, 1982; Feit et al., 1990).

426 In *adgf* mutants, ammonia levels may not be sufficient enough to neutralize the acidic vesicles
427 and hence, NR staining is intense in the pst region and the ALCs (Bonner, 1952). Ammonia has
428 been shown to differentially suppress cAMP chemotaxis in ALC and pst cells in *Dictyostelium*
429 (Feit et al., 2001).

430 **Ammonia's effect on cAMP signaling in *Dictyostelium***

431 Exposing the cells to ammonia is known to increase intracellular cAMP levels in *D. discoideum*
432 (Riley and Barclay, 1990; Feit et al., 2001), but Schindler and Sussman, (1977) and Williams et
433 al., (1984) reported that high ammonia levels inhibit the synthesis and release of cAMP.
434 However, these experiments use ammonium carbonate (Schindler and Sussman, 1977), or
435 ammonium chloride (Williams et al., 1984) as a source of ammonia, and the possibility of
436 carbonate and chloride ions interfering with development cannot be ruled out. Ammonia is
437 reported to show no effect on cAMP levels in *D. discoideum* slugs (Schaap et al., 1995), but in *D.*
438 *mucoroides,* high ammonia levels are known to block the production of extracellular cAMP. The
439 effect of ammonia on aggregation seems to be species specific notably in *P. violaceum, P.*
440 *pallidum, and D. mucoroides* resulting in wider aggregation territories, while it was not observed
441 in other species such as *D. discoideum* and *D. purpureum* (Bonner and Hoffman, 1963).

442 Adenylate cyclase (AC) activity is regulated by various factors (Steer, 1975). At physiological
443 levels, ammonium ions increase AC activity in the rat brain by 40% (Yeung et al., 1989), but
444 lowered its activity in the liver by about 30% (Wiechetek et al., 1979). Ammonia has been
445 shown to increase the activity of AC-G in *Dictyostelium* sori (Cotter et al., 1999). High ammonia
446 levels by altering the pH, can affect the activity of numerous enzymes whose activity is pH
447 dependent and thus the activity of AC can be impacted by pH variations. *adgf* mutants with low
448 ammonia levels have reduced cAMP levels, and increase in ammonia causes a significant

449 increase in *aca*A expression. In rat brain, ammonia is known to interact with manganese (Rivera-
450 Mancía et al., 2012; Lu et al., 2020), that is known to increase *aca*A expression in *Dictyostelium*
451 (Loomis et al., 1979; Khachatrian et al., 1987). Possibly, ammonia interacts with metal ions like
452 manganese to form 'ammine complexes' (Lipkowski and Galus, 1973), particularly in aqueous
453 environments or under specific conditions where the appropriate ligands are available, and
454 enhances cAMP levels, thus rescuing the mound defects of the mutant.
455 Tip organizer development in *Dictyostelium* depends on the differentiation and appropriate
456 sorting of pst and psp cells (Kay et al., 1978; Williams et al., 1989; Saxe et al., 1993; Williams,
457 2006), a process that relies on signaling of different morphogens including cAMP, adenosine,
458 DIF and ammonia (Bloom and Kay, 1988; Williams, 1988; Riley and Barclay, 1990; Gross et al.,
459 1994). These morphogens modify one another's effects, and determine the choice of the
460 differentiation pathway as well as the spatial arrangement of cells (Bloom and Kay, 1988). Thus,
461 the rescue of the *adgf* mutant upon exposure to ammonia is likely due to cAMP signaling and
462 cell-cell contact.

463 **Possible reasons for reduced cAMP levels in the *adgf* mutant**

464 Higher *pde4* and reduced *acaA* expression may result in low cAMP levels in the mutant. ADA
465 significantly regulates adenosine levels, thus reducing the activation of adenosine-mediated
466 receptors (Van Haastert, 1983). Two classes of adenosine receptors including adenosine alpha-
467 and beta-receptors are known to be expressed in *Dictyostelium* (Theibert and Devreotes, 1984).
468 When adenosine concentrations are high, beta-receptors bound with adenosine inhibit the
469 binding of cAMP to its receptors, thereby inhibiting cAMP signaling (Newell, 1982; Van
470 Haastert, 1983; Theibert and Devreotes, 1984). High adenosine levels in the *adgf* mutant may
471 also reduce cAMP levels via a similar mechanism.

472 The mound/slug tip is believed to carry high adenosine levels restricting additional tip formation
473 (Wang and Schaap, 1985), and our results also suggest that *adgf*$^{-}$ cells with high adenosine end
474 up as pst cells.

475 **Distorted cAMP waves in mutant**

476 Collective cell movement within mounds is essential for cell sorting and the progression from
477 mounds to finger structures (Kellerman and McNally, 1999). In WT mounds, cAMP waves
478 propagate as spirals, while in the mutants, the wave propagation was in concentric circles.
479 Initially, the cAMP waves arise as concentric circles, that, upon symmetry breaking, form spiral
480 waves (Siegert and Weijer, 1995). With successive wave propagation, the circular ring distorts,
481 and one end curls towards the pulsatile center, creating a spiral wave around the organizing
482 center. In *adgf* mutants, however, defective cAMP relay prevents this transition. A surge in
483 phosphodiesterase inhibition is thought to regulate this shift from concentric to spiral wave
484 propagation (Palsson and Cox, 1996), and indeed the phosphodiesterase expression was higher in
485 the *adgf* mutant possibly distorting the wave propagation.

486 The mound/slug tip of *Dictyostelium* generates cAMP pulses (Traynor et al., 1992), and is
487 known to suppress additional tip formation (Farnsworth, 1973). Adenosine, that inhibits
488 additional tip formation represses *pde4* expression whereas ammonia, that promotes tip
489 elongation, increases *pde4* expression. Thus, the restoration of cAMP signaling and spiral wave
490 propagation possibly leads to the rescue of the *adgf*$^{-}$ mound arrest phenotype upon exposure to
491 ammonia. Surprisingly adenosine exerts little effect on tip development in WT cells and studies
492 of Inouye (1989) also reinforce our observations, showing that adenosine does not significantly
493 influence the conversion of pst to psp cells in shaking culture conditions.

494 **Adenosine deamination drives tip organizer development**

495 A crucial evidence supporting that adenosine deamination is singularly responsible for the rescue
496 of *adgf* $^{-}$ mound arrest comes from experiments where partitioned dish with buffered solution
497 containing adenosine on one side, and the mutants on the other half of the dish. Addition of ADA
498 to the buffer containing adenosine resulted in *adgf* mutants forming tipped mound. Although
499 ammonia's role in *Dictyostelium* development is well established, this report is the first to show a
500 novel role of ammonia in tip development. If natural variants of *Dictyostelium* that fail to form
501 tips exist in soil ecosystems, it is conceivable that these strains could still form fruiting bodies
502 when in proximity to WT strains. This interaction would likely occur through volatile signals
503 such as ammonia diffusing through the shared environment. These diffusible signals may help
504 rescue or coordinate developmental processes among neighbouring cells. Notably, the
505 development of an organism in its natural environment is strongly influenced by volatile
506 compounds present in its surroundings (Schulz-Bohm et al., 2017).

507 **ADA in organizer development and gastrulation in vertebrates**

508 *ada/adgf* expression is found to be high during gastrulation stages (Figure S8) in several
509 vertebrates (Pijuan-Sala et al., 2019; Tyser et al., 2021), and collective cell migration during
510 gastrulation and collective cell movement within the *Dictyostelium* mound are remarkably
511 similar (Weijer, 2009), suggesting an overlooked role of ammonia in organizer development.
512 The human homologue of *adgf*, CECR1, is a potential gene for the genetic disorder, Cat-eye
513 syndrome and thus, *Dictyostelium* may also serve as a model to study this condition. Ammonia is
514 crucial in regulating differentiation, metabolism, and gene expression (Stein et al., 2013; Liu et
515 al., 2022). Ammonium has been shown to induce aberrant blastocyst differentiation, disrupt
516 normal metabolic processes, alter pH regulation, and subsequently affect fetal development in

517 mice (Lane and Gardner, 2003). Newt *Triturus* exposed to ammonia shows dorsalization of the
518 ventral marginal zone highlighting the capacity of ammonia to alter embryonic axis formation
519 (Yamada, 1950). Furthermore, research on avian embryos has revealed significant ammonia
520 content in developing eggs, suggesting a potential role for ammonia in the energy metabolism
521 during ontogenesis (Needham, 1926).

522 ***dhkD* functions upstream of *adgf***

523 The histidine kinase *dhkD*, a member of the two-component family of histidine kinases, appears
524 to function upstream of *adgf*, adding to our understanding of the signaling cascade in
525 *Dictyostelium*. Histidine kinases play essential roles in regulating developmental transitions, with
526 *dhkC*, for example, initiating the late developmental program that ultimately leads to fruiting
527 body formation (Singleton et al., 1998). This function of *dhkC* is regulated in part by ammonia
528 levels, as low ammonia concentrations have been shown to inhibit the *dhkC* phospho-relay,
529 thereby influencing the developmental outcomes (Kirsten et al., 2005). In *Dictyostelium*, several
530 histidine kinases, including *dhkA*, *dhkB*, *dhkC*, and *dokA*, coordinate cAMP signaling to
531 modulate the activity of PKA, a cAMP-dependent protein kinase that is essential for proper
532 development (Anjard and Loomis, 2003). These findings suggest the interdependencies within
533 the signaling network in regulating multicellular development in *Dictyostelium.*

534 **Model of ADGF action**

535 Ammonia generated from multiple sources is likely to be quenched rapidly by the intracellular
536 acidic vesicles of pst cells, increasing its pH and favoring collective cell movement driving
537 mound/ slug tip development. However, the slime sheath at the back of the slug may prevent the
538 diffusion of ammonia, and thus the major route of ammonia emission will be from the slug front
539 (Farnsworth and Loomis, 1974). Although ammonia is likely to be formed from several sources

540 in *Dictyostelium*, a critical threshold concentration of ammonia may be necessary for tip
541 development. The failure of even one pathway may result in a drop-in ammonia levels, exerting
542 an effect on development (Figure 11). Thus, ammonia is likely to be important for the maturation
543 of tip cells.

544 Our study shows that *adgf* acts downstream of *dhkD* and *in silico* studies have shown that *dhkD*
545 interacts with *adgf*. Therefore, it is likely that in the presence of ammonia, *dhkD* activates the
546 phosphorelay, in turn increasing intracellular cAMP levels, leading to tip formation. Histidine
547 kinase *dhkC* is known to phosphorylate *regA* in *Dictyostelium* (Thomason et al.,1999). However,
548 based on docking we found no direct interaction of *regA* with ADGF (data not shown). Thus, the
549 integration of histidine kinase signaling ensures coordinated multicellular organization in
550 *Dictyostelium* (Aoki et al., 2020). Previous work in other systems have found ADA to be
551 interacting with CD 26 (dpp IV) (Tanaka et al., 1993), and docking DdADGF with AprA (dpp8)
552 also supports this observation. However, adding ADA inhibitor to *aprA* mutant (dpp8), showed
553 no effect on the phenotype (data not shown).

554 **Supplementary Results**

555 **Genes involved in autophagy and tipped mound formation do not show altered expression**
556 **in the *adgf* mutant**

557 Autophagy helps in maintaining cellular homeostasis by promoting the breakdown of damaged
558 proteins and organelles (Mizushima et al., 2008), and ammonia is recognised to be a diffusible
559 regulator of autophagy in human cells (Eng et al., 2010). To investigate if autophagy is impaired
560 in the mutant, the expression of autophagy markers *atg8* and *atg18* were examined and there was
561 no discernible change in the expression levels when compared to WT. The tipless to tipped

562 mound transition as well as late developmental gene expression is regulated by *gbf*A, a G-box
563 binding factor (GBF). However, in the *adgf* mutant the *gbf*A expression levels were comparable
564 with no significant difference between the WT at 16 h (data not shown). Without the assay for
565 autophagy as well as assay for GBF activity, these expression studies alone are not conclusive to
566 rule out the role of these factors in tip formation.

567 **ADA does not deaminate cytokinin**

568 ADA is known to interact with 5'AMP (Hanif et al., 2022) and in *Dictyostelium*, 5′-AMP serves
569 as a direct precursor of cytokinin, playing a significant role in cellular signaling and development
570 (Taya et al., 1978). Although docking studies suggest low to moderate binding of ADGF with
571 cytokinins (zeatin, dihydrozeatin, isopentenyl adenine), we carried a functional assay by mixing
572 cytokinin and ADA with KK2 buffer in one side of the Petridish and found no rescue of the
573 mutant in such conditions (data not shown), suggesting no functional activity between ADA and
574 the versions of cytokinin tested.

575 **Supplementary discussion**

576 **Plausible routes of caffeine action rescuing the mound arrest phenotype**

577 The *adgf* mound arrest could be rescued by the addition of the adenosine antagonist, caffeine but
578 treatment with the *pde4* inhibitor, IBMX failed to rescue the mound arrest. Caffeine is known to
579 reduce adenosine levels in blood plasma (Conlay et al., 1988) and also increase ammonium
580 levels in urine samples of rabbits (Bernheim and Bernheim, 1945). Thus, the mound rescue upon
581 caffeine treatment may be a result of reduced adenosine and increased ammonia levels. With
582 respect to caffeine action on cAMP levels, the reports are contradictory. Caffeine has been
583 reported to increase adenylate cyclase expression thereby increasing cAMP levels (Hagmann,
584 1986) whereas Alvarez-Curto et al., (2007) found that caffeine reduced intracellular cAMP levels

585 in *Dictyostelium*. Although, caffeine is moderately potent in inhibiting PDE enzyme activity, the
586 *in vivo* concentrations are likely to be low to be associated with effective PDE inhibition (Burg
587 and Werner, 1975; Daly, 1993).

588 **Material and Methods**

589 **Bioinformatic analyses of ADGF**

590 The genomic sequence and the protein sequence of ADGF were obtained either from dictybase
591 (http://dictybase.org) or NCBI database (https://www.ncbi.nlm.nih.gov/). The ADA domain
592 within the DdADGF was identified by SMART and BLAST (http://smart.embl-heidelberg.de/)
593 (https://blast.ncbi.nlm.nih.gov/Blast.cgi) (Altschul et al., 1990; Letunic and Bork, 2018) analyses.
594 A phylogenetic tree was generated by aligning multiple amino acid sequences of ADGF from
595 several taxa. Neighbour Joining approach and the MUSCLE alignment tool of the MEGAX
596 programme were used for constructing the tree (Saitou and Nei, 1987). The tertiary structure of
597 ADGF was obtained using the online programme alphafold (https://alphafold.ebi.ac.uk/) (Jumper
598 et al., 2021), and PyMol was used for viewing the images. The expression profiles of *ada* and
599 *ada2* during mouse and human gastrula development were retrieved from the
600 marionilab.cruk.cam.ac.uk/MouseGastrulation2018/ and human-gastrula.net/ databases (Pijuan-
601 Sala et al., 2019; Tyser et al., 2021), respectively. Protein-protein docking was carried out using
602 High Ambiguity Driven Protein-Protein Docking (HADOCK) version 2.4.

603 **Culture and development of *Dictyostelium discoideum***

604 *D. discoideum* (WT-AX4) cells or the mutant *adgf* derived from AX4, (DBS0237637) were
605 cultured in modified maltose-HL5 medium (Formedium, UK) with 100,000 U/L penicillin and
606 0.1 g/L streptomycin. Three independent mutants (GWDI_17_D_7, GWDI_47_C_1,
607 GWDI_132_H_3; insertion in exon 2 in all three mutants) of the *adgf* gene (DDB_G0275179)

608 were obtained from the GWDI bank (https://remi-seq.org), in *Dictyostelium* stock centre, North
609 Western University, USA (Gruenheit et al., 2021). The mound defects were identical in all three
610 and strain GWDI_47_C_1 alone was characterised further. The culture was raised as a
611 monolayer in Petri plates or grown in an Erlenmeyer flask in shaking conditions at 150 rpm and
612 22 °C, to a cell density of 2-4x10^6 cells/ml. The cells were also grown on SM/5 agar plates
613 supplemented with *Klebsiella pneumoniae* at 22 °C (2 g/L glucose, 2 g/L protease peptone, 0.4
614 g/L yeast extract, 1 g/L $MgSO_4.H_2O$, 0.66 g/L K_2HPO_4, 2.225 g/L KH_2PO_4, 1% Bactoagar, pH
615 6.4). For developmental assays, freshly starved cells were washed twice with ice cold KK2
616 buffer (2.25 g KH_2PO_4 and 0.67 g K_2HPO_4 per litre, pH 6.4), and plated on 1% non-nutrient
617 KK2 agar plates at a density of 5x10^5 cells/cm^2 (Nassir et al., 2019). Thereafter, the plates were
618 incubated in dark conditions at 22 °C for development.

619 ***Dictyostelium* genomic DNA isolation**

620 WT and *adgf*$^-$ cells grown axenically were harvested, and the pellet was resuspended in 1 ml of
621 lysis buffer (50 mM Tris-Cl, pH 8; 10 mM EDTA; 0.8% SDS). To this mixture, 200 µl of
622 Nonidet P-40 (NP40), a non-ionic detergent, was added, vortexed and centrifuged at 12,000 g for
623 15 min at room temperature (RT). The resultant pellet was gently vortexed, resuspended in 500
624 µl of lysis solution containing 200 µg/ml Proteinase K, and incubated at 65 °C for 30 min. 300 µl
625 of phenol: chloroform was added to this suspension, centrifuged at 18,000 g for 10 min at RT,
626 and the resultant aqueous phase was extracted carefully. An equal amount of chloroform was
627 added and centrifuged at 18,000 g for 10 min at RT. Following this, 750 µl of pure ethanol was
628 added to the suspension, which was then centrifuged at 12,000 g for 15 min at 4 °C. Genomic
629 DNA was precipitated by adding twice the volume of absolute ethanol and 1/10th the volume of 3
630 M sodium acetate. After a 10 min centrifugation at 15,000 g, the pellet was cleaned using 70%

631 ethanol and stored at 4 °C. Electrophoresis was conducted in TAE buffer at 50 V using a Medox
632 power pack system (India), and the integrity of DNA was confirmed on a 1% agarose gel.

633 **Validation of the *adgf* mutant**

634 To validate the blasticidin (*bs*r) resistance cassette insertion in the *adgf* mutant, WT and *adgf*$^-$
635 genomic DNA were isolated, and a diagnostic PCR was performed using the gene and *bsr* insert
636 specific primers in accordance with the guidelines provided in the GWDI website. A qRT-PCR
637 was carried out to confirm the absence of *adgf* expression in the mutant cells. The primers used
638 for mutant validation are listed in Supplementary Table S2.

639 **Quantitative real-time PCR (qRT-PCR)**

640 Total RNA was extracted from WT and *adgf*$^-$ cells using Trizol reagent (Favorgen, USA) at
641 specified intervals (every four hours from 0 to 24 h). cDNA was synthesized from the total RNA
642 using a PrimeScript 1st Strand cDNA Synthesis Kit (Takara, Japan). Random primers from the
643 manufacturer were used to generate the cDNA from a template of 1 µg total RNA. qRT-PCR
644 was performed using SYBR Green Master Mix (Thermo Scientific, USA) and 1 µl of cDNA.
645 The expression levels of *adgf*, *acaA*, cAMP receptor A (*carA*), phosphodiesterases (*pdsA*, *regA*),
646 5' nucleotidase (*5'nt*), extracellular matrix A (*ecmA*), extracellular matrix B (*ecmB*), prespore A
647 (*pspA*), countin (*ctn*), and small aggregate (*smlA*) were quantified with a QuantStudio Flex 7
648 (Applied Biosystems, USA). The mitochondrial large RNA subunit (*rnlA*) served as an internal
649 control. qRT-PCR data analysis was conducted according to the method described by Schmittgen
650 and Livak (2008). The primer sequences used for qRT-PCR are provided in Supplementary
651 Table S4.

652 **Generation of *adgf* over expression construct**

653 The full-length 1.7 kb *adgf* sequence was PCR-amplified using ExTaq polymerase (Takara,
654 Japan) with WT genomic DNA as the template. The amplified product was then ligated into the
655 pDXA-GFP2 vector at the HindIII and KpnI restriction sites. Both *adgf* $^{-}$ and WT cells were
656 electroporated with this vector, and G418-resistant clones (10 µg/ml) were isolated for further
657 analysis. The expression of *adgf* was confirmed by semi-quantitative PCR. The corresponding
658 primer sequences are listed in Supplementary Table S3.

659 **Transformation of *Dictyostelium discoideum***

660 WT and *adgf* $^{-}$ cells grown axenically were harvested, washed twice with ice-cold EP buffer (10
661 mM KH_2PO_4, 10 mM K_2HPO_4, 50 mM sucrose, pH 6.2), and resuspended in 100 µl of EP++
662 solution (10 K_2HPO_4 mM, 10 mM KH_2PO_4, 50 mM sucrose, 1 mM $MgSO_4$, 1 mM $NaHCO_3$, 1
663 mM ATP, 1 µM $CaCl_2$) containing 10 µg of plasmid vector (Nassir et al., 2019) in pre-cooled
664 cuvettes (BioRad, USA). The cells were electroporated using a BTX ECM830 electroporator
665 (Harvard Apparatus, USA) at 300 V with 2 ms pulses and five square wave pulses at 5-second
666 intervals. The cells were then transferred to a Petri dish with 10 ml of HL5 medium and
667 incubated at 22 °C. After 24 hours, G418 (10 µg/ml) was added to the medium, and resistant
668 colonies were selected for further analysis.

669 **Preparation of conditioned media (CM)**

670 WT and *adgf* $^{-}$ cells grown in HL5 medium were collected at the mid-log (ML) phase,
671 resuspended in KK2 buffer at a density of $1x10^7$ cells/ml, and incubated at 22 °C with shaking
672 for 20 hours. The clarified supernatant obtained after centrifugation was used for the experiments.

673 **Assay for ADA activity**

674 Total ADA activity from *Dictyostelium* was determined as per the protocol of the manufacturer

675 (Abcam, USA; Cat No: ab204695). For sample preparation, $5x10^5$ cells/cm^2 were seeded onto
676 KK2 agar plates and at the mound stage, ice cold ADA assay buffer was flooded, then vigorously
677 pipetted to disrupt the mound integrity. The cell homogenate was agitated on a rotary shaker at
678 4 °C for 15 min and then centrifuged at 12,000 rpm for 10 min in a cold microfuge tube. The
679 supernatant was subjected to the ADA assay. This ADA test relies on adenosine to inosine
680 formation. The intermediate formed combines with the probe to produce uric acid, which is
681 quantified at 293 nm. BCA (Bicinchonic acid) assay kit (Thermoscientific, USA) was used for
682 determining the protein concentration. One unit of ADA activity is defined as the amount of
683 enzyme that hydrolyses adenosine to yield 1 μmol of inosine per min under the assay conditions.

684 **Adenosine quantification**

685 Total adenosine levels from *Dictyostelium* mounds were measured according to the
686 manufacturer's protocol, using the adenosine assay kit (Abcam, USA; Cat No: ab211094). Cells
687 grown in HL5 were collected, washed and plated on KK2 agar plates. The cell lysis buffer was
688 added to the plates with mounds and mixed thoroughly. 50 μl of the lysate was mixed with 2 U
689 of ADA and was subjected to incubation for 15 min at RT. Adenosine quantification involves the
690 use of ADA and after a series of enzymatic reactions, an intermediate is formed which reacts
691 with the adenosine probe generating a fluorescent product. Using a spectrofluorometer (Perkin
692 Elmer, USA; λEx = 544 nm/λEm = 590), the fluorescence intensity was measured, which is
693 proportional to the concentration of adenosine. The adenosine levels were quantified using the
694 adenosine standard curve.

695 **Quantification of ammonia**

696 Ammonia assay kit (Sigma-Aldrich, USA; Cat No: AA0100) was used for estimating the total
697 ammonia levels. WT and *adgf* $^-$ cells developed on KK2 agar plates were sealed with parafilm

698 and incubated at 22 °C. The mounds were collected using lysis solution, and the debris was
699 removed by centrifugation at 10,000 g for 10 min. The supernatant was used for further analysis.
700 For the ammonia assay, 1 ml of assay reagent was mixed thoroughly with either 100 µl of
701 samples or standards, incubated for 5 min at RT, and the absorbance was measured at 340 nm.
702 Then, 10 µl of L-glutamate dehydrogenase (GDH) solution was added to each cuvette, and after
703 a 5-min incubation at 25 °C, the absorbance was measured again at 340 nm using a
704 spectrophotometer (Eppendorf, Germany). In the presence of GDH, ammonia combines with α-
705 ketoglutaric acid and reduced NADPH to produce L-glutamate and oxidised $NADP^+$. The
706 decrease in absorbance at 340 nm is proportional to the ammonia concentration. The ammonia
707 standard curve was used to calculate the ammonia levels.

708 **Volatile ammonia generation**

709 To generate ammonia, 1 ml of 1 N NaOH and 1 ml of NH_4Cl (concentrations used 0.1 mM, 1
710 mM, 10 mM) were mixed thoroughly (Thadani et al., 1977; Feit et al., 1990) and from this mix,
711 2 ml was aliquoted in the upper half of the Petri dish. The other half of the plate with the *adgf*$^-$
712 mounds on KK2 agar were inverted, sealed and incubated at 22 °C. To determine whether WT
713 mounds, physically separated from the mutants could rescue the mound arrest, WT ($1x10^6$
714 cells/cm^2) and *adgf*$^-$ ($5x10^5$ cells/cm^2) cells were developed on KK2 agar plates on either side of
715 compartmentalised and sealed Petri plates. *adgf*$^-$ cells developed on either side of the dish
716 served as controls.

717 **Quantification of cAMP**

718 Using the cAMP-XP test kit and following the manufacturer's instructions, total cAMP levels
719 were determined from both the WT and the mutant (Cell signaling, USA). WT and *adgf*$^-$
720 mounds were disrupted and collected in 1 ml ice cold KK2 buffer. After centrifuging the pellet,

721 100 µl of 1X lysis solution was added, and the mixture was incubated in ice for 10 min.
722 Subsequently, 50 µl of lysate and 50 µl of HRP-conjugated cAMP solution were added to the test
723 plates, which were then shaken horizontally at RT. After 3 h incubation, the wells were emptied
724 and washed three times with 200 µl of 1X wash buffer. 100 µl of stop solution was added to halt
725 the reaction, and the absorbance was measured at 450 nm using a spectrophotometer (Biorad,
726 USA). The cAMP standard curve was used to determine the cAMP levels.

727 **Visualisation of cAMP waves using dark field optics**

728 $5x10^5$ cells/cm^2 were developed on KK2 agar plates under moist, dark conditions to monitor the
729 propagation of cAMP waves. Using a Nikon DS-5MC camera mounted on a Nikon SMZ-1000
730 stereo zoom and Nikon Eclipse TE2000 inverted microscope, a time-lapse video of the
731 aggregation was captured in real-time (Nikon, Japan). cAMP optical density waves were
732 displayed by subtracting the image pairs (Siegert and Weijer, 1995) after processing the images
733 with the NIS-Elements D program or ImageJ (NIH, USA).

734 **Under agarose cAMP chemotaxis assay**

735 The under-agarose cAMP chemotaxis assay (Woznica and Knecht, 2006; Singh and Insall, 2022)
736 was carried out with cells obtained from WT and *adgf*$^-$ mounds. Briefly, the cells were starved
737 in KK2 buffer at $1x10^7$ cells/ml density. Three parallel troughs, each measuring 2 mm in width,
738 were set up on a Petri dish containing 1% agarose. In the outer two troughs, 100 µl of WT and
739 *adgf*$^-$ cell suspension was aliquoted respectively and 10 µM cAMP was added to the central
740 trough. Cell migration toward cAMP was recorded every 30 s over a total duration of 20 min
741 using the NIS-Elements D software and an inverted Nikon Eclipse TE2000 microscope (Nikon,
742 Japan). 35 cells were tracked each time and subsequently analysed using ImageJ (NIH, USA).

743 **Mixing WT with mutant cells**

744 WT and *adgf* $^{-}$ cells cultured in HL5 medium, were harvested at the mid log (ML) phase by
745 centrifugation, rinsed twice with ice-cold KK2 buffer. The cells mixed in different ratios (1:9,
746 2:8 and 1:1) were adjusted to a final density of $5x10^5$ cells/cm^2, plated on 1% KK2 agar plates,
747 and incubated at 22 °C for development.

748 **Tracking cell fate after mixing**

749 *Dictyostelium* cells harvested from fresh HL5 media were resuspended at a density of $1x10^6$
750 cells/ml in KK2 buffer, followed by incubation at 22 °C for 1.5 h in shaking conditions with 0.2
751 µM DIL (Invitrogen, USA). DIL has been used extensively as a cell tracker in *C. elegans*,
752 *Xenopus and* mice (Schultz and Gumienny, 2012; Xu et al., 2020; Erdogan et al., 2016). WT or
753 *adgf* $^{-}$ cells labelled with DIL were mixed with the unlabelled cells in a ratio of 1:9, 2:8 and 1:1
754 and plated for development. In the ratios mentioned, the smaller fraction represents the stained
755 cells. DIL is a lipophilic dye that selectively stains the plasma membranes of living cells,
756 allowing visualization and analysis of cell morphology.

757 **Neutral red staining of mounds and slugs**

758 WT and *adgf* $^{-}$ cells harvested from HL5 cultures were resuspended at a density of $1x10^7$ cells
759 per ml in KK2 buffer and treated with 0.005% neutral red (NR) solution for 15 min at RT in
760 shaking conditions (Bonner, 1952). The stained cells were washed twice with KK2 buffer, plated
761 on buffered agar plates and thereafter, NR stained slugs were observed using an upright
762 microscope.

763 **Cell-type specific expression analysis of *adgf***

764 To determine the differential expression of *adgf,* if any, between the two major cell types, psp-
765 GFP cells in AX4 background were developed on KK2 agar plates at a density of 5×10^5
766 cells/cm² until they reached the slug stage, as described by Ratner and Borth (1983).
767 Fluorescence was initially monitored using microscopy to confirm GFP expression. Slugs were
768 then dissociated in 20 mM phosphate buffer containing 40 mM EDTA, pH 7.0 (Nadin et al.,
769 2000), filtered through a 10-µm nylon mesh, chilled on ice, and using FACS (FACS Discover S8
770 Image Sorter (BD Biosciences, USA)) the two cell types were sorted. Sorting was performed at a
771 rate of 10,000 cells/s with a 488 nm laser. GFP-positive prespore (psp) cells and GFP-negative
772 prestalk (pst) cells were collected separately on ice over several hours. Total RNA was extracted
773 from both cell populations, and the expression of *adgf* was analyzed using RT-PCR.

774 **Cell-cell adhesion assay**

775 After 14 h of development on phosphate buffered agar plates, WT and *adgf* $^-$ mounds were
776 disaggregated by repeated pipetting and vortexing using ice-cold KK2 buffer. Dissociated cells
777 were resuspended in KK2 buffer and incubated at 150 rpm for 45 min. Single and non-adherent
778 cells were counted using a Neubauer chamber (Lam et al., 1981).

779 **Treatment of *Dictyostelium* cells with different compounds**

780 A highly specific ADA inhibitor, DCF that inhibits both extra and intra-cellular ADAs (Cha et
781 al., 1975) was mixed with the WT cell suspension and plated on 1% non- nutrient KK2 agar
782 plates at a density of $5x10^5$ cells/cm^2. Of the different DCF concentrations tested (10 nM, 50 nM,
783 100 nM and 1 µM), 100 nM showed complete tip inhibition.

784 For the enzymatic rescue assay, 10 U of bovine ADA dissolved in KK2 buffer (Sigma-Aldrich,
785 USA) was added onto mutant mounds. The concentrations of 8-Br-cAMP (2 mM), cAMP (0.1

786 mM, 0.5 mM), c-di-GMP (0.1 mM, 0.5 mM), adenosine (1 μM, 10 μM, 100 μM, 1 mM),
787 caffeine (10 nM, 100 nM, 1 μM) and IBMX (0.5 mM) were based on previous publications
788 (Chen et al., 2017; Chen and Schaap, 2012; Nassir et al., 2019; Siegert and Weijer, 1989) and
789 these compounds were added independently either on top of the mounds or supplemented while
790 plating. All the fine chemicals were from Sigma-Aldrich, USA except when mentioned.

791 **Microscopy**

792 Microscopy was performed using a Nikon SMZ-1000 stereo zoom microscope with
793 epifluorescence optics, Nikon 80i Eclipse upright microscope, or a Nikon Eclipse TE2000
794 inverted microscope, connected with a digital sight DS-5MC camera (Nikon). Image processing
795 was carried out using NIS-Elements D (Nikon) or Image J.

796 **Statistical tools**

797 Data analyses were carried out using Microsoft Excel (2016). Statistical significance was
798 determined by paired or unpaired, two-tailed Student's t-test and ANOVA analysis (GraphPad
799 Prism, version 7).

800 **Acknowledgements**

801 We gratefully acknowledge the help of NBRP Nenkin, Japan and *Dictyostelium* Stock Center
802 (DSC), Northwestern University, USA for providing various strains and plasmids used in this
803 study. We thank Prof. Richard Gomer, Texas A&M, USA for providing *aprA* mutant strain. We
804 thank Prof. Kei Inouye, Kyoto University, Japan, Prof. Kees Weijer, University of Dundee, UK
805 and Prof. Gad Shaulsky, Baylor College of Medicine USA for their comments on an earlier
806 version of the manuscript/ thesis. We acknowledge Dr. Srividhya, Facility-in-Charge, Flow
807 Cytometry facility, Bio-SAIF, IIT Madras, for assistance with FACS and technical support. We

808 gratefully acknowledge the help from Indian Council of Medical Research (ICMR), New Delhi
809 for their support in this project. We thank Steve Hawthorne from Scholarly memory for his
810 feedback and suggestions on an earlier version of the manuscript.

811 **Author contributions**

812 P.H. and R.B. conceptualized the work. P.H. performed all experiments. P.H. and R.B. analysed
813 the data and wrote the manuscript.

814 **Competing interests**

815 The authors declare no competing interests.

816 **References**

817 Aoki, M. M., Emery, R. J., Anjard, C., Brunetti, C. R., and Huber, R. J. (2020). Cytokinins in
818 *Dictyostelia*–A unique model for studying the functions of signaling agents from species to
819 kingdoms. *Frontiers in Cell and Developmental Biology*, 511.

820 Altschul, S. F., Gish, W., Miller, W., Myers, E. W. and Lipman, D. J. (1990). Basic local
821 alignment search tool. *J. Mol. Biol.* 215, 403–410.

822 Alvarez-Curto, E., Weening, K. E., and Schaap, P. (2007). Pharmacological profiling of the
823 *Dictyostelium* adenylate cyclases ACA, ACB and ACG. *Biochemical Journal*, 401(1), 309-316.

824 Anjard, C., and Loomis, W. F. (2003). Histidine kinases of *Dictyostelium*. In *Histidine Kinases*
825 *in Signal Transduction* (pp. 421-438). Academic Press.

826 Bader, S., Kortholt, A., and Van Haastert, P. J. (2007). Seven *Dictyostelium discoideum*
827 phosphodiesterases degrade three pools of cAMP and cGMP. *Biochemical Journal*, 402(1), 153-
828 161.

829 Bagorda, A., Das, S., Rericha, E. C., Chen, D., Davidson, J., and Parent, C. A. (2009). Real-time
830 measurements of cAMP production in live *Dictyostelium* cells. *Journal of Cell Science*, 122(21),
831 3907-3914.

832 Bernheim, F., and Bernheim, M. L. (1945). Note on the effect of caffeine on ammonia and urea
833 excretion in rabbits. *American Journal of Physiology-Legacy Content*, 145(1), 115-117.

834 Bloom, L., and Kay, R. R. (1988). The search for morphogenes in *Dictyostelium*. *Bioessays*, 9(6),
835 187-191.

836 Bonner, J. T. (1952). Morphogenesis: an essay on development (Vol. 28). Princeton, NJ:
837 Princeton University Press.

838 Bonner, J. T., Suthers, H. B., and Odell, G. M. (1986). Ammonia orients cell masses and speeds
839 up aggregating cells of slime moulds. *Nature*, 323(6089), 630-632.

840 Bonner, J. T., and Hoffman, M. E. (1963). Evidence for a substance responsible for the spacing
841 pattern of aggregation and fruiting in the cellular slime molds. *Development*, 11(3), 571-589.

842 Bradbury, J. M., and Gross, J. D. (1989). The effect of ammonia on cell-type-specific enzyme
843 accumulation in *Dictyostelium discoideum*. *Cell Differentiation and Development*, 27(2), 121-
844 128.

845 Brock, D. A., and Gomer, R. H. (1999). A cell-counting factor regulating structure size in
846 *Dictyostelium*. *Genes and Development*, 13(15), 1960-1969.

847 Brock, D. A., Ehrenman, K., Ammann, R., Tang, Y., and Gomer, R. H. (2003). Two components
848 of a secreted cell number-counting factor bind to cells and have opposing effects on cAMP
849 signal transduction in *Dictyostelium*. *Journal of Biological Chemistry*, 278(52), 52262-52272.

850 Burg, A. W., and Werner, E. (1975). Effect of orally-administered caffeine and theophylline on
851 tissue concentrations of 3', 5'cyclic-amp and phospho-diesterase. *Federation Proceedings,* 34(3),
852 332-332.

853 Carpousis, A. J., Vanzo, N. F., and Raynal, L. C. (1999). mRNA degradation: a tale of poly (A)
854 and multiprotein machines. *Trends in Genetics*, 15(1), 24-28.

855 Carrin, I., Murgia, I., McLachlan, A., and Kay, R. R. (1996). A mutational analysis of
856 *Dictyostelium discoideum* multicellular development. *Microbiology*, 142(4), 993-1003.

857 Cha, S., Agarwal, R. P., and Parks Jr, R. E. (1975). Tight-binding inhibitors—II: Non-steady
858 state nature of inhibition of milk xanthine oxidase by allopurinol and alloxanthine and of human
859 erythrocytic adenosine deaminase by coformycin. *Biochemical Pharmacology*, 24(23), 2187-
860 2197.

861 Chen, Z. H., and Schaap, P. (2012). The prokaryote messenger c-di-GMP triggers stalk cell
862 differentiation in *Dictyostelium*. *Nature*, 488(7413), 680-683.

863 Chen, Z. H., Singh, R., Cole, C., Lawal, H. M., Schilde, C., Febrer, M., Barton, G. J. and Schaap,
864 P. (2017). Adenylate cyclase A acting on PKA mediates induction of stalk formation by cyclic
865 diguanylate at the *Dictyostelium* organizer. *Proceedings of the National Academy of Sciences*
866 *(USA)*, 114(3), 516-521.

867 Chien, S., Chung, C. Y., Sukumaran, S., Osborne, N., Lee, S., Ellsworth, C., Mc Nally, G. Y.,
868 and Firtel, R. A. (2000). The *Dictyostelium* LIM domain-containing protein LIM2 is essential for
869 proper chemotaxis and morphogenesis. *Molecular Biology of the Cell*, *11*(4), 1275-1291.

870 Cristalli, G., Costanzi, S., Lambertucci, C., Lupidi, G., Vittori, S., Volpini, R., and Camaioni, E.
871 (2001). Adenosine deaminase: functional implications and different classes of
872 inhibitors. *Medicinal Research Reviews*, 21(2), 105-128.

873 Coates, J. C., and Harwood, A. J. (2001). Cell-cell adhesion and signal transduction during
874 *Dictyostelium* development. *Journal of Cell Science*, 114(24), 4349-4358.

875 Conlay, L. A., Evoniuk, G., and Wurtman, R. J. (1988). Endogenous adenosine and hemorrhagic
876 shock: effects of caffeine administration or caffeine withdrawal. *Proceedings of the National*
877 *Academy of Sciences (USA)*, 85(12), 4483-4485.

878 Costenla, A. R., Cunha, R. A., and De Mendonça, A. (2010). Caffeine, adenosine receptors, and
879 synaptic plasticity. *Journal of Alzheimer's Disease*, 20(s1), S25-S34.

880 Cotter, D. A., Dunbar, A. J., Buconjic, S. D., and Wheldrake, J. F. (1999). Ammonium
881 phosphate in sori of *Dictyostelium discoideum* promotes spore dormancy through stimulation of
882 the osmosensor ACG. *Microbiology*, 145(8), 1891-1901.

883 Daly, J. W. (1993). Mechanism of action of caffeine. *Caffeine, coffee, and health*, 97-150. Raven
884 press.

885 Davies, L., Satre, M., Martin, J. B., and Gross, J. D. (1993). The target of ammonia action in
886 *Dictyostelium*. *Cell*, 75(2), 321-327.

887 Dolezal, T., Dolezelova, E., Zurovec, M., and Bryant, P. J. (2005). A role for adenosine
888 deaminase in *Drosophil*a larval development. *PLoS Biology*, 3(7), e201.

889 Eichinger, L et al., (2005). The genome of the social amoeba *Dictyostelium discoideum*. *Nature*.
890 435(7038):43-57.

891 Eidhammer, I., Jonassen, I., and Taylor, W. R. (2000). Structure comparison and structure
892 patterns. *Journal of Computational Biology*, *7*(5), 685-716.

893 Eng, C. H., Yu, K., Lucas, J., White, E., and Abraham, R. T. (2010). Ammonia derived from
894 glutaminolysis is a diffusible regulator of autophagy. *Science signaling*, 3(119).

895 Erdogan, B., Ebbert, P. T., and Lowery, L. A. (2016). Using *Xenopus laevis* retinal and spinal
896 neurons to study mechanisms of axon guidance in vivo and in vitro. *Seminars in Cell and*
897 *Developmental Biology,* 51, 64-72. Academic Press. USA.

898 Farnsworth, P. (1973). Morphogenesis in the cellular slime mould *Dictyostelium discoideum*; the
899 formation and regulation of aggregate tips and the specification of developmental axes.
900 *Development,* 29(2), 253-266.

901 Farnsworth, P. A., and Loomis, W. F. (1974). A barrier to diffusion in pseudoplasmodia of
902 *Dictyostelium discoideum*. *Developmental Biology*, 41(1), 77-83.

903 Feit, I. N. (1988). Ammonia can stimulate or inhibit aggregate density in *Dictyostelium*
904 *mucoroides*: A quantitative test of the hypothesis that ammonia is the aggregation-suppressing
905 gas. *Developmental Genetics*, 9(4-5), 639-652.

906 Feit, I. N., Bonner, J. T., and Suthers, H. B. (1990). Regulation of the anterior-like cell state by
907 ammonia in *Dictyostelium discoideum*. *Developmental Genetics*, 11(5-6), 442-446.

908 Feit, I. N., Medynski, E. J., and Rothrock, M. J. (2001). Ammonia differentially suppresses the
909 cAMP chemotaxis of anterior-like cells and prestalk cells in *Dictyostelium discoideum*. *Journal*
910 *of Biosciences*, 26, 157-166.

911 Felsenstein, J. (1985). Confidence limits on phylogenies: an approach using the
912 bootstrap. *Evolution*, 39(4), 783-791.

913 Firtel, R. A. (1996). Interacting signaling pathways controlling multicellular development in
914 *Dictyostelium*. *Current Opinion in Genetics and Development*, 6(5), 545-554.

915 Follstaedt, S. C., Kirsten, J. H., and Singleton, C. K. (2003). Temporal and spatial expression of
916 ammonium transporter genes during growth and development of *Dictyostelium*
917 *discoideum. Differentiation*, 71(9-10), 557-566.

918 Gaspar, H. B. (2010). Bone marrow transplantation and alternatives for adenosine deaminase
919 deficiency. *Immunology and Allergy Clinics*, 30(2), 221-236.

920 Gee, K., Russell, F., and Gross, J. D. (1994). Ammonia hypersensitivity of slugger mutants of *D.*
921 *discoideum*. *Journal of Cell Science*, 107(2), 701-708.

922 Godecke, A. (2008). cAMP: fuel for extracellular adenosine formation? *British Journal of*
923 *Pharmacology*, 153(6), 1087-1089.

924 Gruenheit, N. et al., (2021). Mutant resources for functional genomics in *Dictyostelium*
925 *discoideum* using REMI-seq technology. *BMC Biology*, 19(1), 172.

926 Gross, J. D., Bradbury, J., Kay, R. R., and Peacey, M. J. (1983). Intracellular pH and the control
927 of cell differentiation in *Dictyostelium discoideum*. *Nature*, 303(5914), 244-245.

928 Gross, J. D., Peacey, M. J., and Von Strandmann, R. P. (1988). Plasma membrane proton
929 pump inhibition and stalk cell differentiation in *Dictyostelium discoideum*. *Differentiation*,
930 38(2), 91-98.

931 Gross, J. D. (1994). Developmental decisions in *Dictyostelium discoideum*.
932 *Microbiological Reviews*, 58(3), 330-351.

933 Gross, J. D. (2009). Acidic Ca2+ stores, excitability, and cell patterning in *Dictyostelium*
934 *discoideum*. *Eukaryotic Cell*, 8(5), 696-702.

935 Hagmann, J. (1986). Caffeine and heat shock induce adenylate cyclase in *Dictyostelium*
936 *discoideum*. *The EMBO Journal*, 5(13), 3437-3440.

937 Hames, B. D., and Ashworth, J. M. (1974). The metabolism of macromolecules during the
938 differentiation of myxamoebae of the cellular slime mould *Dictyostelium discoideum* containing
939 different amounts of glycogen. *Biochemical Journal*, 142(2), 301-315.

940 Hanif, M. A., Hossen, S., Cho, Y., Sukhan, Z. P., Choi, C. Y., and Kho, K. H. (2022).
941 Characterization and expression analysis of mollusk-like growth factor: A secreted protein
942 involved in Pacific abalone embryonic and larval development. *Biology*, 11(10), 1445.

943 Harrison, M. J. (2005). signaling in the arbuscular mycorrhizal symbiosis. *Annu. Rev. Microbiol*.,
944 59, 19-42.

945 Headrick, J. P., and Willis, R. J. (1989). 5' -Nucleotidase activity and adenosine formation in
946 stimulated, hypoxic and underperfused rat heart. *Biochemical Journal*, 261(2), 541-550.

947 Helgason, T., Daniell, T. J., Husband, R., Fitter, A. H., and Young, J. P. W. (1998). Ploughing up
948 the wood-wide web. *Nature*, 394(6692), 431-431.

949 Hiraoka, H., Wang, J., Nakano, T., Hirano, Y., Yamazaki, S., Hiraoka, Y., and Haraguchi, T.
950 (2022). ATP levels influence cell movement during the mound phase in *Dictyostelium*
951 *discoideum* as revealed by ATP visualization and simulation. *FEBS Open bio*, 12(11), 2042-2056.

952 Honorato, R. V., Koukos, P. I., Jiménez-García, B., Tsaregorodtsev, A., Verlato, M., Giachetti,
953 A., Rosato, A., and Bonvin, A. M. (2021). Structural biology in the clouds: the WeNMR-EOSC
954 ecosystem. *Frontiers in Molecular Biosciences*, 8, 729513.

955 Honorato, R. V., Trellet, M. E., Jiménez-García, B., Schaarschmidt, J. J., Giulini, M., Reys, V.,
956 Koukos, P. I., Rodrigues, J. P. G. L. M., Karaca, E., van Zundert, G. C. P., Roel-Touris, J., van
957 Noort, C. W., Jandova, Z., Melquiond, A. S. J., and Bonvin, A. M. (2024). The HADDOCK2. 4
958 web server for integrative modeling of biomolecular complexes. *Nature Protocols*, 1-23.

959 Huber, R. J., Williams, R. S., and Müller-Taubenberger, A. (2022). *Dictyostelium*: A Tractable
960 Cell and Developmental Model in Biomedical Research. *Frontiers in Cell and Developmental*
961 *Biology*, 10, 909619.

962 Iijima, R., Kunieda, T., Yamaguchi, S., Kamigaki, H., Fujii-Taira, I., Sekimizu, K., Kubo, T.,
963 Natori, S., Homma, K. J. (2008). The extracellular adenosine deaminase growth factor,
964 ADGF/CECR1, plays a role in *Xenopus* embryogenesis via the adenosine/P1 receptor. *J Biol*
965 *Chem*. 283(4):2255–2264.

966 Inouye, K. (1989). Control of cell type proportions by a secreted factor in *Dictyostelium*
967 *discoideum*. *Development*, 107(3), 605-609.

968 Jaiswal, P., Soldati, T., Thewes, S., and Baskar, R. (2012). Regulation of aggregate size and
969 pattern by adenosine and caffeine in cellular slime molds. *BMC Developmental Biology*, *12*, 1-19.

970 Jang, W., and Gomer, R. H. (2011). Initial cell type choice in *Dictyostelium*. Eukaryotic Cell,
971 10(2), 150-155.

972 Jumper, J et. al., (2021). Highly accurate protein structure prediction with
973 alphafold. *Nature*, 596(7873), 583-589.

974 Kay, R. R., Tilly, R., and Garrod, D. (1978). Requirement for cell differentiation in
975 *Dictyostelium discoideum*. *Nature*, 271(5640), 58-60.

976 Kellerman, K. A., and McNally, J. G. (1999). Mound-Cell Movement and Morphogenesis in
977 *Dictyostelium*. *Developmental Biology*, *208*(2), 416-429.

978 Kessin, R. H. (2001). *Dictyostelium*: evolution, cell biology, and the development of
979 multicellularity (Vol. 38). Cambridge University Press.

980 Khachatrian, L., Klein, C., and Howlett, A. (1987). Regulation of *Dictyostelium discoideum*
981 adenylate cyclase by manganese and adenosine analogs. *Biochimica et Biophysica Acta (BBA)-*
982 *Molecular Cell Research*, 927(2), 235-246.

983 Kirsten, J. H., Xiong, Y., Dunbar, A. J., Rai, M., and Singleton, C. K. (2005). Ammonium
984 transporter C of *Dictyostelium discoideum* is required for correct prestalk gene expression and
985 for regulating the choice between slug migration and culmination. *Developmental*
986 *Biology*, 287(1), 146-156.

987 Koehl, P. (2001). Protein structure similarities. *Current Opinion in Structural Biology*, 11(3),
988 348-353.

989 Konijn, T. M., Van De Meene, J. G., Bonner, J. T., and Barkley, D. S. (1967). The acrasin
990 activity of adenosine-3', 5'-cyclic phosphate. *Proceedings of the National Academy of Sciences*
991 *(USA)*, 58(3), 1152-1154.

992 Kosugi, T., and Inouye, K. (1989). Negative chemotaxis to ammonia and other weak bases by
993 migrating slugs of the cellular slime moulds. *Microbiology*, 135(6), 1589-1598.

994 Kumar, S., Stecher, G., Li, M., Knyaz, C., and Tamura, K. (2018). MEGA X: molecular
995 evolutionary genetics analysis across computing platforms. *Molecular Biology and*
996 *Evolution*, 35(6), 1547.

997 Lam, T., Pickering, G., Geltosky, J., and Siu, C. H. (1981). Differential cell cohesiveness
998 expressed by prespore and prestalk cells of *Dictyostelium discoideum*. *Differentiation*, *20*(1-3),
999 22-28.

1000 Lane, M., and Gardner, D. K. (2003). Ammonium induces aberrant blastocyst differentiation,
1001 metabolism, pH regulation, gene expression and subsequently alters fetal development in the
1002 mouse. *Biology of Reproduction*, 69(4), 1109-1117.

1003 Letunic, I., and Bork, P. (2018). 20 years of the SMART protein domain annotation
1004 resource. *Nucleic Acids Research*, 46(D1), D493-D496.

1005 Li, S., and Aksoy, S. (2000). A family of genes with growth factor and adenosine deaminase
1006 similarity are preferentially expressed in the salivary glands of *Glossina m. morsitans*. *Gene*,
1007 252(1-2), 83-93.

1008 Lipkowski, J., and Galus, Z. (1973). Electrode kinetics in mixed solvents Investigations of the
1009 kinetics and equilibrium properties of manganese (II)—ammonia complexes in water and mixed

1010 solvents of n-propanol, isopropanol, t-butanol and water. *Journal of Electroanalytical Chemistry*
1011 *and Interfacial Electrochemistry*, 48(3), 337-352.

1012 Liu, Y., Zhang, X., Wang, W., Liu, T., Ren, J., Chen, S., Lu, T., Yuan, X., Mo, F., Yang, J, Wei,
1013 Y., and Wei, X. (2022). Ammonia promotes the proliferation of bone marrow-derived
1014 mesenchymal stem cells by regulating the Akt/mTOR/S6k pathway. *Bone Research*, 10(1), 57.

1015 Lonski, J. (1976). The effect of ammonia on fruiting body size and microcyst formation in the
1016 cellular slime molds. *Developmental Biology*, 51(1), 158-165.

1017 Loomis, W. F., Klein, C., and Bracket, P. (1979). The effect of divalent cations on aggregation of
1018 *Dictyostelium discoideum*. *Differentiation*, 12(1-3), 83-89.

1019 Lu, J., Li, Y., Zhang, C., Yang, X., and Qiang, J. W. (2020). Interaction of manganese and
1020 ammonia in the brain of hepatic encephalopathy rats. *Hepatitis Monthly*, 20(8).

1021 Mahadeo, D. C., and Parent, C. A. (2006). Signal relay during the life cycle of
1022 *Dictyostelium*. *Current topics in Developmental Biology*, *73*, 115-140.

1023 Maier, S. A., Galellis, J. R., and McDermid, H. E. (2005). Phylogenetic analysis reveals a novel
1024 protein family closely related to adenosine deaminase. *Journal of Molecular Evolution*, 61, 776-
1025 794.

1026 Mann, S. K., and Firtel, R. A. (1993). cAMP-dependent protein kinase differentially regulates
1027 prestalk and prespore differentiation during *Dictyostelium* development. *Development*, *119*(1),
1028 135-146.

1029 Marone, G., Plaut, M., and Lichtenstein, L. M. (1980). The role of adenosine in the control of
1030 immune function. *Ricerca in clinica e in laboratorio*., 10(2), 303-312.

1031 Martín-González, J., Montero-Bullón, J. F., and Lacal, J. (2021). *Dictyostelium discoideum* as a
1032 non-mammalian biomedical model. *Microbial Biotechnology*, 14(1), 111-125.

1033 Meinhardt, H. (1983). A model for the prestalk/prespore patterning in the slug of the slime
1034 mold *Dictyostelium discoideum*. *Differentiation*, 24(1-3), 191-202.

1035 Mizushima, N., Levine, B., Cuervo, A. M., and Klionsky, D. J. (2008). Autophagy fights disease
1036 through cellular self-digestion. *Nature*, 451(7182), 1069-1075.

1037 Moreno, E., Canet, J., Gracia, E., Lluís, C., Mallol, J., Canela, E. I., Cortés. A. and Casadó, V.
1038 (2018). Molecular Evidence of Adenosine Deaminase Linking Adenosine A2A Receptor and
1039 CD26 Proteins. *Frontiers in Pharmacology*, 9, 106.

1040 Müller-Taubenberger, A., Kortholt, A., and Eichinger, L. (2013). Simple system–substantial
1041 share: the use of *Dictyostelium* in cell biology and molecular medicine. *European Journal of Cell*
1042 *Biology*, 92(2), 45-53.

1043 Nadin, B. M., Mah, C. S., Scharff, J. R., and Ratner, D. I. (2000). The regulative capacity of
1044 prespore amoebae as demonstrated by fluorescence-activated cell sorting and green fluorescent
1045 protein. *Developmental Biology*, 217(1), 173-178.

1046 Nassir, N., Hyde, G. J., and Baskar, R. (2019). A telomerase with novel non-canonical roles:
1047 TERT controls cellular aggregation and tissue size in *Dictyostelium*. *PLoS Genetics*, *15*(6),
1048 e1008188.

1049 Neave, N., Sobolewski, A., and Weeks, G. (1983). The effect of ammonia on stalk cell formation
1050 in submerged monolayers of *Dictyostelium discoideum*. *Cell Differentiation*, 13(4), 301-307.

1051 Needham, J. (1926). The energy-sources in ontogenesis: III. The ammonia content of the
1052 developing avian egg and the theory of recapitulation. *Journal of Experimental Biology*, 4(2),
1053 145-154.

1054 Newell, P. C., Telser, A., and Sussman, M. (1969). Alternative developmental pathways
1055 determined by environmental conditions in the cellular slime mold *Dictyostelium*
1056 *discoideum*. *Journal of Bacteriology*, 100(2), 763-768.

1057 Newell, P. C. (1982). Cell surface binding of adenosine to *Dictyostelium* and inhibition of
1058 pulsatile signaling. *FEMS Microbiology Letters*, 13(4), 417-421.

1059 Notarangelo, L. D. (2016). T cell immunodeficiencies. *Paediatric Allergy, E-Book: Principles*
1060 *and Practice*, 80-89.

1061 Otto, G. P., Wu, M. Y., Kazgan, N., Anderson, O. R., and Kessin, R. H. (2003). Macroautophagy
1062 is required for multicellular development of the social amoeba *Dictyostelium discoideum*.
1063 *Journal of Biological Chemistry*, 278(20), 17636-17645.

1064 Otto, G. P., Wu, M. Y., Clarke, M., Lu, H., Anderson, O. R., Hilbi, H., Shuman, H, A and Kessin,
1065 R. H. (2004). Macroautophagy is dispensable for intracellular replication of *Legionella*
1066 *pneumophila* in *Dictyostelium discoideum*. *Molecular Microbiology*, *51*(1), 63-72.

1067 Oyama, M., and Blumberg, D. D. (1986). Cyclic AMP and $NH_3/NH^+{}_4$ both regulate cell-type-
1068 specific mRNA accumulation in the cellular slime mold, *Dictyostelium*
1069 *discoideum*. *Developmental Biology*, 117(2), 557-566.

1070 Palsson, E., and Cox, E. C. (1996). Origin and evolution of circular waves and spirals in
1071 *Dictyostelium discoideum* territories. *Proceedings of the National Academy of Sciences (USA)*,
1072 93(3), 1151-1155.

1073 Pijuan-Sala, B., Griffiths, J. A., Guibentif, C., Hiscock, T. W., Jawaid, W., Calero-Nieto, F. J.,
1074 Mulas, C., Ibarra-Soria, X., Tyser, R. C. V, Ho, D. L. L., Reik, W., Srinivas, S., Simons, D. B.,
1075 Nichols, J., Marioni, J.C., and Göttgens, B. (2019). A single-cell molecular map of mouse
1076 gastrulation and early organogenesis. *Nature*, 566(7745), 490-495.

1077 Raper, K. B. (1940). Pseudoplasmodium formation and organization in *Dictyostelium*
1078 discoideum. *Journal of the Elisha Mitchell Scientific Society*, 56(2), 241-282.

1079 Riazi, A. M., Arsdell, G. V., and Buchwald, M. (2005). Transgenic expression of CECR1
1080 adenosine deaminase in mice results in abnormal development of heart and kidney. *Transgenic*
1081 *Research*, 14, 333-336.

1082 Ribeiro, J. A., and Sebastiao, A. M. (2010). Caffeine and adenosine. *Journal of Alzheimer's*
1083 *Disease*, 20(s1), S3-S15.

1084 Riley, B. B., and Barclay, S. L. (1990). Ammonia promotes accumulation of intracellular cAMP
1085 in differentiating amoebae of *Dictyostelium discoideum*. *Development*, 109(3), 715-722.

1086 Rivera-Mancía, S., Ríos, C., and Montes, S. (2012). Manganese and ammonia interactions in the
1087 brain of cirrhotic rats: effects on brain ammonia metabolism. *Neurochemical Research*, 37,
1088 1074-1084.

1089 Roisin-Bouffay, C., Jang, W., Caprette, D. R., and Gomer, R. H. (2000). A precise group size in
1090 *Dictyostelium* is generated by a cell-counting factor modulating cell–cell adhesion. *Molecular*
1091 *Cell*, 6(4), 953-959.

1092 Rubin, J., and Robertson, A. (1975). The tip of the *Dictyostelium discoideum* pseudoplasmodium
1093 as an organizer. *Development*, 33(1), 227-241.

1094 Saitou, N., and Nei, M. (1987). The neighbor-joining method: a new method for reconstructing
1095 phylogenetic trees. *Molecular Biology and Evolution*, 4(4), 406-425.

1096 Saxe, C. 3., Ginsburg, G. T., Louis, J. M., Johnson, R., Devreotes, P. N., and Kimmel, A. R.
1097 (1993). CAR2, a prestalk cAMP receptor required for normal tip formation and late development
1098 of *Dictyostelium discoideum*. *Genes and Development*, 7(2), 262-272.

1099 Schaap, P., Brandt, R., and van Es, S. (1995). Regulation of *Dictyostelium* adenylylcyclases by
1100 morphogen-induced modulation of cytosolic pH or Ca^{2+} levels. *Developmental Biology*, 168(1),
1101 179-188.

1102 Schaap, P., and Wang, M. (1986). Interactions between adenosine and oscillatory cAMP
1103 signaling regulate size and pattern in *Dictyostelium*. *Cell*, 45(1), 137-144.

1104 Schindler, J., and Sussman, M. (1977). Ammonia determines the choice of morphogenetic
1105 pathways in *Dictyostelium discoideum*. *Journal of Molecular Biology*, 116(1), 161-169.

1106 Schindler, J., and Sussman, M. (1979). Inhibition by ammonia of intracellular cAMP
1107 accumulation in *Dictyostelium discoideum*: its significance for the regulation of
1108 morphogenesis. *Developmental Genetics*, 1(1), 13-20.

1109 Schmittgen, T. D., and Livak, K. J. (2008). Analyzing real-time PCR data by the comparative CT
1110 method. *Nature protocols*, 3(6), 1101-1108.

1111 Schulz-Bohm, K., Martín-Sánchez, L., and Garbeva, P. (2017). Microbial volatiles: small
1112 molecules with an important role in intra and inter-kingdom interactions. *Frontiers in*
1113 *Microbiology*, 8, 289291.

1114 Schultz, R. D., and Gumienny, T. L. (2012). Visualization of *Caenorhabditis elegans* cuticular
1115 structures using the lipophilic vital dye DiI. *Journal of Visualized Experiments*, (59), e3362.

1116 Siegert, F., and Weijer, C. (1989). Digital image processing of optical density wave propagation
1117 in *Dictyostelium discoideum* and analysis of the effects of caffeine and ammonia. *Journal of Cell*
1118 *Science*, 93(2), 325-335.

1119 Siegert, F., and Weijer, C. J. (1995). Spiral and concentric waves organize multicellular
1120 *Dictyostelium* mounds. *Current Biology*, 5(8), 937-943.

1121 Singer, G., Araki, T., and Weijer, C. J. (2019). Oscillatory cAMP cell-cell signaling persists
1122 during multicellular *Dictyostelium* development. *Communications Biology*, *2*(1), 139.

1123 Singh, S. P., and Insall, R. H. (2022). Under-Agarose Chemotaxis Chemotaxis and Migration
1124 Assays for *Dictyostelium*. In *Cell Polarity Signaling: Methods and Protocols* (pp. 467-482). New
1125 York, NY: Springer US.

1126 Singleton, C. K., Zinda, M. J., Mykytka, B., and Yang, P. (1998). The histidine kinase dhkC
1127 regulates the choice between migrating slugs and terminal differentiation in *Dictyostelium*
1128 *discoideum*. *Developmental Biology*, 203(2), 345-357.

1129 Singleton, C. K., Kirsten, J. H., and Dinsmore, C. J. (2006). Function of ammonium transporter
1130 A in the initiation of culmination of development in *Dictyostelium discoideum*. *Eukaryotic*
1131 *Cell*, 5(7), 991-996.

1132 Singleton, C. K., and Xiong, Y. (2013). Loss of the histidine kinase DhkD results in mobile
1133 mounds during development of *Dictyostelium discoideum*. *Plos One*, 8(9), e75618.

1134 Siu, C. H., Lam, T. Y., and Choi, A. H. (1985). Inhibition of cell-cell binding at the aggregation
1135 stage of *Dictyostelium discoideum* development by monoclonal antibodies directed against an
1136 80,000-dalton surface glycoprotein. *Journal of Biological Chemistry*, 260(29), 16030-16036.

1137 Steer, M. L. (1975). Adenyl cyclase. *Annals of Surgery*, 182(5), 603.

1138 Stege, J. T., Laub, M. T., and Loomis, W. F. (1999). Tip genes act in parallel pathways of early
1139 *Dictyostelium* development. *Developmental Genetics*, 25(1), 64-77.

1140 Stein, L. Y., Campbell, M. A., and Klotz, M. G. (2013). Energy-mediated vs. ammonium-
1141 regulated gene expression in the obligate ammonia-oxidizing bacterium, *Nitrosococcus oceani*.
1142 *Frontiers in Microbiology*, 4, 277.

1143 Sternfeld, J., and David, C. N. (1979). Ammonia plus another factor are necessary for
1144 differentiation in submerged clumps of *Dictyostelium*. *Journal of Cell Science*, 38(1), 181-191.

1145 Sternfeld, J., and David, C. N. (1982). Fate and regulation of anterior-like cells in *Dictyostelium*
1146 slugs. *Developmental Biology*, 93(1), 111-118.

1147 Tanaka, T., Kameoka, J., Yaron, A., Schlossman, S. F., and Morimoto, C. (1993). The
1148 costimulatory activity of the CD26 antigen requires dipeptidyl peptidase IV enzymatic activity.
1149 *Proceedings of the National Academy of Sciences (USA)*, 90(10), 4586-4590.

1150 Taya, Y., Tanaka, Y., and Nishimura, S. (1978). 5′-AMP is a direct precursor of cytokinin in
1151 *Dictyostelium discoideum*. *Nature*, 271(5645), 545-547.

1152 Thadani, V., Pan, P., and Bonner, J. T. (1977). Complementary effects of ammonia and cAMP
1153 on aggregation territory size in the cellular slime mold *Dictyostelium mucoroides*. *Experimental*
1154 *Cell Research*, 108(1), 75-78.

1155 Theibert, A., and Devreotes, P. N. (1984). Adenosine and its derivatives inhibit the cAMP
1156 signaling response in *Dictyostelium discoideum*. *Developmental Biology*, 106(1), 166-173.

1157 Thomason, P., Traynor, D., and Kay, R. (1999). Taking the plunge: terminal differentiation in
1158 *Dictyostelium*. *Trends in Genetics*, 15(1), 15-19.

1159 Torija, P., Vicente, J. J., Rodrigues, T. B., Robles, A., Cerdán, S., Sastre, L., Martínez, P., and
1160 Escalante, R. (2006). Functional genomics in *Dictyostelium*: MidA, a new conserved protein, is
1161 required for mitochondrial function and development. *Journal of Cell Science*, 119(6), 1154-
1162 1164.

1163 Traynor, D., Kessin, R. H., and Williams, J. G. (1992). Chemotactic sorting to cAMP in the
1164 multicellular stages of *Dictyostelium* development. *Proceedings of the National Academy of*
1165 *Sciences (USA)*, 89(17), 8303-8307.

1166 Tung, S. M., Ünal, C., Ley, A., Peña, C., Tunggal, B., Noegel, A. A., Krut, O., Steinert, M., and
1167 Eichinger, L. (2010). Loss of *Dictyostelium* ATG9 results in a pleiotropic phenotype affecting
1168 growth, development, phagocytosis and clearance and replication of *Legionella pneumophila*.
1169 *Cellular Microbiology*, 12(6), 765-780.

1170 Tyser, R. C., Mahammadov, E., Nakanoh, S., Vallier, L., Scialdone, A., and Srinivas, S. (2021).
1171 Single-cell transcriptomic characterization of a gastrulating human embryo. *Nature*, 600(7888),
1172 285-289.

1173 Tzertzinis, G., Ganatra, M. B., Ruse, C., Taron, C. H., Causey, B., Wang, L., and Schildkraut, I.
1174 (2023). The AMP deaminase of the mollusk *Helix pomatia* is an unexpected member of the
1175 adenosine deaminase-related growth factor (ADGF) family. *PloS One*, 18(7), e0286435.

1176 Ubeidat, M., Eristi, C. M., and Rutherford, C. L. (2002). Expression pattern of 5′-nucleotidase in
1177 *Dictyostelium*. *Mechanisms of Development*, *110*(1-2), 237-239.

1178 Van Haastert, P. J. (1983). Binding of cAMP and adenosine derivatives to *Dictyostelium*
1179 *discoideum* cells. Relationships of binding, chemotactic, and antagonistic activities. *Journal of*
1180 *Biological Chemistry*, 258(16), 9643-9648.

1181 Wakamiya, M., Blackburn, M. R., Jurecic, R., McArthur, M. J., Geske, R. S., Cartwright Jr, J.,
1182 and Kellems, R. E. (1995). Disruption of the adenosine deaminase gene causes hepatocellular
1183 impairment and perinatal lethality in mice. *Proceedings of the National Academy of Sciences*
1184 *(USA)*, 92(9), 3673-3677.

1185 Walsh, J., and Wright, B. E. (1978). Kinetics of net RNA degradation during development in
1186 *Dictyostelium discoideum*. *Microbiology*, 108(1), 57-62.

1187 Wang, B., and Kuspa, A. (2002). CulB, a putative ubiquitin ligase subunit, regulates prestalk cell
1188 differentiation and morphogenesis in *Dictyostelium* spp. *Eukaryotic Cell*, 1(1), 126-136.

1189 Wang, M., and Schaap, P. (1985). Correlations between tip dominance, prestalk/prespore pattern,
1190 and cAMP-relay efficiency in slugs of *Dictyostelium discoideum*. *Differentiation*, 30(1), 7-14.

1191 Wang, M., and Schaap, P. (1989). Ammonia depletion and DIF trigger stalk cell differentiation
1192 in intact *Dictyostelium discoideum* slugs. *Development*, 105(3), 569-574.

1193 Weeks, G., and Weijer, C. J. (1994). The *Dictyostelium* cell cycle and its relationship to
1194 differentiation. *FEMS Microbiology Letters*, 124(2), 123-130.

1195 Weijer, C. J. (2009). Collective cell migration in development. *Journal of Cell Science*, 122(18),
1196 3215-3223.

1197 Weijer, C. J., and Durston, A. J. (1985). Influence of cyclic AMP and hydrolysis products on cell
1198 type regulation in *Dictyostelium discoideum*. *Development*, 86(1), 19-37.

1199 White, G. J., and Sussman, M. (1961). Metabolism of major cell components during slime mold
1200 morphogenesis. *Biochimica et biophysica acta*, 53(2), 285-293.

1201 Wiechetek, M., Breves, G., and Höller, H. (1979). The effect of ammonium ion concentration on
1202 the activity of adenylate cyclase in various rat tissues in vitro. *Quarterly Journal of Experimental*
1203 *Physiology and Cognate Medical Sciences: Translation and Integration*, 64(3), 169-174.

1204 Williams, G. B., Elder, E. M., and Sussman, M. (1984). Modulation of the cAMP relay in
1205 *Dictyostelium discoideum* by ammonia and other metabolites: possible morphogenetic
1206 consequences. *Developmental Biology*, 105(2), 377-388.

1207 Williams, J. G. (1988). The role of diffusible molecules in regulating the cellular differentiation
1208 of *Dictyostelium discoideum*. *Development*, 103(1), 1-16.

1209 Williams, J. G. (2006). Transcriptional regulation of *Dictyostelium* pattern formation. *EMBO*
1210 *Reports*, 7(7), 694-698.

1211 Williams, J. G., Duffy, K. T., Lane, D. P., McRobbie, S. J., Harwood, A. J., Traynor, D., Kay, R.
1212 R. and Jermyn, K. A. (1989). Origins of the prestalk-prespore pattern in *Dictyostelium*
1213 development. *Cell*. 59(6), 1157–1163.

1214 Xu, J., Wang, X., Chen, J., Chen, S., and Li, Z., Liu, H., Bai, Y and Zhi, F. (2020). Embryonic
1215 stem cell-derived mesenchymal stem cells promote colon epithelial integrity and regeneration by
1216 elevating circulating IGF-1 in colitis mice. *Theranostics,* 10(26), 12204.

1217 Yamada, T. (1950). Dorsalization of the ventral marginal zone of the *Triturus* gastrula. I.
1218 Ammonia-treatment of the medio-ventral marginal zone. *The Biological bulletin*, 98(2), 98-121.

1219 Yeung, S. M. H., Shoshani, I., Stübner, D., and Johnson, R. A. (1989). Ammonium ions enhance
1220 proteolytic activation of adenylate cyclase and decrease its sensitivity to inhibition by "P"-site
1221 agonists. *Archives of Biochemistry and Biophysics*, 271(2), 332-345.

1222 Yoshino, R., Morio, T., Yamada, Y., Kuwayama, H., Sameshima, M., Tanaka, Y., Sesaki, H.,
1223 and Iijima, M. (2007). Regulation of ammonia homeostasis by the ammonium transporter AmtA
1224 in *Dictyostelium discoideum*. *Eukaryotic Cell*, 6(12), 2419-2428.

1225 Zavialov, A. V., Yu, X., Spillmann, D., Lauvau, G., and Zavialov, A. V. (2010). Structural basis
1226 for the growth factor activity of human adenosine deaminase ADA2. *Journal of Biological*
1227 *Chemistry*, 285(16), 12367-12377.

1228 Zhou, Q et al. (2014). Early-onset stroke and vasculopathy associated with mutations in
1229 ADA2. *New England Journal of Medicine*, 370(10), 911-920.

1230 Zurovec, M., Dolezal, T., Gazi, M., Pavlova, E., and Bryant, P. J. (2002). Adenosine deaminase-
1231 related growth factors stimulate cell proliferation in *Drosophila* by depleting extracellular
1232 adenosine. *Proceedings of the National Academy of Sciences (USA)* 99(7), 4403-4408.

Figure 1

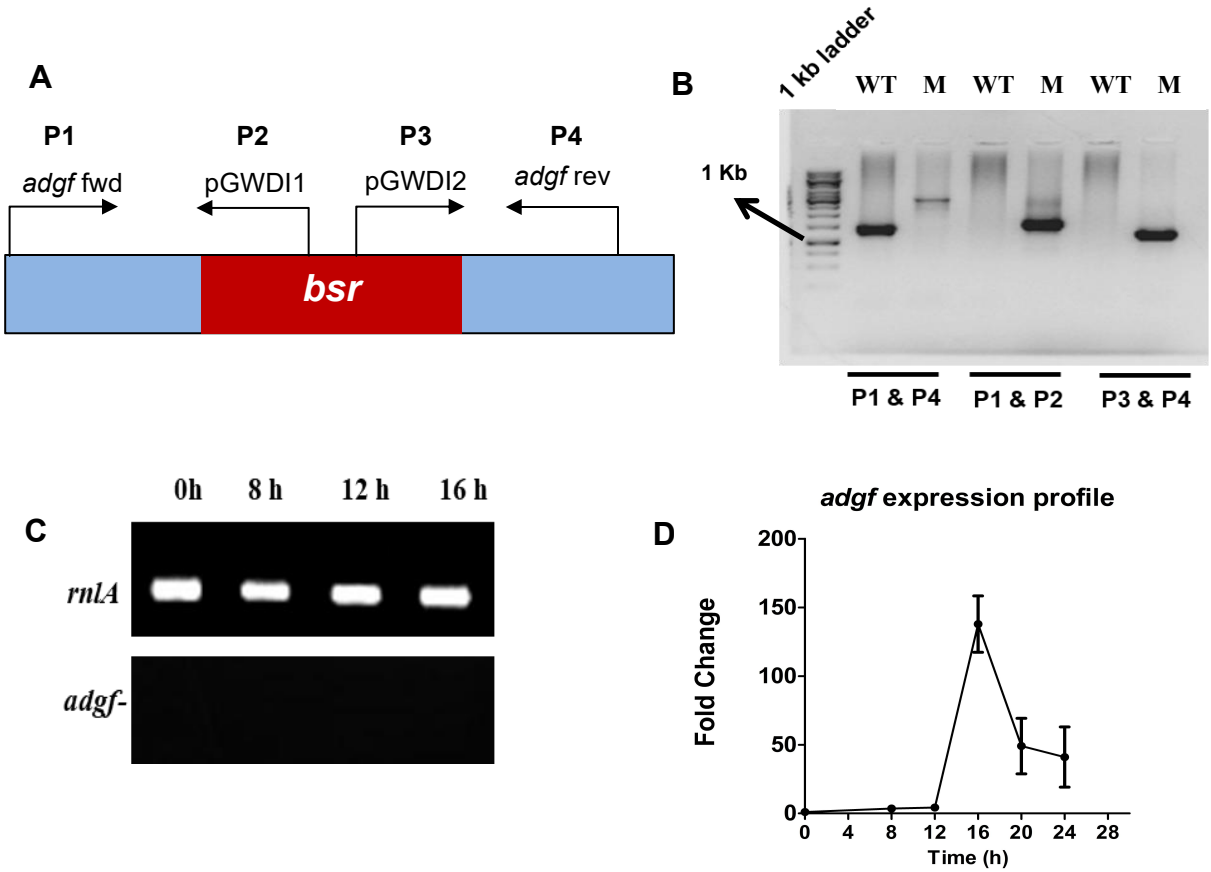

Figure 1. *adgf* mutant validation

A) Schematic representation of *adgf* locus showing the relative positions of the primers (P1–P4) and the blasticidin resistance cassette (*bsr*). Primer P1 (*adgf* fwd) is at the start codon of *adgf*, and primer P4 (*adgf* rev) is 264 bp upstream of the stop codon, flanking the insertion site. Primers P2 (pGWD2) and P3 (pGWD1) are located within the *bsr* cassette. *bsr* insertion is in exon 2 of *adgf*. **B)** PCR analyses using P1 and P4 primers. A 1.4 kb shift in the *adgf* mutant. PCR using P1 and P2 primers showed an amplicon from the mutant (M) and not from the wild type (WT). PCR using P3 and P4 primers showed an amplicon with the *adgf* mutant while WT did not show any amplicon. **C)** Semi-quantitative RT-PCR of the internal control, *rnlA* and *adgf*$^{-}$. *adgf* expression during development in *Dictyostelium*. **D)** Total RNA was isolated from *Dictyostelium* during vegetative growth and development using TRIzol method. To quantify *adgf* expression, qRT-PCR was carried out with *rnlA* as a control and the fold change was calculated accordingly. Time points are shown in hours (bottom). Error bars represent the mean and SEM (n = 3).

Figure 2

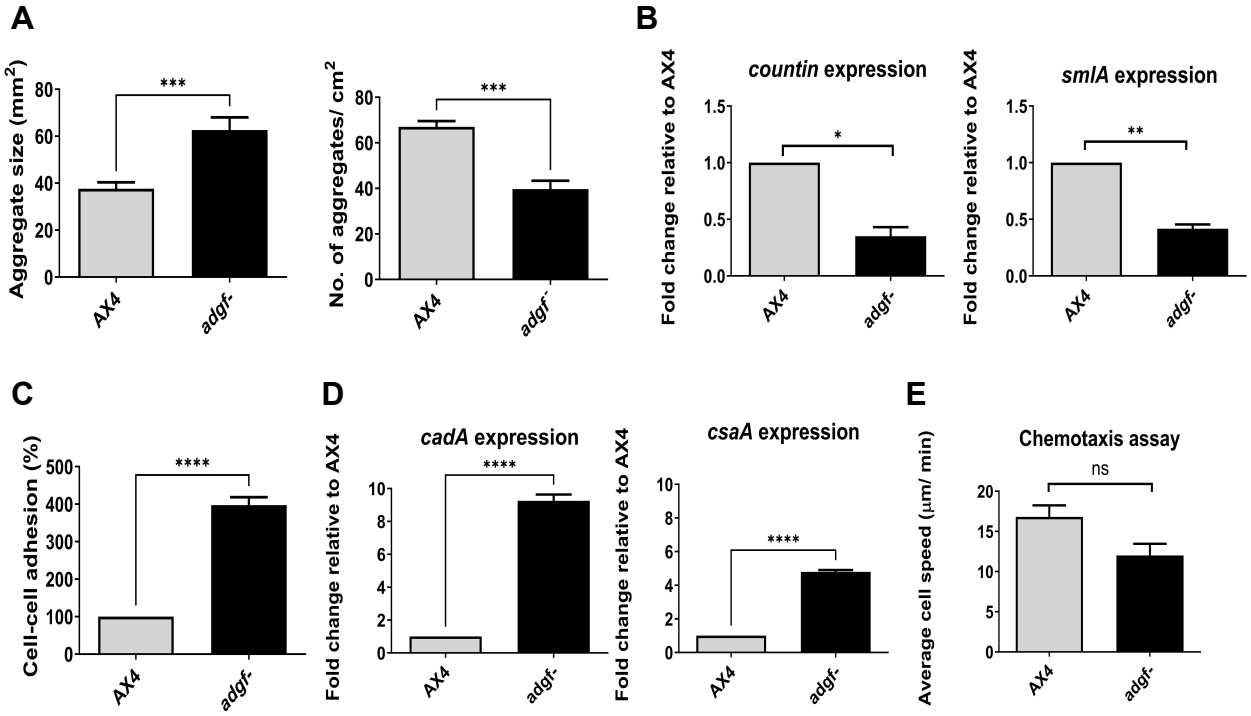
A
Aggregate size (mm²)
***
AX4
adgf-
No. of aggregates/ cm²
***
AX4
adgf-
B
countin expression
Fold change relative to AX4
*
AX4
adgf-
smlA expression
Fold change relative to AX4
**
AX4
adgf-
C
Cell-cell adhesion (%)
****
AX4
adgf-
D
cadA expression
Fold change relative to AX4
****
AX4
adgf-
csaA expression
Fold change relative to AX4
****
AX4
adgf-
E
Chemotaxis assay
Average cell speed (µm/ min)
ns
AX4
adgf-

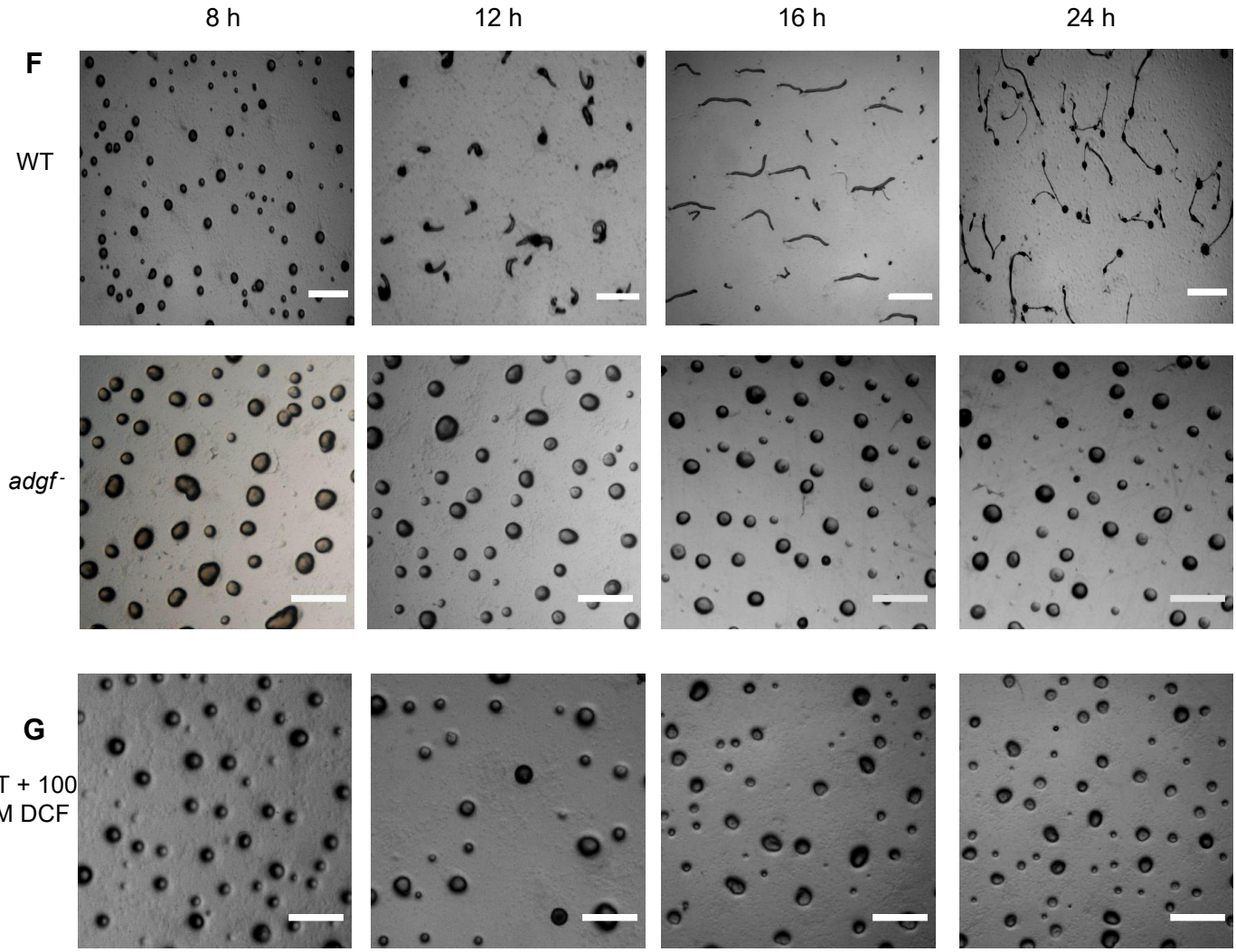
8 h
12 h
16 h
24 h
F
WT
adgf-
G
WT + 100 nM DCF

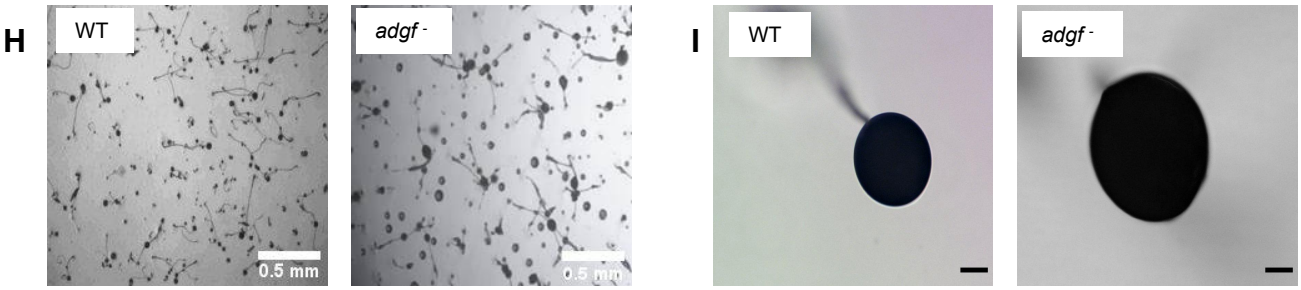

Figure 2. Aggregates formed by *adgf* mutants were larger in size

A) The graph shows the mound size and the number of aggregates formed by WT and *adgf* $^{-}$. The values represent mean ± S.E; n=3. **B)** Expression levels of the genes, countin (*ctn*) and small aggregates (*smlA*) during aggregation in *adgf* $^{-}$ compared to WT. *rnlA* was used as the internal control. **C)** WT and *adgf* $^{-}$ cells were developed on KK2 agar, and after 16 h, the multicellular mounds/slugs were dissociated by vigorous vortexing in KK2 buffer. Individual cells were counted using a hemocytometer and resuspended in a phosphate buffer. Non-adherent single cells were counted 45 min after incubation. The percent cell-cell adhesion was plotted by normalizing the values to the non-adherent WT count to 100%. Error bars represent the mean ± SEM (n=3). **D)** qRT-PCR analysis of cadherin (*cadA*) and contact site (*csA*) during aggregation. The fold-change in RNA transcript levels is relative to WT at the indicated time points. (n=3). ns = not significant. Significance level is indicated as *p< 0.05, **p< 0.01, ***p< 0.001, ****p< 0.0001. (Student's t-test). **E)** Under agarose chemotaxis assay. The average cell speed in response to 10 µM cAMP was recorded. The graph represents the mean ± SEM (n=3). **Developmental phenotype of *adgf* $^{-}$. F)** WT and *adgf* $^{-}$ cells were washed, plated on 1% KK2 agar plates at a density of $5x10^5$ cells/cm^2, incubated in a dark, moist chamber and images were taken at different time intervals. **G)** WT cells treated with 100 nM of DCF mimicked the mound arrest phenotype of the mutant. The time points are indicated in hours at the top of the figure. Scale bar: 2 mm; (n=3). **H)** WT and *adgf* $^{-}$ cells after 36 h of development. Scale bar: 0.5 mm; (n=3). **I)** Fruiting bodies of WT and *adgf* $^{-}$. Scale bar: 2 mm; (n=3).

Figure 3

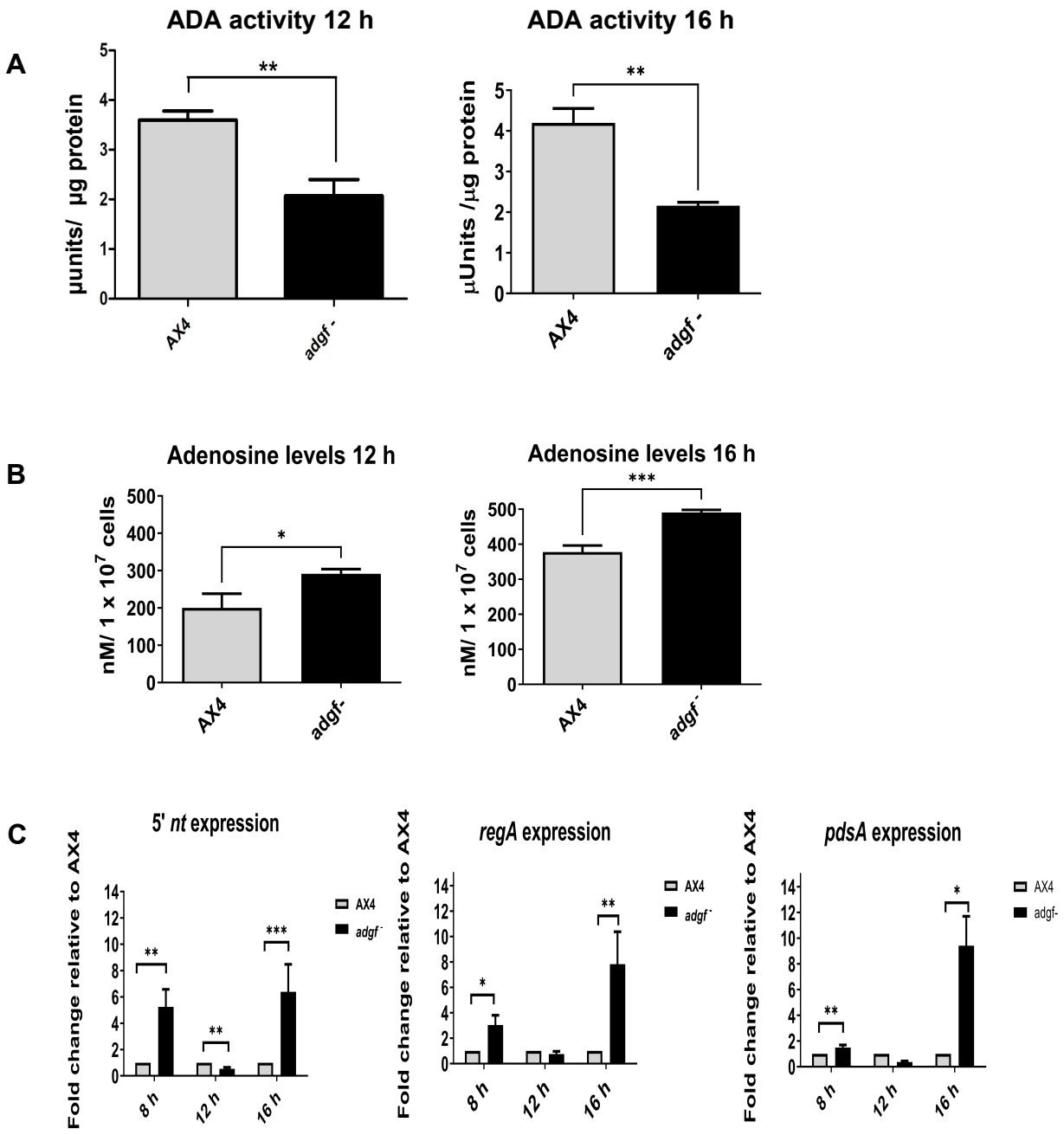

Figure 3. *adgf* mounds have reduced ADA activity and high adenosine levels.

A) ADA activity in WT and *adgf* $^{-}$ harvested at 12 h and 16 h. The enzymatic assay for ADA was performed in *adgf* $^{-}$ with the corresponding WT control. Error bars represent the mean and SEM (n=3). Significance level is indicated as **p< 0.01. **B)** Quantification of adenosine levels in WT and *adgf* mutants at 12 h and 16 h. Level of significance is indicated as *p< 0.05, **p< 0.01, ***p< 0.001; (n=3). **C)** Expression profile of 5' nucleotidase (*5'nt*) and phosphodiesterases (*regA*, *pdsA*) involved in cAMP-to-adenosine conversion. The fold-change in RNA transcript levels is relative to WT at the indicated time points. *rnlA* was used as an internal control. Error bars represent the mean and SEM (n=3).

Figure 4

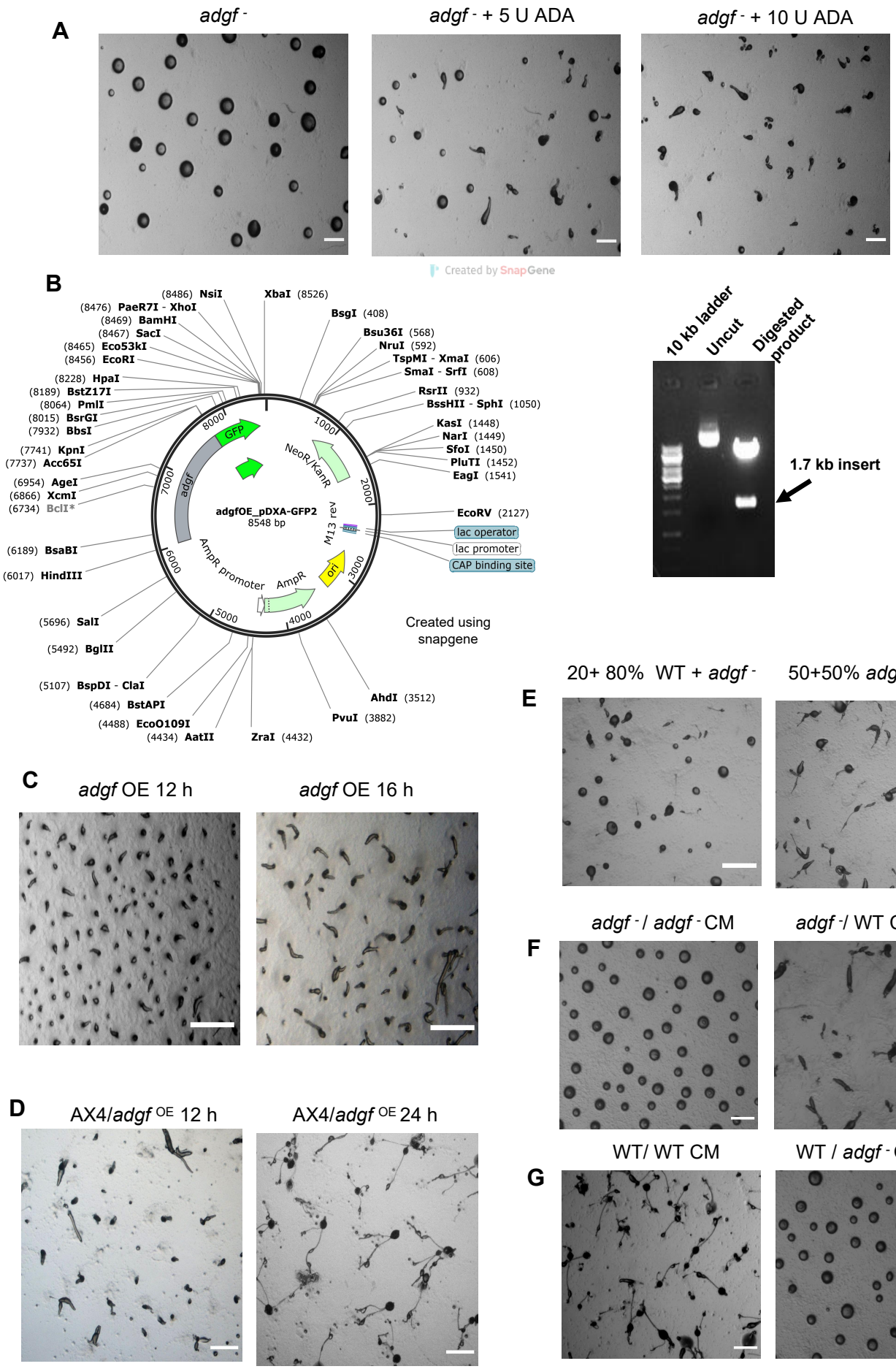
A
adgf -
adgf - + 5 U ADA
adgf - + 10 U ADA
B
Created by SnapGene
(8486) NsiI
XbaI (8526)
(8476) PaeR7I - XhoI
(8469) BamHI
(8467) SacI
(8465) Eco53kI
(8456) EcoRI
(8228) HpaI
(8189) BstZ17I
(8064) PmlI
(8015) BsrGI
(7932) BbsI
(7741) KpnI
(7737) Acc65I
(6954) AgeI
(6866) XcmI
(6734) BclI*
(6189) BsaBI
(6017) HindIII
(5696) SalI
(5492) BglII
(5107) BspDI - ClaI
(4684) BstAPI
(4488) EcoO109I
(4434) AatII
ZraI (4432)
PvuI (3882)
AhdI (3512)
BsgI (408)
Bsu36I (568)
NruI (592)
TspMI - XmaI (606)
SmaI - SrfI (608)
RsrII (932)
BssHII - SphI (1050)
KasI (1448)
NarI (1449)
SfoI (1450)
PluTI (1452)
EagI (1541)
EcoRV (2127)
lac operator
lac promoter
CAP binding site
1000
2000
3000
4000
5000
6000
7000
8000
GFP
adgf
NeoR/KanR
M13 rev
ori
AmpR
AmpR promoter
adgfOE_pDXA-GFP2
8548 bp
Created using
snapgene
10 kb ladder
Uncut
Digested
product
1.7 kb insert
C
adgf OE 12 h
adgf OE 16 h
D
AX4/adgf OE 12 h
AX4/adgf OE 24 h
E
20+ 80% WT + adgf -
50+50% adgf - + WT
F
adgf - / adgf - CM
adgf -/ WT CM
G
WT/ WT CM
WT / adgf - CM

Figure 4. Overexpression of *adgf* rescued the mound arrest phenotype

A) *adgf*$^-$ mounds were treated with 5 U and 10 U ADA enzyme, and imaged at 16 h. Scale bar: 2 mm; (n=3). **B)** The full-length *adgf* gene was cloned in the vector pDXA-GFP2. The overexpression construct was verified by restriction digestion with HindIII and KpnI enzymes. **C)** *adgf* overexpression in the mutant rescued the mound arrest. **D)** Overexpression of *adgf* in WT background. Scale bar: 2 mm; (n=3). The time points in hours are shown at the top. **WT cells mixed with *adgf*$^-$ rescued the *adgf* mutant phenotype. E)** Mixing of WT with *adgf*$^-$ in a 1:4 ratio showed a partial rescue, and a full rescue of the *adgf*$^-$ mound arrest phenotype in a 1:1 ratio with WT. **F)** Development of *adgf* mutants in the presence of *adgf*$^-$ CM and WT CM on KK2 agar plates. WT CM rescued the mound arrest. **G)** Development of WT in the presence of WT CM and *adgf*$^-$ CM on KK2 agar plates. *adgf*$^-$ CM induced mound arrest in WT cells. Scale bar: 2 mm; (n=3).

Figure 5

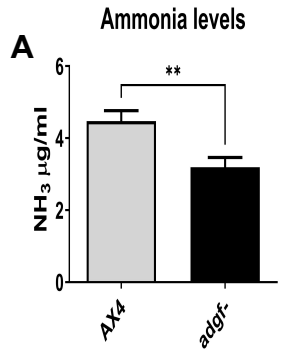
A
Ammonia levels
**
NH3 µg/ml
0
2
4
6
AX4
adgf-

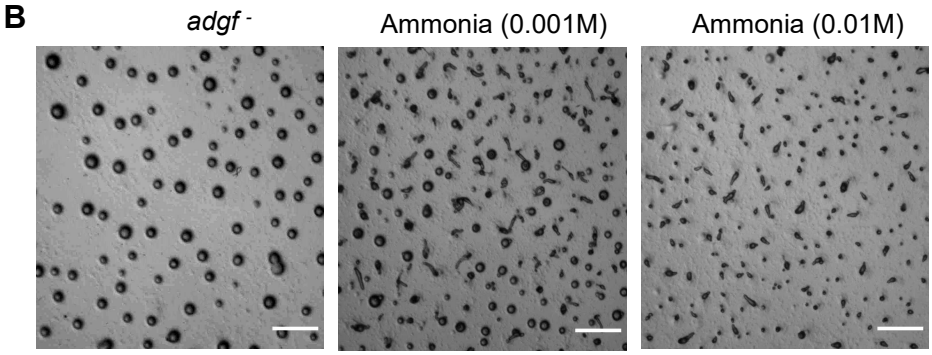
B
adgf -
Ammonia (0.001M)
Ammonia (0.01M)

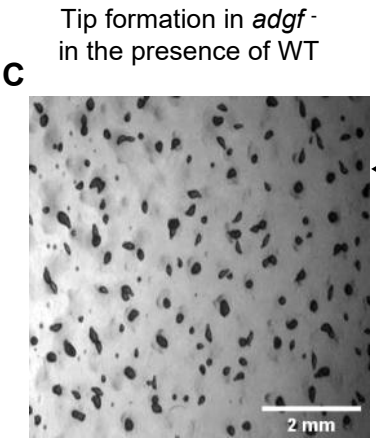
C
Tip formation in adgf -
in the presence of WT
2 mm

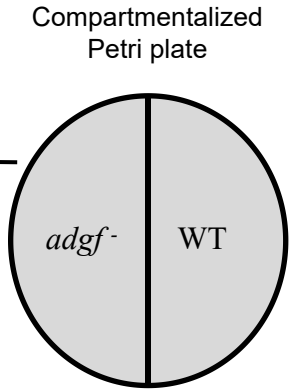
Compartmentalized
Petri plate
adgf -
WT

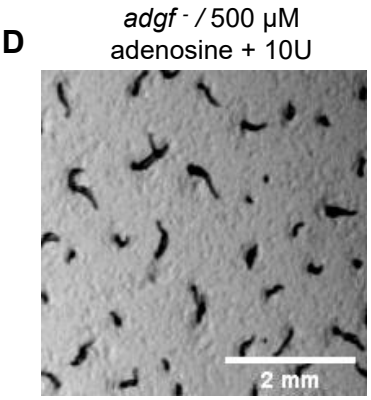
D
adgf - / 500 µM
adenosine + 10U
2 mm

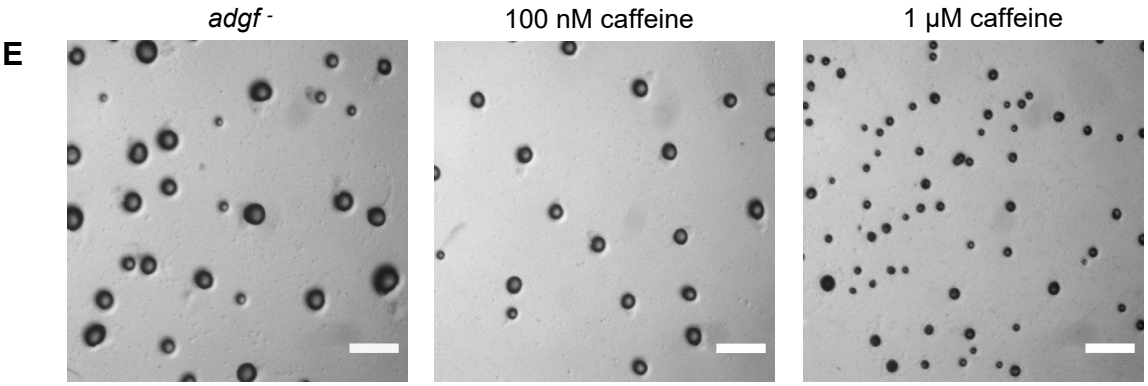
E
adgf -
100 nM caffeine
1 µM caffeine

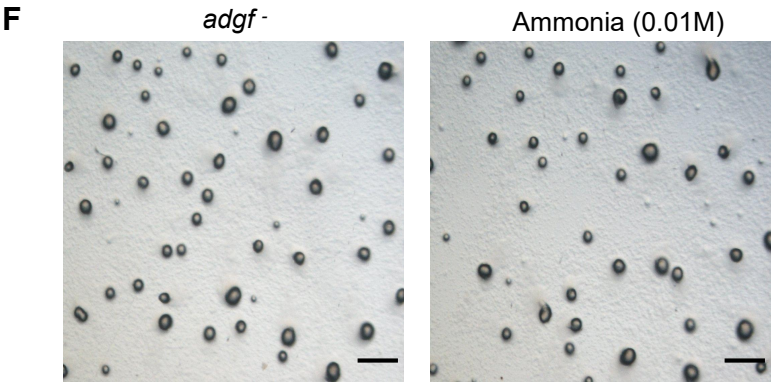
F
adgf -
Ammonia (0.01M)

Figure 5. Adenosine deamination reaction rescues the mound arrest of *adgf* $^{-}$

A) Quantification of ammonia using the ammonia assay kit. WT and *adgf* $^{-}$ mounds were harvested and lysed using a cell lysis buffer. Cell debris was removed by centrifugation, and the supernatant was used to quantify ammonia. **B)** Treatment of *adgf* $^{-}$ mounds with ammonia. Ammonia was generated by mixing 2 ml of NH_4Cl and 2 ml of 1N NaOH. The mixture was poured on top of the lid and the KK2 plates with the mounds were inverted and sealed thereafter. Images were taken 3.5 h post treatment. Dose dependent effect of ammonia on the rescue. Scale bar: 2 mm; (n=3). **C)** WT and *adgf* $^{-}$ cells on either side of a compartmentalized Petri dish led to tip fornation in *adgf* $^{-}$. **D)** *adgf* $^{-}$ cells on one side and KK2 buffer containing adenosine and ADA on the other side of the compartmentalized dish, rescued the mound defect. **Caffeine rescues the large mound size of *adgf* mutant. E)** *adgf* $^{-}$ cells were treated with different concentrations of caffeine (100 nM, 1 µM) while plating, and images were taken during mound stage. Scale bar: 2 mm; n=3. **F)** Exposure to ammonia does not rescue the mound size of *adgf* mutant. *adgf* $^{-}$ mounds were exposed to 0.01 M ammonia and images were captured 3.5 h post chemical treatment. Scale bar: 2 mm; (n=3).

Figure 6

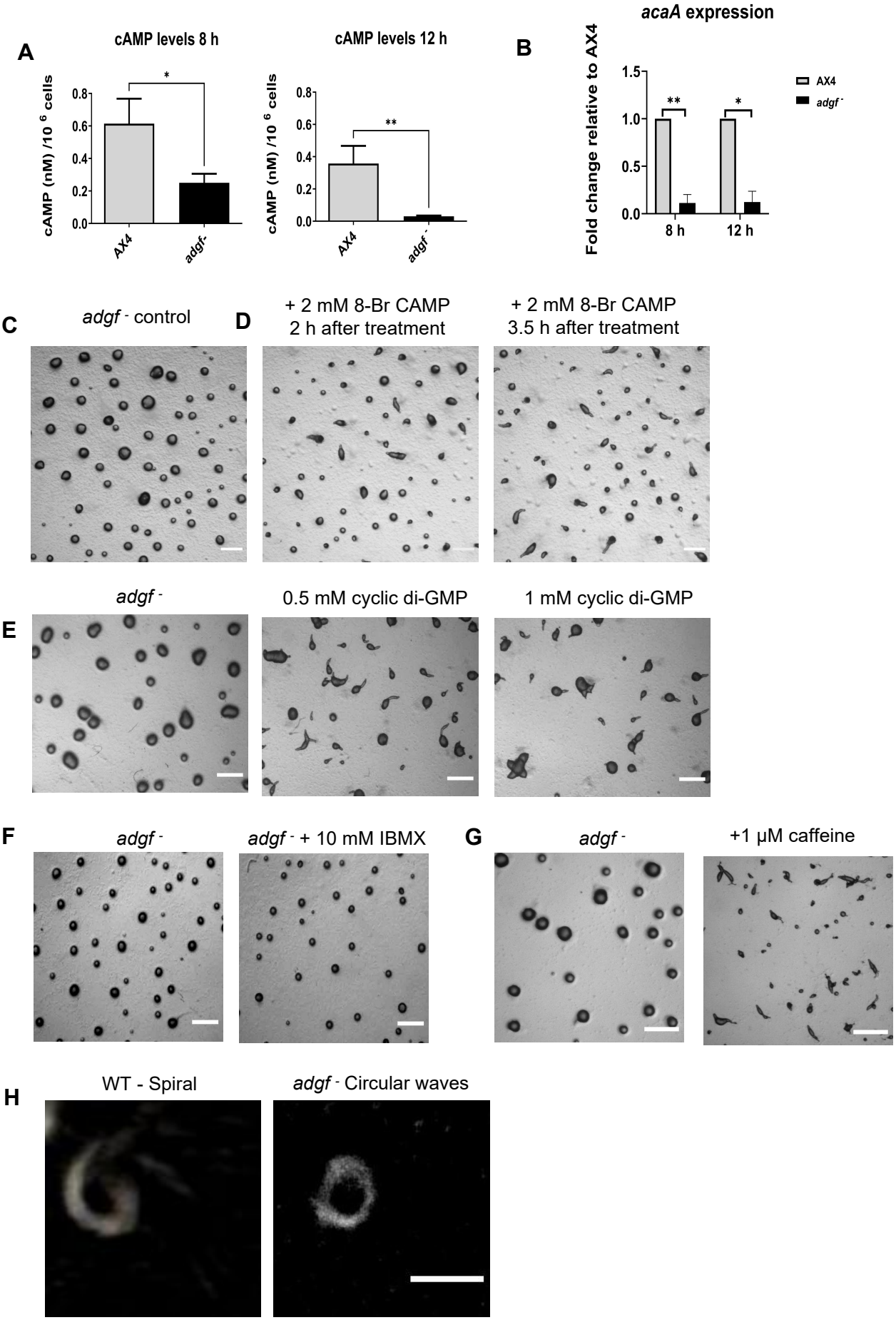
A
cAMP levels 8 h
cAMP levels 12 h
cAMP (nM) /10 6 cells
0.0
0.2
0.4
0.6
0.8
*
**
AX4
adgf-
B
acaA expression
Fold change relative to AX4
0.0
0.5
1.0
1.5
**
*
8 h
12 h
AX4
adgf -
C
adgf - control
D
+ 2 mM 8-Br CAMP
2 h after treatment
+ 2 mM 8-Br CAMP
3.5 h after treatment
E
adgf -
0.5 mM cyclic di-GMP
1 mM cyclic di-GMP
F
adgf -
adgf - + 10 mM IBMX
G
adgf -
+1 μM caffeine
H
WT - Spiral
adgf - Circular waves

Figure 6. Impaired cAMP signaling in *adgf*$^{-}$

A) Total cAMP levels in WT and *adgf*$^{-}$ mounds were quantified using cAMP-XP assay kit (Cell signaling, USA). Level of significance is indicated as *$p < 0.05$, **$p < 0.01$; (n=3). **B)** *acaA* expression was quantified using qRT-PCR. The error bars represent the mean ± SEM (n=3). **C)** *adgf*$^{-}$ mounds. **D)** Time course of *adgf*$^{-}$ mounds treated with 8-Br-cAMP and imaged at different intervals. Scale bar: 2 mm; (n=3). **Treatment with cyclic di-GMP and caffeine rescues the mound arrest phenotype. E)** Addition of cyclic-di-GMP restored tip formation in *adgf*$^{-}$ 3.5 h after the treatment. Scale bar: 1 mm; (n=3). **F)** PDE inhibitor (IBMX) treatment failed to rescue the *adgf*$^{-}$ mound arrest. Scale bar 1 mm; (n=3). **G)** *adgf*$^{-}$ mounds treated with caffeine formed tips 3.5 h post treatment. Scale bar: 2 mm; (n=3). **Altered cAMP wave pattern in *adgf* mutants. H)** Optical density waves depicting cAMP wave generating centers in WT and *adgf*$^{-}$. WT shows spiral and *adgf*$^{-}$ exhibits circular wave propagation.

Figure 7

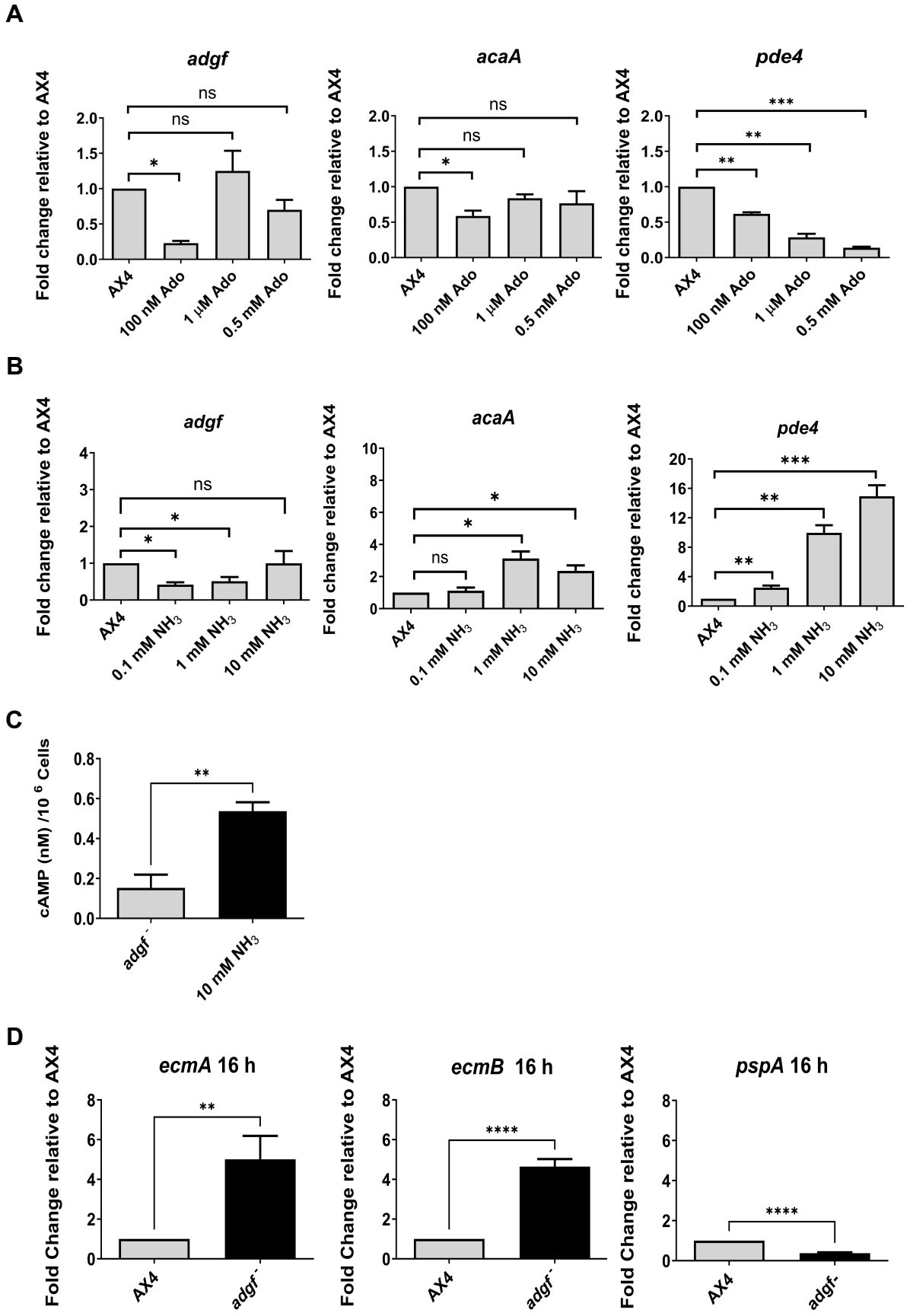
A
adgf
acaA
pde4
Fold change relative to AX4
ns
*
**
***
AX4
100 nM Ado
1 μM Ado
0.5 mM Ado
B
0.1 mM NH3
1 mM NH3
10 mM NH3
C
cAMP (nM) /10 6 Cells
adgf-
D
ecmA 16 h
ecmB 16 h
pspA 16 h
****

Figure 7. Expression levels of *adgf*, *acaA* and *pde4* in response to adenosine and ammonia treatment

A) Expression levels of *adgf*, *acaA* and *pde4* in response to adenosine treatment (100 nM, 500 nM, 1 µM). **B)** And ammonia treatment (0.1 mM, 1 mM, 10 mM). Level of significance is indicated as *p<0.05, **p<0.01, and ***p<0.001; (n=3). **C)** cAMP levels in *adgf* mutants rescued with ammonia. Level of significance is indicated as **p< 0.01; (n=3). **Expression levels of prestalk (pst), *ecmA, ecmB* and prespore (psp), *pspA* cell type markers in *adgf*$^-$.** The expression profile of **D)** pst (*ecmA*, *ecmB*) and psp (*pspA*) specific markers in WT and *adgf*$^-$ were quantified using qRT-PCR. Level of significance is indicated as **p<0.01 and ****p<0.0001; (n=3). Three independent biological replicates were performed and the error bars represent the mean and SEM. The fold-change in RNA transcript levels is relative to WT at the indicated time points. *rnlA* was used as the internal control (n=3). ns = not significant.

Figure 8

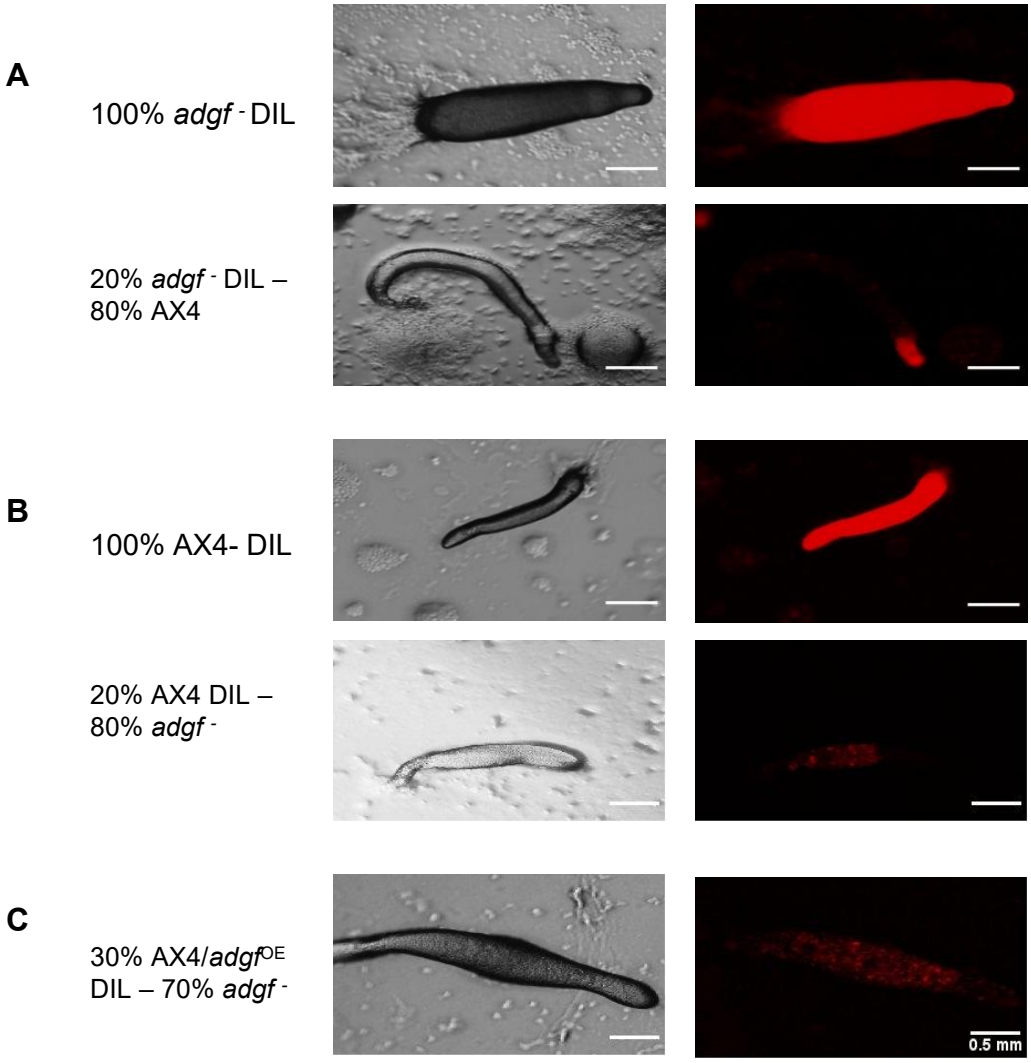

Figure 8. Mixing of WT cells with *adgf* - following DIL staining

A-C) DIL labelled cells were mixed with unlabelled cells and plated on KK2 agar. Images were captured during the migrating slug stage. The left panel shows bright field, and the right panel shows the corresponding fluorescence images. Scale bar: 0.5 mm; (n=3).

Figure 9

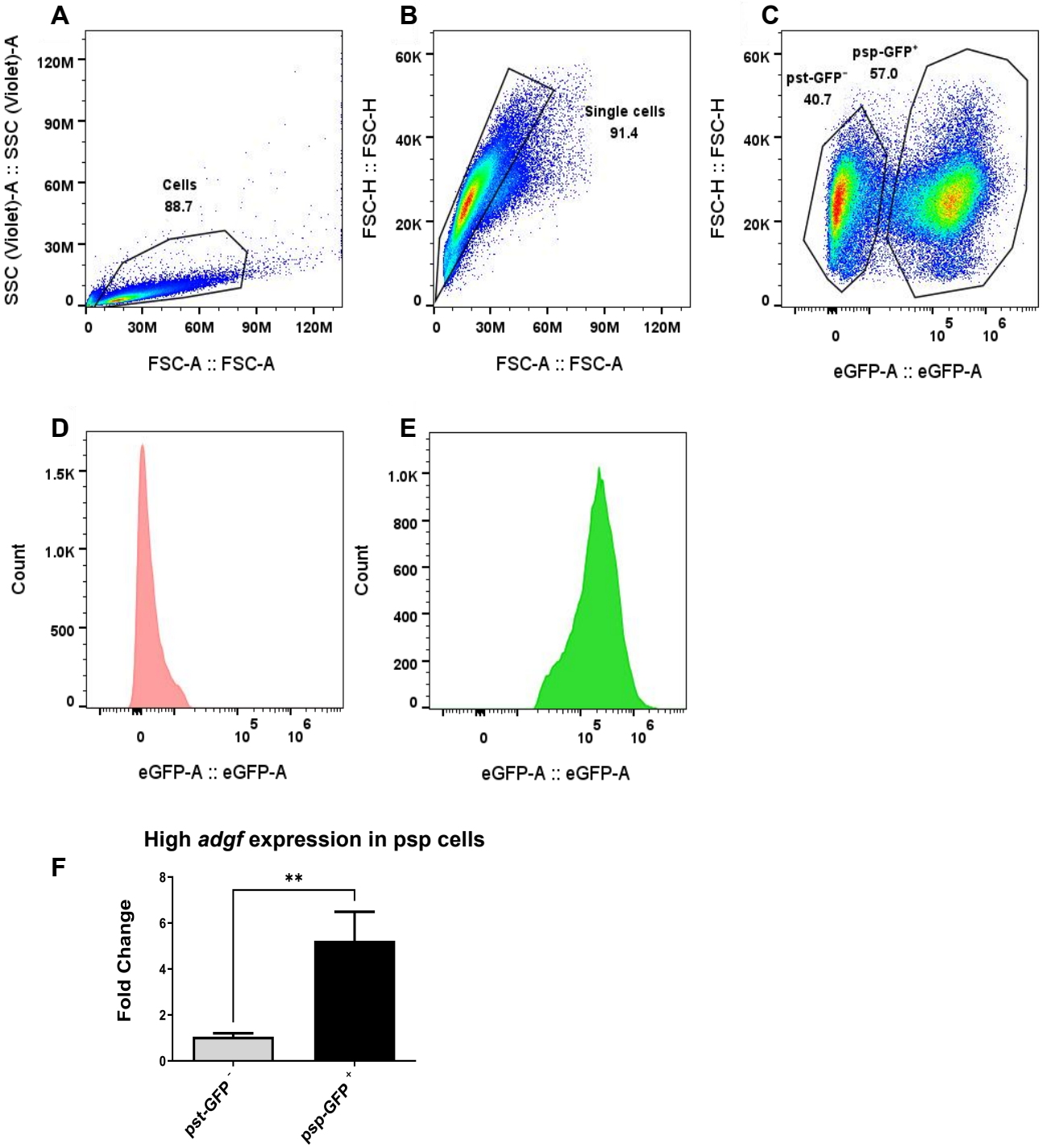

Figure 9. Sorting of pst-GFP⁻ and psp-GFP⁺ *Dictyostelium* cells by fluorescence activated cell sorter

A) Forward scatter (FSC) vs. side scatter (SSC) plot used to gate total cells. **B)** Singlets were gated based on FSC-H vs. FSC-A to exclude doublets and aggregates. **C)** GFP fluorescence profile of gated single cells reveals two populations: pst-GFP⁻ and psp-GFP⁺, corresponding to pst and psp cells, respectively. **D)** GFP⁻ (pst) and **E)** GFP⁺ (psp) fractions. **F)** *adgf* expression in FACS sorted samples was quantified by qRT-PCR. Level of significance is indicated as **$p<0.01$ (n=3).

Figure 10

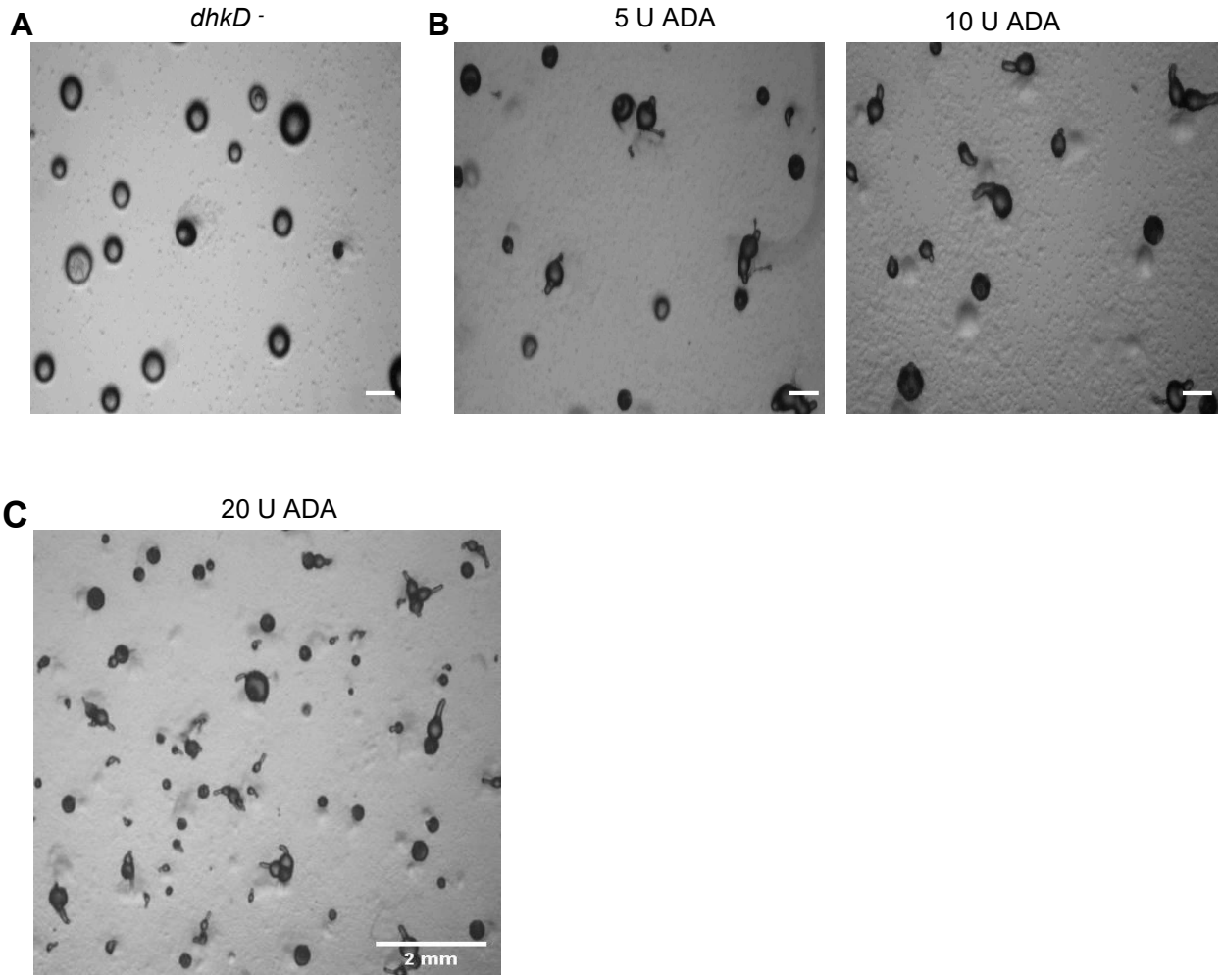

Figure 10. *adgf* acts downstream of the histidine kinase *dhkD*

A) *dhkD* mutants on KK2 agar plates. **B)** 5 U, 10 U ADA rescued the mound arrest phenotype in a dose dependent manner. Scale bar: 1 mm; (n=3). Images were taken 3.5 h post treatment. **C)** Addition of 20 U ADA led to formation of multiple tips. Scale bar: 2 mm; (n=3).

Figure 11

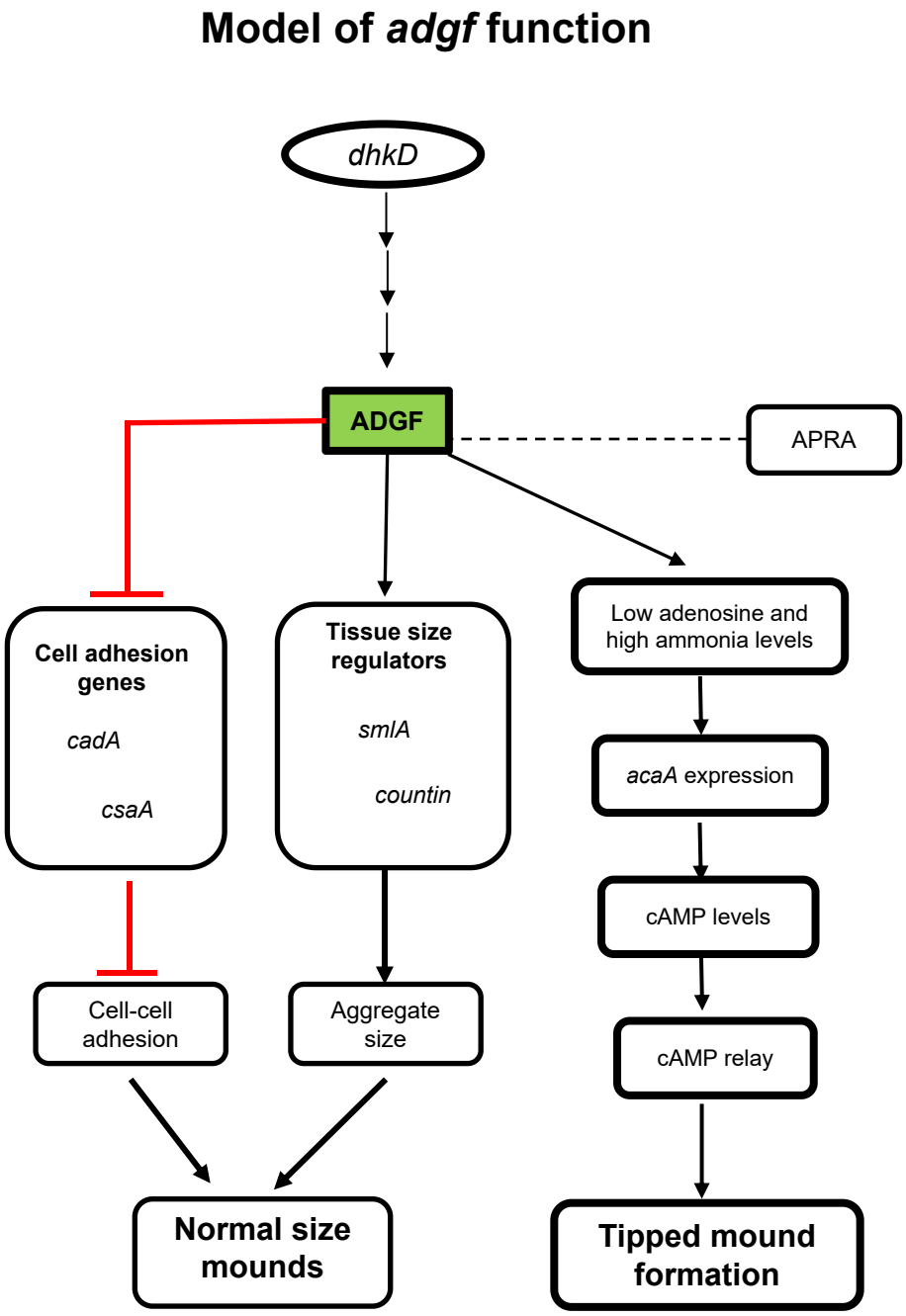

Figure 11. Model illustrating the role of *adgf* in development

adgf suppresses the expression of genes involved in cell adhesion, *cadA* and *csaA,* and regulates the mound size and tip development by directly acting on adenosine, ammonia levels and cAMP signaling. Line ending in an arrow indicates that the previous gene/factor either directly or indirectly raises the activity or levels of the second; line ending in a cross-bar indicates inhibition. Dotted lines indicate ADGF interacting with APRA.

Supplementary Figure 1

A

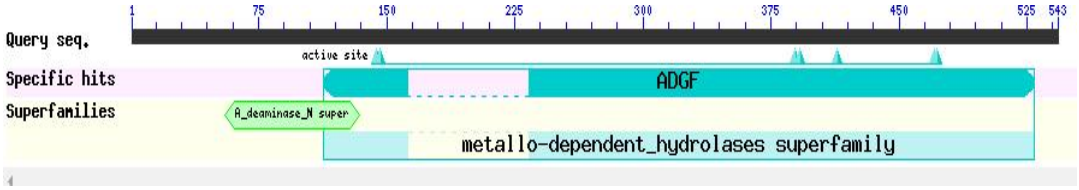

B

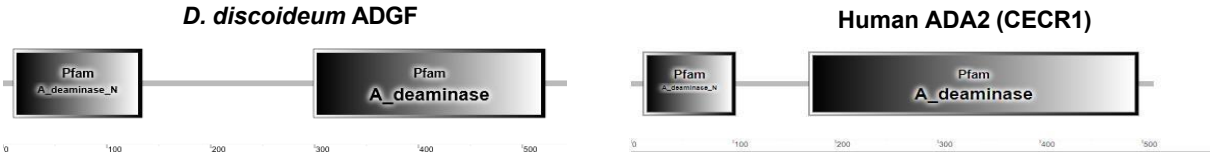

C

```
Q553U5     ADA2_DICDI        1   MFLK-------FKNIFFIVLTLSIVFNGLIVNSKNIHINNKNNNNNNNNKDLSSSESGSS   53
A0A3Q2UK74 A0A3Q2UK74_CHICK  1   --MK----PPSGQGIRLACL-LGLASLCL-------------------------------   22
A0A3Q1NIS4 A0A3Q1NIS4_BOVIN  1   -----MSGRLAPPSLLLALV-VSSFCPAT-------------------------------   23
Q9NZK5     ADA2_HUMAN        1   MLVDGPSERPALCFLLLAVA-MSFFGSAL-------------------------------   28
G3QXR5     G3QXR5_GORGO      1   MLVDGPSERPALRFLLLAVA-MSFFGSAL-------------------------------   28
A0A287BDN3 A0A287BDN3_PIG    1   -----MSGWPVLPALLLAVA-MSSFHSAT-------------------------------   23
Q1X7G4     Q1X7G4_XENLA      1   ----------MTCISHWLLL-LSLASAAL-------------------------------   18
F6NKG5     F6NKG5_DANRE      1   --MSSISLKD-VSAAVMVVL-LVCVSECK-------------------------------   25
Q9VVK5     Q9VVK5_DROME      1   -------MSPVIRRNLIACL-TLGLCVCLSFGPGPVE--SRTRPKNQVDRKLL-TIYGST   49
```

D

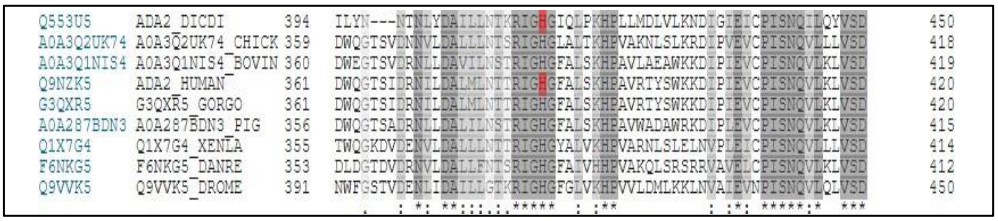

```
Q553U5     ADA2_DICDI        394   ILYN---NTNLYDAILLNTKRIGHGIQLPKHPLLMDLVLKNDIGIEICPISNQILQYVSD   450
A0A3Q2UK74 A0A3Q2UK74_CHICK  359   DWQGTSVDNNVLDALLLNTSRIGHGLALTKHPVAKNLSLKRDIPVEVCPISNQVDLLVSD   418
A0A3Q1NIS4 A0A3Q1NIS4_BOVIN  360   DWEGTSVDRNILDAVILNSTRIGHGFALSKHPAVLAEAWKKDIPIEVCPISNQVDKLVSD   419
Q9NZK5     ADA2_HUMAN        361   DWQGTSIDRNILDALMLNTTRIGHGFALSKHPAVRTYSWKKDIPIEVCPISNQVDKLVSD   420
G3QXR5     G3QXR5_GORGO      361   DWQGTSIDRNILDALMLNTTRIGHGFALSKHPAVRTYSWKKDIPIEVCPISNQVDKLVSD   420
A0A287BDN3 A0A287BDN3_PIG    356   DWQGTSADRNILDALILNSTRIGHGFALSKHPAVWADAWRKDIPLEVCPISNQVDKLVSD   415
Q1X7G4     Q1X7G4_XENLA      355   TWQGKDVDENVLDALLLNTTRIGHGYALVKHPVARNLSLELNVPLEICPISNQVDLLVSD   414
F6NKG5     F6NKG5_DANRE      353   DLDGTDVDRNVLDALLFNTSRIGHGFALVHHPVAKQLSRSRRVAVELCPISNQVDKLVSD   412
Q9VVK5     Q9VVK5_DROME      391   NWFGSTVDENLIDAILLGTKRIGHGFGLVKHPVVLDMLKKLNVAIEVNPISNQVDQLVSD   450
                                       . : *: **:::::.:*****  : :**          : :*: *****:*  ***
```

E

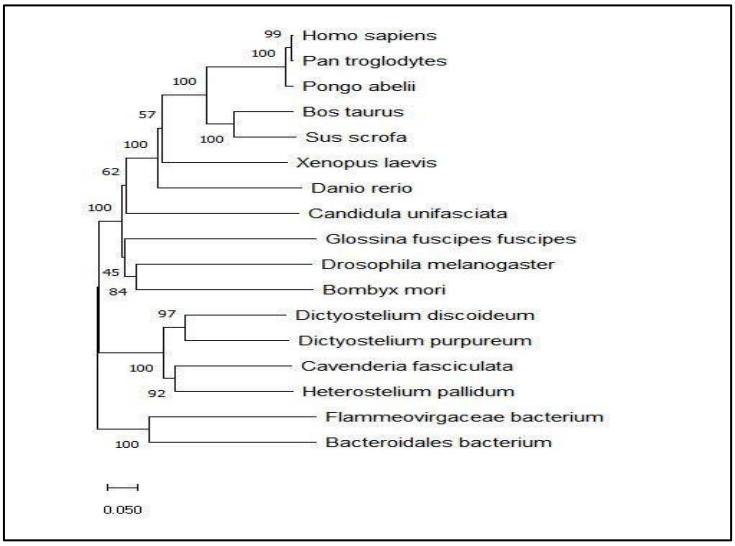

F ADA2 (CECR1) *Homo sapiens*

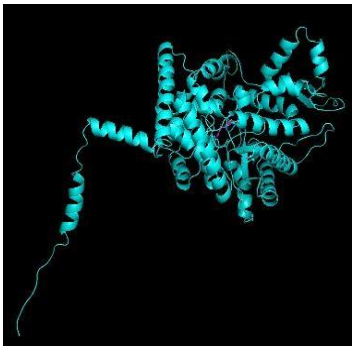

G ADGF *D. discoideum*

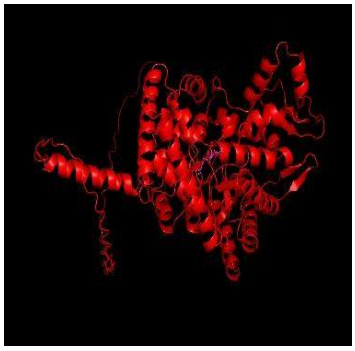

H Overlap

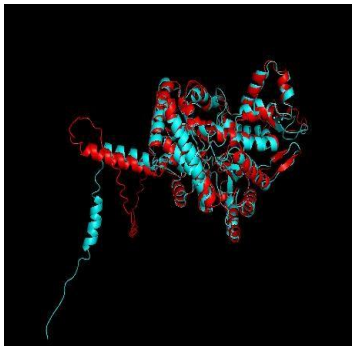

Figure S1. Bioinformatic analyses of ADGF

A) BLAST analysis of ADGF. **B)** SMART analysis depicting different ADA domains within ADGF. ADGF has an ADA and an N-terminal deaminase domain similar to human ADA2. **Multiple sequence alignment of *Dictyostelium* ADGF with ADGF from other organisms. C)** The shaded region depicts the N-terminal signal sequence characteristic of extracellular proteins. **D)** The active site residue highlighted in red, is conserved between *D.discoideum* and human *ada2*. **E)** Phylogenetic analysis of ADGF across different organisms. Maximum likelihood method was used for constructing the tree using molecular evolutionary genetic analysis X (MEGAX). **Structural comparison of human ADA2 and *Dictyostelium* ADGF**. Identical tertiary structures of human ADA2 and *Dictyostelium* ADGF. **F)** ADA2 (CECR1) *Homo sapiens* and **G)** DdADGF **H)** Alignment of *Dictyostelium* ADGF with Human ADA2 (CECR1).

Supplementary Figure 2

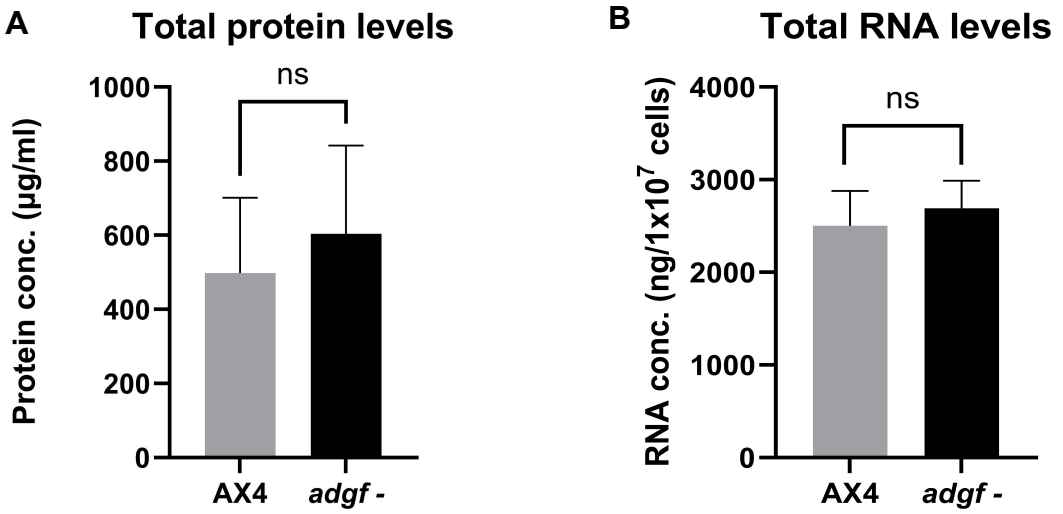

Figure S2. Total protein and RNA levels during mound stage of development.

A) Total protein levels were estimated using BCA assay. **B)** Total RNA levels in the WT and *adgf* $^{-}$. The error bars represent the mean ± SEM (n=3). ns = not significant.

Supplementary Figure 3

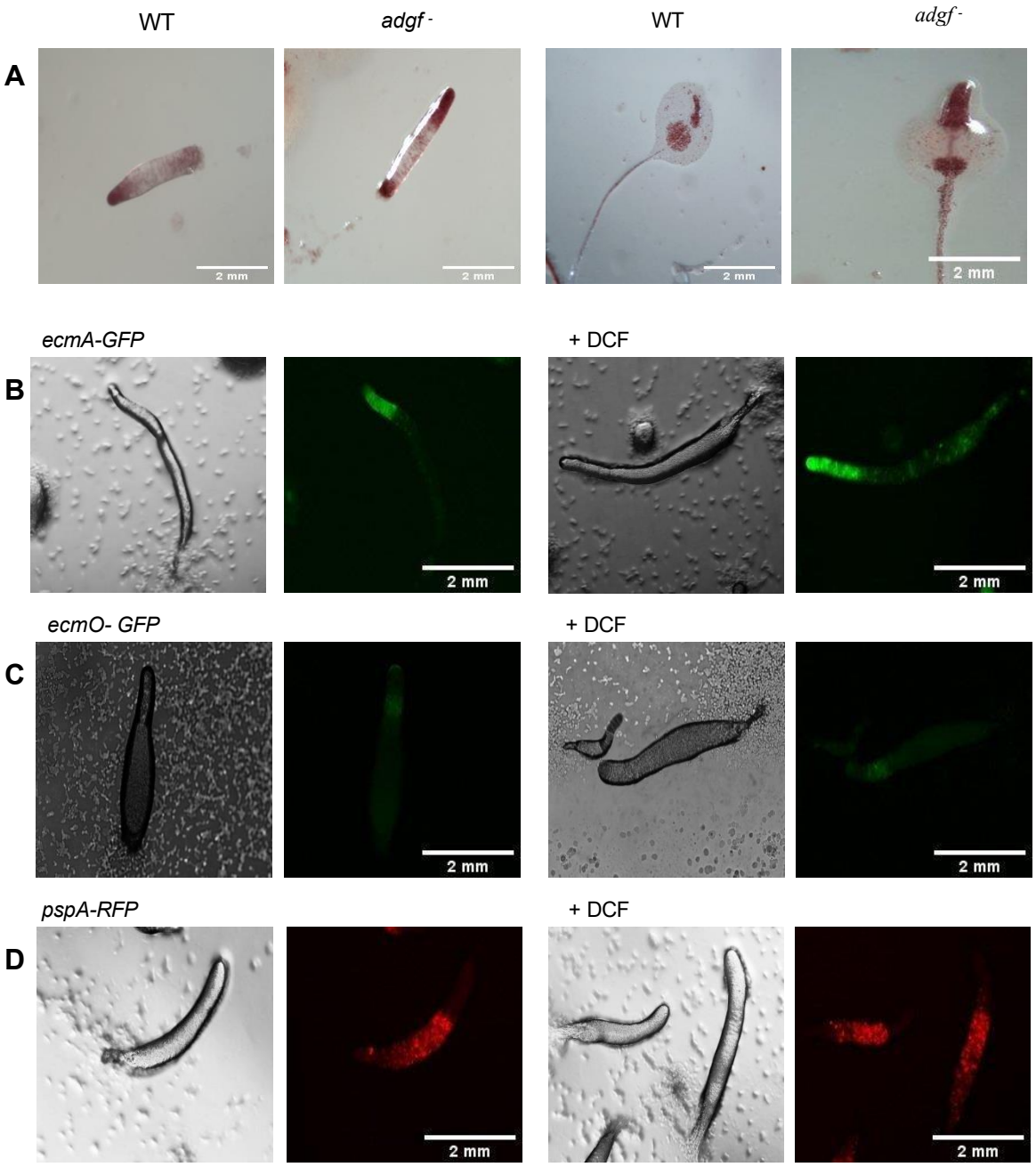

Figure S3. Neutral red staining of mounds and slugs.

A) WT and *adgf* $^{-}$ cells were stained with NR, plated and images were captured at different time intervals. Scale bar: 2 mm; (n=3). **Pst/psp marker expression in slugs after inhibitor treatment. B.** *ecmA*-GFP. **C)** *ecmO*-GFP. **D)** *pspA*-RFP expression in the slugs after DCF treatment. Scale bar: 2 mm.

Supplementary Figure 4

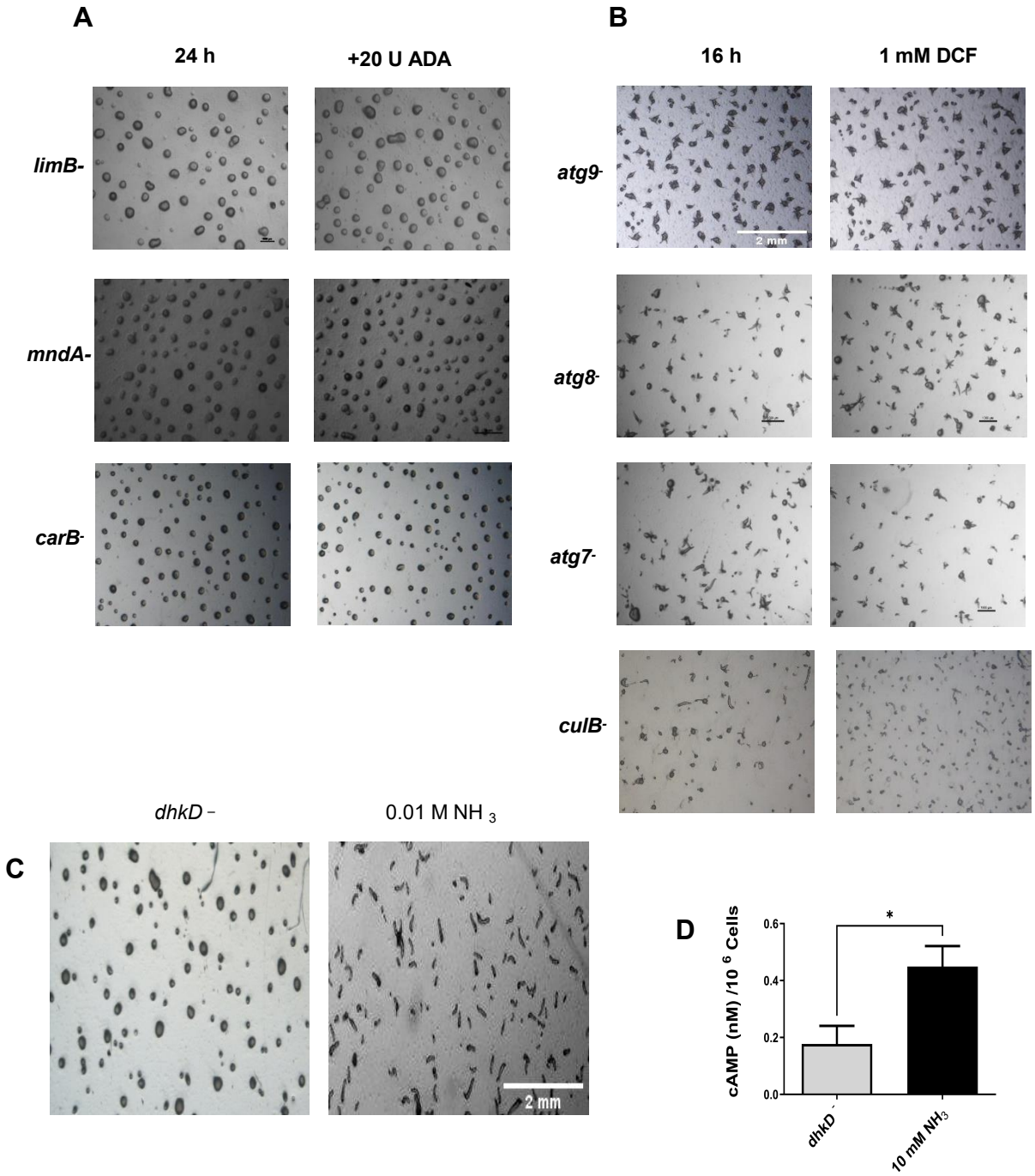

Figure S4. Treatment of mounds with ADA and DCF.

A) ADA enzyme was directly added on top of the mound arrest mutants at 12 h, and images were taken after 3.5 h. Scale bar: 2 mm; n=3. **B)** Multi tipped mutants were treated with 1 mM DCF, plated for development and images were taken after 16 h. Scale bar: 2 mm; n=3. **C)** Ammonia restores tip formation in *dhkD* - mounds.. Scale bar: 2 mm; n=3. **D)** cAMP levels in *dhkD* mutants rescued with ammonia.

Supplementary Figure 5

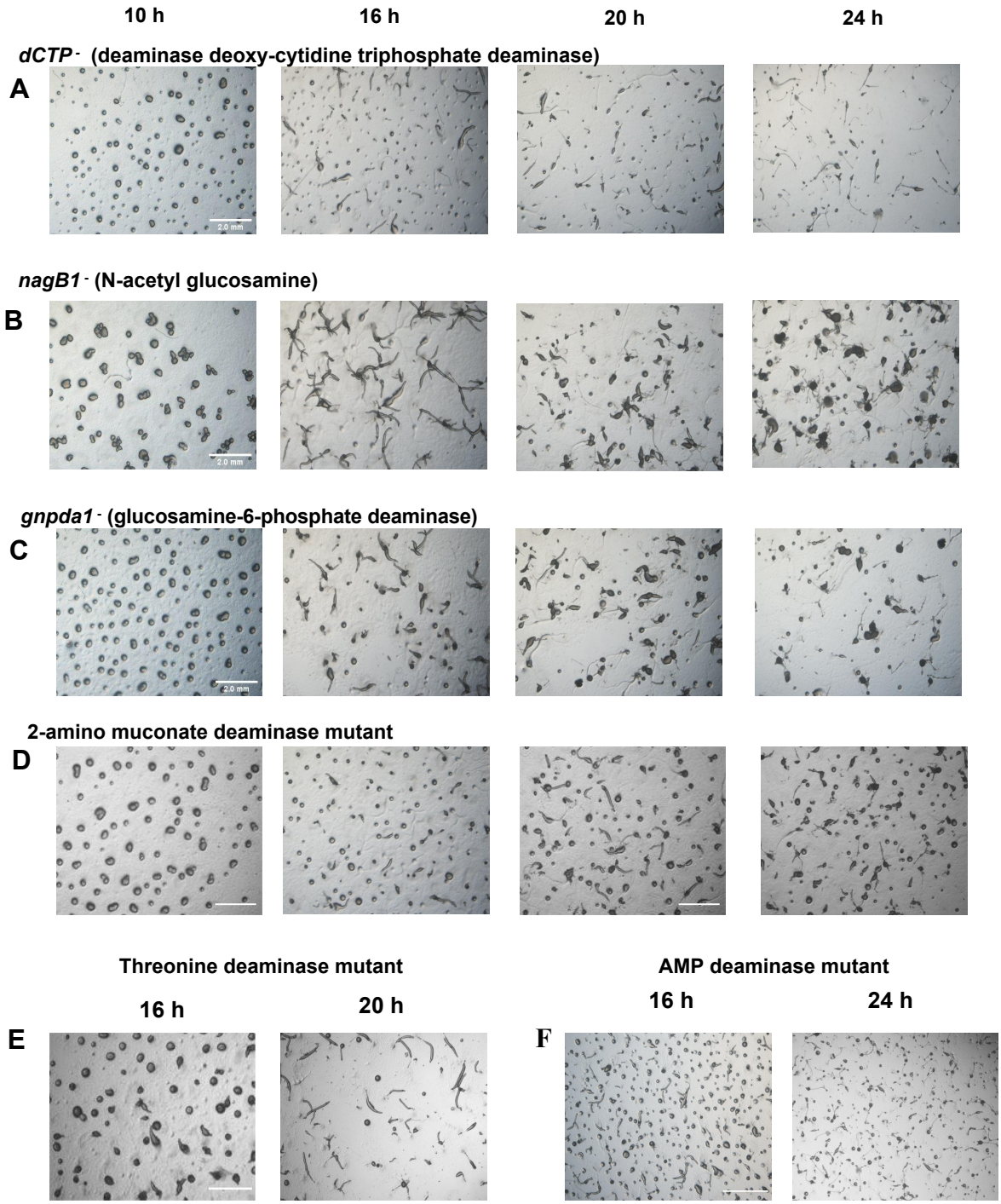

Figure S5. Developmental phenotype of different deaminase gene knockouts .

A) deoxy-cytidine triphosphate deaminase **B)** N-acetyl glucosamine **C)** glucosamine-6-phosphate deaminase **D)** 2-amino muconate deaminase. **E)** Threonine deaminase **F)** Adenosine monophosphate deaminase. Scale bar: 2 mm; n=3.

Supplementary Figure 6

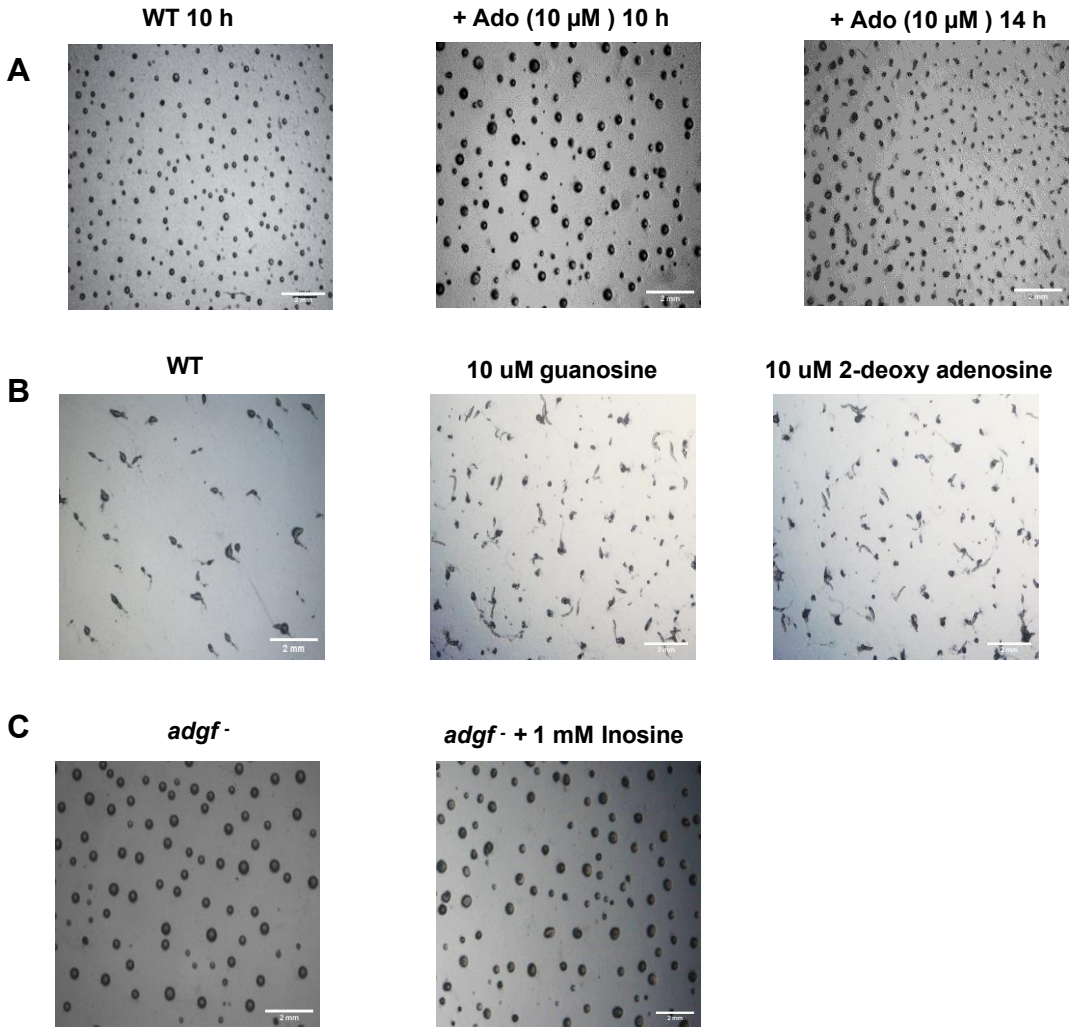

Figure S6. Treatment with adenosine and other purines does not induce mound arrest in WT.

A) WT cells were treated with adenosine (10 µM) while plating, and imaged at different time intervals. Scale bar: 1 mm; n=3. **B)** WT cells were treated with 10 µM guanosine and 10 µM 2-deoxy adenosine, plated for development and images were taken after 16 h. Scale bar: 2 mm; n=3. **C)** *adgf* $^{-}$ mounds were treated with inosine and images were captured 3.5 h post chemical treatment. Scale bar: 2 mm; (n=3).

Supplementary Figure 7

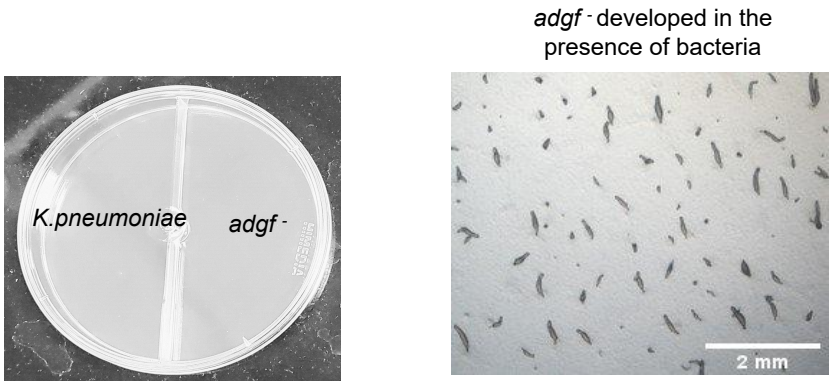

Figure S7. Volatiles released from *K. pneumoniae* rescues the mound arrest phenotype of *adgf* -

Picture depicting *K. pneumoniae* and *adgf* - cells on either side of a compartmentalized Petri dish. Scale bar: 2 mm; (n=3). *K. pneumoniae* and *adgf* - cells were developed on either side of compartmentalised dish, and photographs were captured at 16 h.

Supplementary Figure 8

A

ada

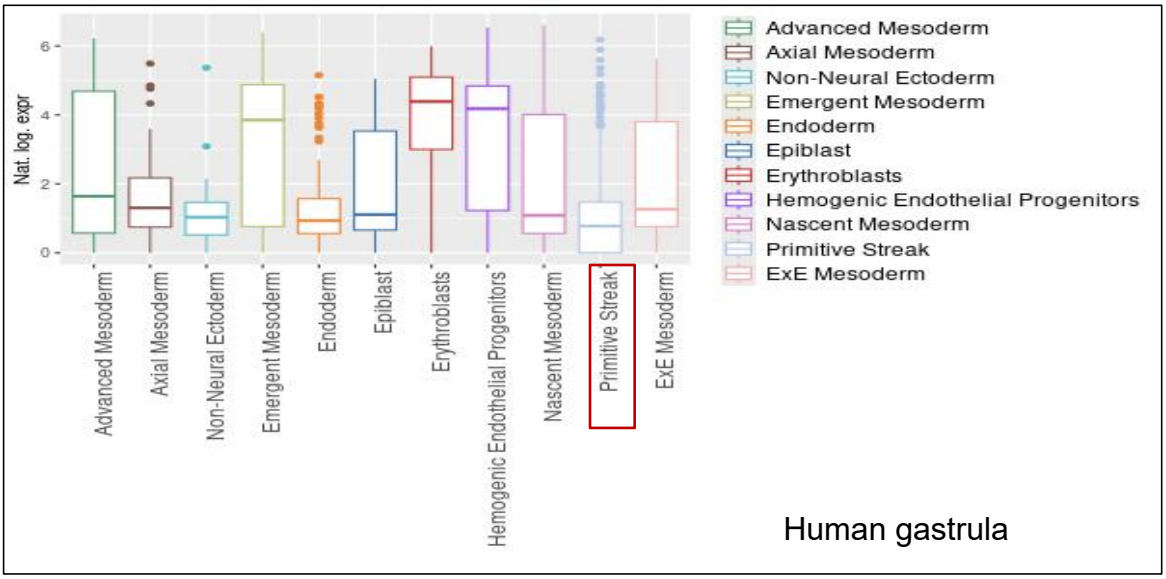

ada2

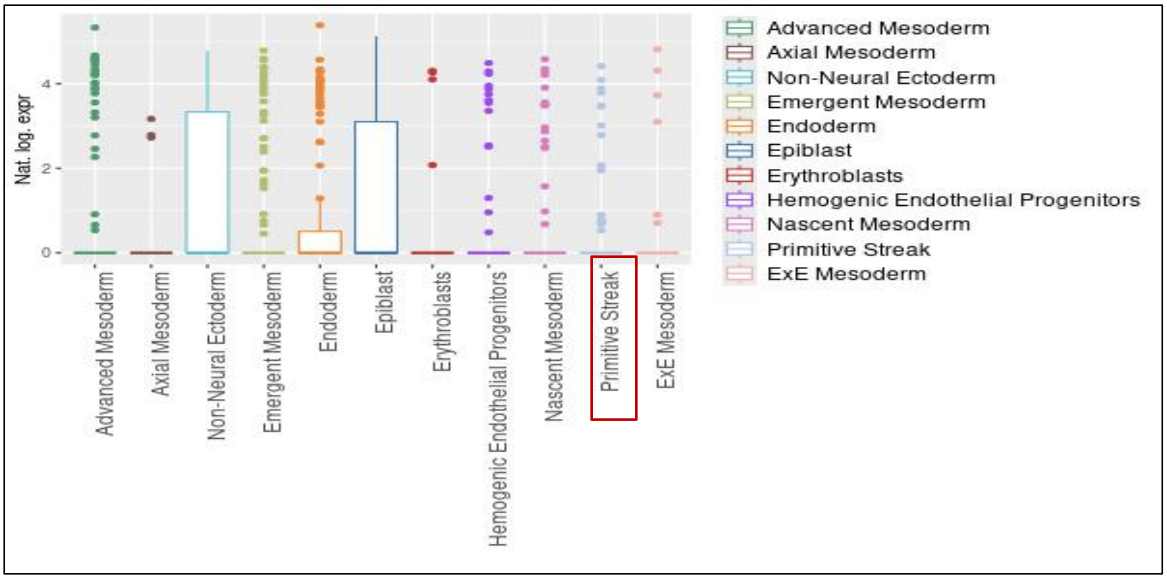

B

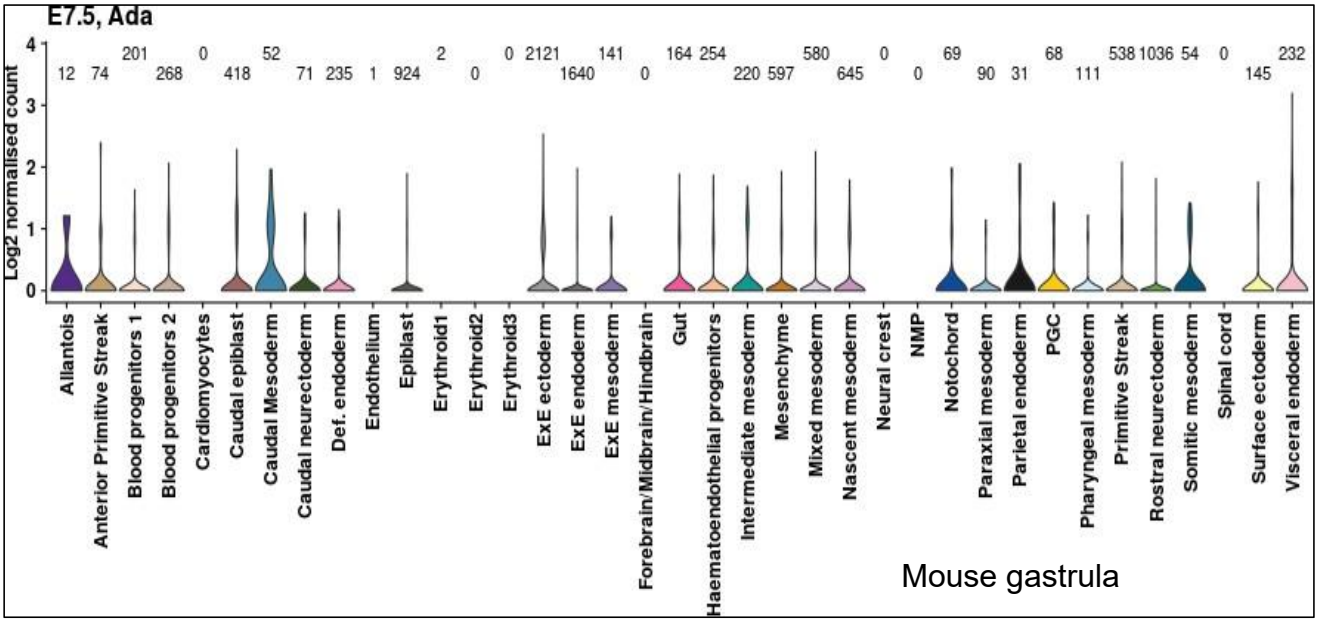

Figure S8. *ada* expression during gastrulation and pre-gastrulation stages in different organisms.

A) Single cell RNA sequencing data of the human gastrulating embryo were obtained from the human- gastrula.net/ database. *ada* expression was observed in the primitive streak (vertebrate organizer). **B)** Single cell RNA sequencing data of mice (E7.5) were obtained from the marionilab.cruk.cam.ac.uk/MouseGastrulation2018/ database. *ada* expression in the primitive streak indicates its possible role in organizer formation.

Supplementary Table 1

Various deaminases annotated in *D. discoideum*

Gene	Gene ID
2-aminomuconate deaminase	DDB_G0275081
adenosine deaminase	DDB_G0287371
adenosine deaminase acting on tRNA 1	DDB_G0278943
adenosine deaminase, tRNA-specific	DDB_G0288099
adenosine deaminase-related growth factor	DDB_G0275179
AMP deaminase	DDB_G0292266
CMP/dCMP deaminase, zinc-binding domain-containing protein	DDB_G0282255 | DDB_G0271914 | DDB_G0286161 | DDB_G0288019
cytidine deaminase	DDB_G0292096
cytidine deaminase-like protein	DDB_G0278841
cytidine/deoxycytidylate deaminase zinc-binding domain-containing protein	DDB_G0292096
dCTP deaminase	DDB_G0293580, DDB_G0268194
glucosamine-6-phosphate deaminase	DDB_G0278873, DDB_G0286195
guanine deaminase	DDB G0277743
porphobilinogen deaminase	DDB_G0284697
putative arginine deaminase	DDB_G0289195
serine deaminase	DDB_G0272787
threonine deaminase	DDB_G0277245
glutamine synthetase	DDB_G0276835,DDB_G0295755
glutamate dehydrogenase	DDB_G0280319, DDB_G0287469
Glutaminase	DDB_G0291984
Allantoicase	DDB_G0280267
Aconitase	DDB_G0279159
Arginine deiminase	DDB_G0272182
Formimidoyl transferase-cyclo deaminase	DDB_G0287977
Fatty acid amide hydrolase	DDB_G0275967

Supplementary Table 2

Primers used for *adgf* semi-quantitative PCR

Primer	**Sequence**
P1	CCGAAGCTTAAAATGTTTTTAAAGTTTA
P2	ATAGAAATGAATGGCAAGTTAG
P3	GTTGAGAAATGTTAAATTGATCC
P4	TGGATGAGCACGCATATCAG

Supplementary Table 3

Primers used for *adgf* over expression and vector construction

Primer	**Sequence**
adgf OE FP	CCGAAGCTTAAAATGTTTTTAAAGTTTA
adgf OE RP	GGCGGTACCTTAAATATTTGAATAAGTATTA

Supplementary Table 4

Primers used for real time-PCR

Primer	**Sequence**
adgf FP	GTGGTGTATGATGCAATGGTAATG
adgf RP	TGGATGAGCACGCATATCAG
ada FP	GAAACGGGTTAACTAAAGAGCAAG
ada RP	TGGATCATCAGAGGTTGAAGAAG
adat FP	ACCAATTTCAGGAGAGTGGAC
adat RP	TTCCTAAACACCTATTACCAGTACC
ada-tRNA FP	GAACAAGACACGCAGAACTTG
ada-tRNA RP	GCACATCAAACATGGCTCTAC
countin FP	CAACCGGTAATGCTTTTGGT
countin RP	CACAAACGAGAGCTGACA
smlA FP	TGGATTACACCATGTTCAGCA
smlA RP	CCGACTGAAACTGATGCTTTGG
acaA FP	CATTCTAGAGGCGGTATTGGC
acaA RP	GGAGAAAATGTCTGATTTCGCTT
carA FP	ATGTTGGGTTGTATGGCAGTG
carA RP	AGGGAAACCACCATTGACAG
pdsA FP	CCATTGGGTACAACTGGTGGA
pdsA RP	AACTGCCCATGATGGATAGGT
regA FP	TAAAGCAACGTTGGCACAAG
regA RP	ATGGTGATTCCATTGCTTCC
pde4 FP	GATCTTGATACACCAATCGAA
pde4 RP	CTTCTGCATCATCTGTACATG
5'nt FP	CAGCTGAACAAGTAGCAATGG
5'nt RP	TGGTGGAAGACTTGATGCTG
cadA FP	TTCCAAGAATTGGCTCAAGG
cadA RP	CATCAACTGCCCATTGAAAA
csaA FP	GCCAAATACAATCGCTGGTG
csaA RP	TGGTTGGTGTGAGATCAAAAGC
ecmA FP	CCAATTAGCTGTCCAAAACC
ecmA RP	GCAATCACCTTTACCTCCTG
ecmB FP	TGATTCATGTTGTTCAACTGG
ecmB RP	TAAATCATCGCCACATTTTCC
pspA FP	CATTGGCCAATCAAAATCCAG
pspA RP	ACAACAGTTGAAGCAGAACC
rnlA FP_qRT	TTACATTTATTAGACCCGAAACCAAGCG
rnlA RP_qRT	TTCCCTTTAGACCTATGGACCTTAGCG